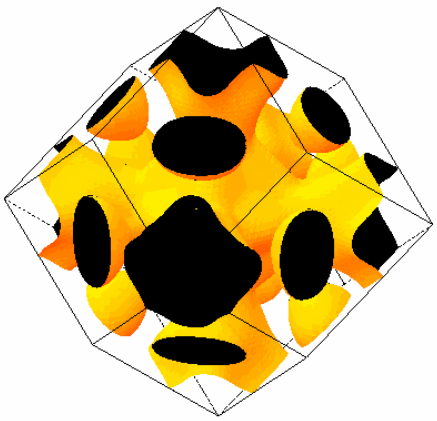
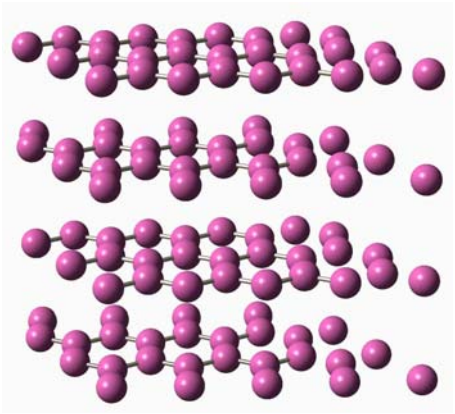
CONDENSED MATTER PHYSICS









R. GRIESSEN
Department of Physics and Astronomy
Faculty of Sciences
Vrije Universiteit Amsterdam
The Netherlands

griessen@nat.vu.nl
April 2007

Table of content

I	INTRODUCTION	4
II	A SIMPLE MOLECULE	6
II.1	The hydrogen atom	6
II.2	Binding by quantum tunnelling: The H_2^+ molecule	10
II.3	The H_2 molecule (this part can be skipped in a first reading)	16
III	A ONE DIMENSIONAL SOLID	22
III.1	Bloch's theorem	23
III.2	The Born-von Karman boundary condition	23
III.3	The Brillouin zone	25
III.4	Energy bands in solids: The tight-binding approximation (B&M596-606)	25
III.5	The ground state	31
IV	CRYSTAL STRUCTURE	33
IV.1	Bravais lattices and primitive cells	34
IV.2	Crystal structure of the elements	37
IV.2.1	Body-centered cubic structure (BCC)	37
IV.2.2	Face centered cubic structure (FCC)	39
IV.2.3	Hexagonal close-packed structure (HCP)	40
IV.2.4	Diamond structure	41
IV.2.5	Density of materials	42
V	THE RECIPROCAL LATTICE AND THE BRILLOUIN ZONE	44
V.1	Bloch theorem in three dimensions	44
V.2	The reciprocal lattice	44
V.2.1	Reciprocal lattice of the BCC-structure	46
V.2.2	Reciprocal lattice of the FCC-structure	47
V.3	The Brillouin zone	48
VI	X-RAY AND NEUTRON SCATTERING IN SOLIDS	51
VI.1	Simple theory of scattering	51
VI.2	Elastic scattering	54
VI.3	Inelastic scattering of neutrons	56
VII	ELECTRON STATES IN THREE DIMENSIONS	57
VII.1	Periodic boundary conditions	57
VII.2	Band structure and ground state	59
VII.2.1	Band structure for a particular choice of k	60
VII.2.2	Following a path in k-space	61
VII.2.3	Surfaces of constant energies.	62
VII.3	The Fermi surface	63
VII.4	The density of states	64
VII.5	The free electron gas	65
VII.6	Effective mass of the electron	67

VIII METALS, SEMICONDUCTORS AND INSULATORS 69
VIII.1 The crystal momentum 69
VIII.2 The true momentum of an electron 70
VIII.3 Bloch electron in an electric field 73
VIII.4 The relaxation time 74
VIII.5 The electric current 75
VIII.6 Various types of materials 77

IX SEMICONDUCTORS 80
IX.1 Properties 80
IX.2 Band structure of a semiconductor 82
IX.3 Impurity states 85
IX.4 p-n junctions 90

X LATTICE VIBRATIONS AND PHONONS 97
X.1 Linear chain of atoms 97
X.2 Periodic boundary conditions 100
X.3 Longitudinal and transverse modes 101
X.4 Phonons 102
X.5 The specific heat of insulators 104
X.6 Specific heat of electrons compared to that of ions 109

XI SUPERCONDUCTIVITY 112
XI.1 The Meissner effect 113
XI.2 London theory 114
XI.3 Cooper pairs 116
XI.4 High temperature superconductors 121

I INTRODUCTION

For many years solid state physics has been focused on the study and description of materials, preferably in crystalline form. Typical questions are:

- why are some materials insulators, other good conductors and some other semiconductors?
- why is diamond so hard and lead so soft?
- why are iron, cobalt and nickel ferromagnetic?
- why is the resistivity of metals increasing with increasing temperature?
- how is it possible that the 10^{23} electrons in a superconductor can transport electricity without electrical resistivity and Joule heating?
- why is copper reddish, gold yellowish, diamond and quartz transparent and nickel so shiny?
- what holds solids together?
- why does semiconducting Si become metallic and even superconducting under high pressures?
- and many more

In the last decades of the 20^{th} century, however, more and more attention was given to disordered systems, such as amorphous semiconductors and metallic glasses, to liquids and to polymers. It is therefore, more appropriate nowadays to talk about **Condensed Matter Physics** rather than about Solid State Physics.

For this course we shall leave the traditional path which starts with a geometric description of ideal crystal structures and scattering of X-rays and neutrons in such structures. We will instead immediately start with a description of electron tunneling from atom to atom in condensed matter, a process which is independent of the exact arrangement of atoms. The basic ingredients which enter the theory are introduced by means of treatment of the simplest system, that of two protons and two electrons, i.e. the H_2-molecule. With this simple example it is already possible to understand, of course very qualitatively, electron hopping, correlation effects and the occurrence of magnetism.

Evidently, a two atomic molecule is quite different form a solid containing approximately 10^{23} atoms per cubic centimeter. In order to explore the profound influence of the presence of many atoms we shall then consider a very long chain of atoms and see that translation invariance leads to the formation of *allowed* as well as *forbidden* energy bands. These bands play a vital role in the description of metals, semiconductors and insulators. The band structure approach is however, not always adequate. For example, for the switchable metal-hydride materials found recently in our group (see cover picture) the semiconductor character of YH_3 is probably due to electron correlation effects of a local nature. Strong electron correlation effects are also playing an important role in high temperature superconductors. The essential aspects of electron correlation effects in solids can be understood by considering a chain of hydrogen atoms.

The determination of electronic states in materials is only one ingredient of condensed

matter physics. It is quite evident that in systems with so many particles statistical physics is eminently needed. We will see that while electrons are described by the Fermi-Dirac statistics, lattice vibrations (whose quanta are called phonons) obey the Bose-Einstein statistics. In that sense, one could popularly define Condensed Matter Physics as a marriage of Statistical Physics and Quantum Mechanics. It is a fascinating playground where various skills are required to understand the many facets of existing and future materials. It is also a playground full of surprises, one of the most spectacular being the discovery of high temperature superconductivity.

Condensed Matter Physics has also had and still has a major impact on our everyday life: without semiconductors, for example, the whole chip industry and informatics revolution would not exist.

Now, to conclude I would like to stress that as Condensed Matter Physics is such a vast subject of physics the present course treats only a few of the basic ideas used in the description of materials. For more information the reader is referred to the excellent book “Solid State Physics” by Ashcroft and Mermin (published by Holt, Rinehart and Winston, 1976).

II A SIMPLE MOLECULE

Many basic properties of solids may be understood by considering the simplest possible solid, a system consisting of two atoms, each atom having only one electron, e.g. a H_2 molecule. The purpose of this section is thus to investigate how cohesion in solids may arise from the delocalisation of electrons without having to solve very complex problems. Furthermore, this section also serves as a reminder of basic quantum-mechanical concepts introduced in the lecture "From Quantum to Matter" (1st year course).

II.1 The hydrogen atom

To start with, let us consider the simplest atom - Hydrogen - with one proton and one electron. The state of the electron is described by Schrödinger´s equation

$$\left[-\frac{\hbar^2}{2m}\Delta + V(\mathbf{R}-\mathbf{r})\right]\phi(\mathbf{r}) = \varepsilon\,\phi(\mathbf{r}) \qquad \text{(II.1)}$$

where **R** indicates the position of the proton and **r** that of the electron. The potential V(**R**-**r**) is simply due to the Coulomb attraction between proton and electron, i.e.

$$V(\mathbf{R}-\mathbf{r}) = \frac{-e^2}{4\pi\varepsilon_0\left|\mathbf{R}-\mathbf{r}\right|} \qquad \text{(II.2)}$$

Equation II.1 has been solved in Quantum Physics. We simply remind here that:

i. the energy eigenstates are:

$$\varepsilon_n = \frac{m\ e^4}{8\,\varepsilon_0^2 h^2}\ \frac{1}{n^2} \qquad \text{(II.3)}$$

ii. eigenstates ϕ_{nlm} depend on three quantum numbers (four, if one includes the electron spin) which are:

n : the principal quantum number
l: the orbital angular momentum quantum number
m_l: the orbital magnetic quantum number (not to be confused with m the mass of the electron

For a given n we have

$$l = 0,\ 1,\ \ldots.,\ n-1 \qquad \text{(II.4)}$$

and

$$m_l = -l,\ -l+1,\ \ldots..,\ l-1,\ l \qquad \text{(II.5)}$$

This implies that the energy level, ε_n is n^2-times degenerate. Remembering that the spin of the electron is either +1/2 or - 1/2 we can thus accommodate $2n^2$ electrons in levels of energy ε_n. An easy way to remember these results is shown in Table II.1

iii. Far from the nucleus all the wave functions decrease exponentially with increasing distance $|\mathbf{R}-\mathbf{r}|$ from the nucleus so that

$$\phi_{nlm}(r,\theta,\varphi) \propto e^{-\frac{|\mathbf{R}-\mathbf{r}|}{na_0}} \tag{II.6}$$

where $a_0 = \dfrac{\varepsilon_0 h^2}{\pi\, me^2}$ (II.7)

is the Bohr radius. It is equal to 0.529 Å (52.9 pm). Near the nucleus ϕ_{nlm} can exhibit nodes. These are, however, not of primary importance in condensed matter physics.

iv. The angular dependence of ϕ_{nlm} is, however, very important as it is responsible for the orientation of bonds in solids.

$$\phi_{n00}(r,\theta,\varphi) \propto 1 \qquad \text{(s-states)} \tag{II.8}$$

$$\phi_{n10}(r,\theta,\varphi) \propto \cos\theta \qquad \text{(p-states)} \tag{II.9}$$
$$\phi_{n1\pm1}(r,\theta,\varphi) \propto \sin\theta\, e^{\pm i\varphi}$$

$$\phi_{n20}(r,\theta,\varphi) \propto 3\cos^2\theta - 1$$
$$\phi_{n2\pm1}(r,\theta,\varphi) \propto \sin\theta\cos\theta\; e^{\pm i\varphi} \qquad \text{(d-states)} \tag{II.10}$$
$$\phi_{n2\pm2}(r,\theta,\varphi) \propto \sin^2\theta\; e^{\pm 2i\varphi}$$

Instead of working with complex wave functions, one can construct real ϕ's by means of linear combinations. For example, $e^{i\varphi} + e^{-i\varphi} = 2\cos\varphi$ and $e^{i\varphi} - e^{-i\varphi} = 2i\sin\varphi$.

For p-states we have then

$$\phi_{n10} \propto \cos\theta$$
$$\phi_{n11} \propto \sin\theta\cos\varphi \tag{II.11}$$
$$\phi_{n1-1} \propto \sin\theta\sin\varphi$$

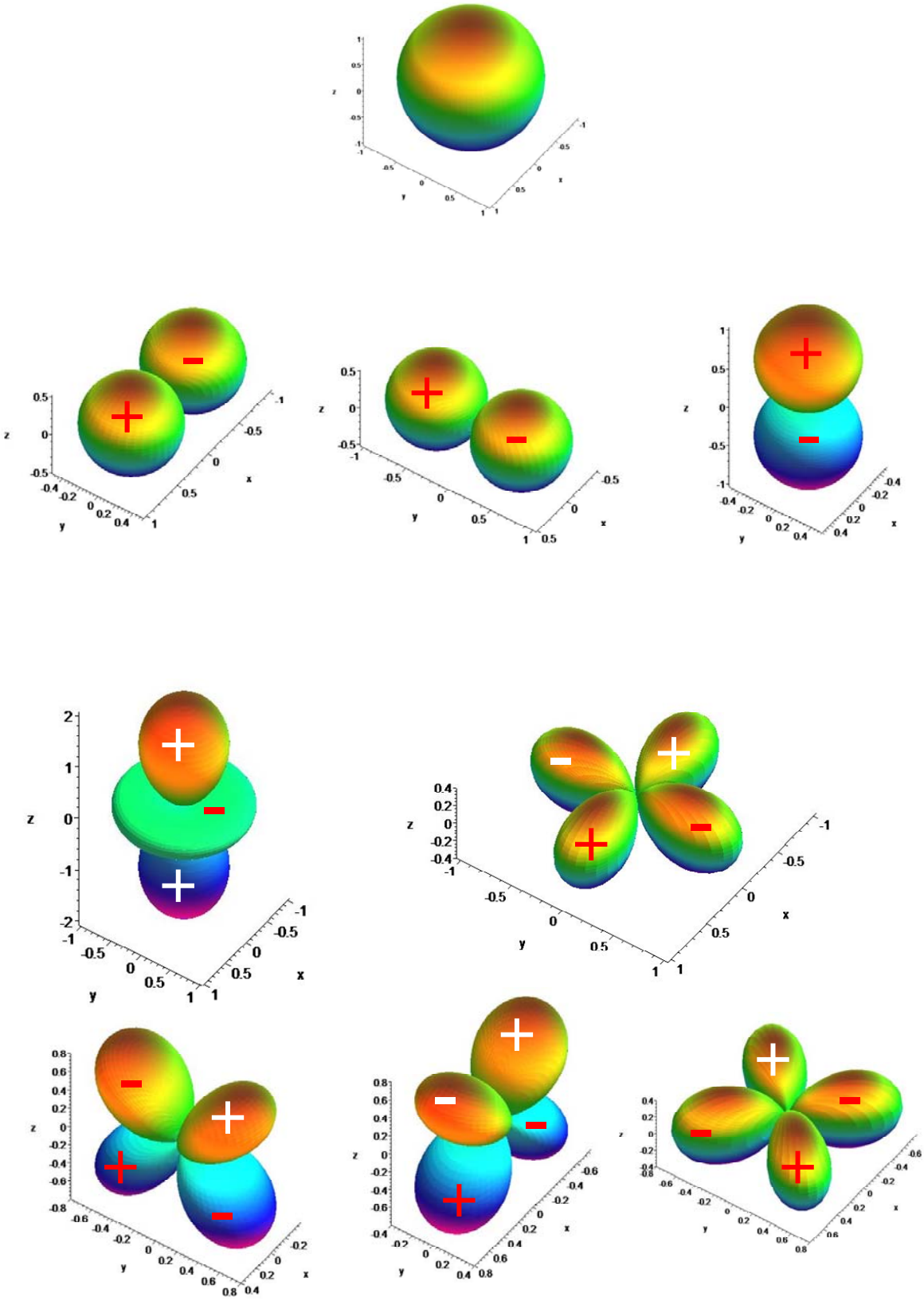


Fig. II.1: Angular dependence of s-states (top) , p-states (middle) and d-states (bottom). The + and – indicate the sign of the wave function.

and for d-states we have

$$\begin{aligned}
\phi_{n2\,0} &\propto 3\cos^2\theta - 1 \\
\phi_{n2\,1} &\propto \sin\theta\cos\theta\ \sin\varphi \\
\phi_{n2-1} &\propto \sin\theta\cos\theta\ \cos\varphi \qquad \text{(II.12)} \\
\phi_{n2\,2} &\propto \sin^2\theta\ \sin 2\varphi \\
\phi_{n2-2} &\propto \sin^2\theta\ \cos 2\varphi
\end{aligned}$$

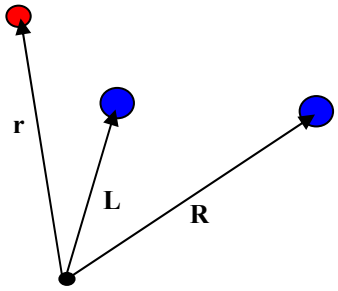
It is important to point out that the angular part of the wave functions shown in Fig. II.1 are very useful to understand, at least qualitatively, the properties of transition metals. Transition metals are all the elements in the periodic system between Scandium and Nickel, Yttrium and Palladium and Lanthanum and Platinum.

This is all for our brief review of the hydrogen atom! We continue now with a slightly more complicated problem.

Table II.1: Energy levels of the hydrogen atom for the four lowest levels. For historical reasons a state with $l = 0$ is called a s-state, one with $l = 1$ a p-state, one with l = 2 a d-state and one with a $l = 3$ f-state.

n	ε_n (eV)	l=0	l=1	l=2	l=3	l=….	degeneracy
n							n^2
..	…..						…..
4	ε_4 = -0.85	4s	4p	4d	4f		1+3+5+7 = 16
3	ε_3 = -1.51	3s	3p	3d			1+3+5 = 9
2	ε_2 = -3.40	2s	2p				1+3 = 4
1	ε_1 = -13.6	1s					1

II.2 Binding by quantum tunneling: The H_2^+ molecule



Consider two protons fixed at L and **R** and one electron at **r**, i.e. a H_2^+-molecule. Then we have the following Schrödinger equation for the electron.

$$\left[-\frac{\hbar^2}{2m}\Delta + V(\mathbf{L}-\mathbf{r}) + V(\mathbf{R}-\mathbf{r}) + V(\mathbf{L}-\mathbf{R})\right]\psi(\mathbf{r}) = \varepsilon\psi(\mathbf{r}) \qquad \text{(II.13)}$$

As we are primarily interested in the state with lowest energy, the so-called **groundstate** of the system, we try to find a solution of Eq. II.13 in the form of a linear combination of the ground state wave function $\phi_{1s}(\mathbf{r})$ of the one electron - one proton problem (the previous H-problem; $\phi_{1s} = \phi_{100}$). As here there are *two* protons we have to specify where ϕ_{1s} is centred (at **L** or **R**) so that $\phi_{1s}(\mathbf{L} - \mathbf{r})$ and $\phi_{1s}(\mathbf{R} - \mathbf{r})$ need to be considered. The linear combination is then

$$\psi(\mathbf{r}) = a\,\phi_{1s}(\mathbf{L}-\mathbf{r}) + b\,\phi_{1s}(\mathbf{R}-\mathbf{r}) \qquad \text{(II.14)}$$

As ϕ_{1s} is a rapidly decreasing function of $|\mathbf{R} - \mathbf{r}|$ (see Eq. II.6) we assume that

$$\int d^3r\ \phi_{1s}^*(\mathbf{L}-\mathbf{r})\,\phi_{1s}(\mathbf{R}-\mathbf{r}) \cong 0 \qquad \text{(II.15)}$$

as long as the distance between the two protons, $|\mathbf{R} - \mathbf{L}|$ is not too small. In other words, we assume that the two states $\phi_{1s}(\mathbf{L} - \mathbf{r})$ and $\phi_{1s}(\mathbf{R} - \mathbf{r})$ are orthogonal. As in the following part of this course we shall often encounter integrals of the type II.15, we introduce here a more compact notation

$$\int d^3r\ \Psi_1^*\,\hat{A}\,\Psi_2 \equiv \left\langle \Psi_1 \middle| \hat{A} \middle| \Psi_2 \right\rangle \qquad \text{(II.16)}$$

where $\hat{A}$ is an operator. In the special case of Eq. II.15, $\hat{A} = 1$ and one writes simply

$$\int d^3r\ \phi_{1s}^*(\mathbf{L}-\mathbf{r})\,\phi_{1s}(\mathbf{R}-\mathbf{r}) \equiv \left\langle \phi_{1s}(\mathbf{L}-\mathbf{r}) \,\middle|\, \phi_{1s}(\mathbf{R}-\mathbf{r}) \right\rangle \cong 0 \qquad \text{(II.17)}$$

Note, however, that

$$\left\langle \phi_{1s}\left(\mathbf{R}-\mathbf{r}\right) \middle| \phi_{1s}\left(\mathbf{R}-\mathbf{r}\right) \right\rangle = \left\langle \phi_{1s}\left(\mathbf{L}-\mathbf{r}\right) \middle| \phi_{1s}\left(\mathbf{L}-\mathbf{r}\right) \right\rangle = 1 \tag{II.18}$$

because we choose ϕ_{1s} (**L** - **r**) and ϕ_{1s} (**R** - **r**)to be normalised.

The standard way to solve Eq. II.13 proceeds in several steps that are used so often in condensed matter physics that we indicate them explicitly.

Step 1: Introduce the Ansatz (Eq. II.14) into Eq. II.13.

Step 2: Multiply both sides of the equation either by $\phi^*_{R1} \equiv \phi^*_{1s}\left(\mathbf{R}_1 - \mathbf{r}\right)$ or $\phi^*_{R2} \equiv \phi^*_{1s}\left(\mathbf{R}_2 - \mathbf{r}\right)$. Two relations are obtained.

Step 3: Integrate both relations over whole space and make use of the orthonormalisation properties (II.15) and (II.18).

Introducing the following notations for simplification

$$T \equiv -\frac{\hbar^2}{2m}\Delta \tag{II.19}$$

$$L \equiv \phi_{1s}\left(\mathbf{L}-\mathbf{r}\right) \quad \text{and} \quad R \equiv \phi_{1s}\left(\mathbf{R}-\mathbf{r}\right) \tag{II.20}$$

$$V_L \equiv V\left(\mathbf{L}-\mathbf{r}\right), \quad V_R \equiv V\left(\mathbf{R}-\mathbf{r}\right), \quad V_{pp} \equiv V\left(\mathbf{R}-\mathbf{L}\right) \tag{II.21}$$

we obtain by the three steps indicated above

$$\begin{aligned} &a\left\langle L\middle|\left(T+V_L\right)+V_R+V_{pp}\middle|L\right\rangle + b\left\langle L\middle|\, V_L+\left(T+V_R\right)+V_{pp}\middle|\, R\right\rangle \\ &= \varepsilon\left\langle L\middle|\, a\,L+b\,R\right\rangle \end{aligned} \tag{II.22}$$

and

$$\begin{aligned} &a\left\langle R\middle|\left(T+V_L\right)+V_R+V_{pp}\middle|L\right\rangle + b\left\langle R\middle|\, V_L+\left(T+V_R\right)+V_{pp}\middle|\, R\right\rangle \\ &= \varepsilon\left\langle R\middle|\, a\,L+b\,R\right\rangle \end{aligned} \tag{II.23}$$

In Eqs. II.22 and II.23 we have written the total Hamiltonian of Eq. II.13 as

$$\bar{H} = \left(T+V_L\right)+V_R+V_{pp} = \left(T+V_R\right)+V_L+V_{pp} \tag{II.24}$$

to explicitly make use of the fact that

$$\left(T+V_L\right)L=\varepsilon_{1s}\,L,\qquad \left(T+V_R\right)\,R=\varepsilon_{1s}\,R \tag{II.25}$$

here ε_{1s} = - 13.6 eV is the ground state energy of the hydrogen atom.
Defining

$$G\equiv\left\langle L\middle|V_R+V_{pp}\middle|L\right\rangle=\left\langle R\middle|V_L+V_{pp}\middle|R\right\rangle=-V+V_{pp} \tag{II.26}$$

and

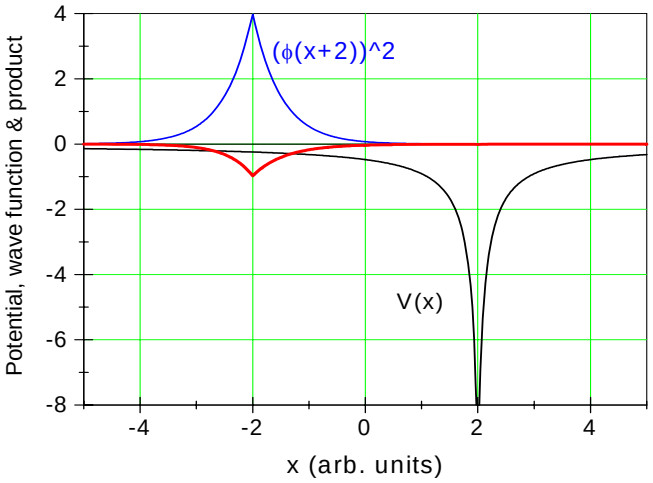
$$-t\equiv\left\langle L\middle|V_L+V_{pp}\middle|R\right\rangle=\left\langle L\middle|V_L\middle|R\right\rangle=\left\langle R\middle|V_R+V_{pp}\middle|L\right\rangle=\left\langle L\middle|V_R\middle|R\right\rangle \tag{II.27}$$

Eqs. II.22 and II.23 become simply

$$a\left(\varepsilon_{1s}+G\right)-b\,t=\varepsilon\,a \tag{II.28}$$

$$-at+b\left(\varepsilon_{1s}+G\right)=\varepsilon\,b \tag{II.29}$$

Note that because V_L and V_R are attractive potentials and V_{pp} is positive, the matrix elements V and t in Eqs. II.28 and II.29 are positive. When the protons are separated by a large distance V is almost exactly compensated by V_{pp}, the repulsive potential energy between the two protons. G is thus small. At small separations the proton-proton repulsion dominates as it varies like $1/\left|\mathbf{R}-\mathbf{L}\right|$. The overlap tunneling matrix element t increases steadily when the two protons are brought together.



:

Fig. II.2: Contribution to the integral V when the protons are far apart. The blue curves indicate the square of the wave function and the black curve the potential. The red curve is the product which appears in the definition for V.

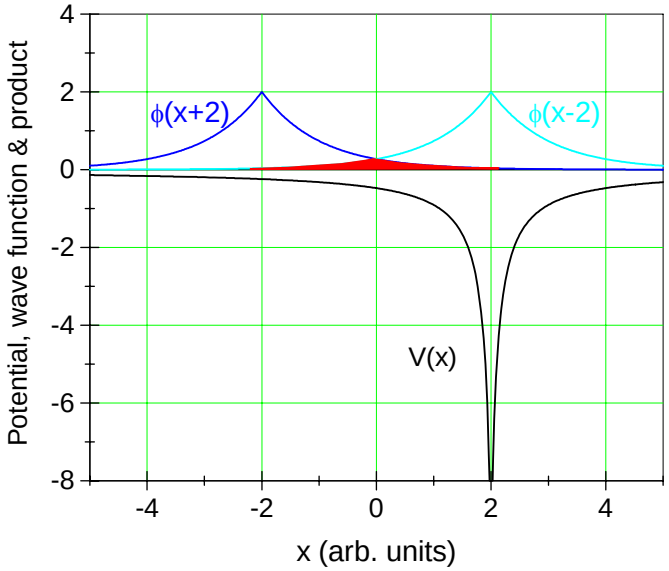


Fig. II.3: Contribution to the overlap integral t when the protons are far apart. The blue curves indicate the wave functions and the black curve the potential. The red region contributes most to the product that appears in the definition of t.

In Fig. II.2 and Fig. II.3 we indicate which terms contribute most to V and t when the protons are far apart. From these schematic pictures it is evident that t depends sensitively on the overlap of the wave functions L and R. This is the reason why t is called the **overlap matrix element** or **overlap integral**. When t is large the electron can easily tunnel from one atom to the other. When $t \to 0$ this is impossible and the electron remains permanently near one proton. The H_2^+-molecule is then, in fact, made of a neutral H atom and a lonely proton.

The two equations II.28 and II.29 form a system of equations that has a non-trivial solution ($a \neq 0$, $b \neq 0$) if the following determinant vanishes, i.e.

$$\begin{vmatrix} \varepsilon_{1s} + G - \varepsilon & -t \\ -t & \varepsilon_{1s} + G - \varepsilon \end{vmatrix} = 0 \qquad \text{(II.30)}$$

This condition determines the eigenvalues of the problem. The determinant is equal to

$$\left[\varepsilon_{1s} + G - \varepsilon\right]^2 - t^2 = 0 \qquad \text{(II.31)}$$

and, therefore,

$$\varepsilon = \varepsilon_{1s} + G \pm t \qquad \text{(II.32)}$$

Note that as the Coulomb interaction is attractive both G and t are negative when the protons are far apart. Compared to the neutral H-atom in which the electron has an energy ε_{1s}, in the H_2^+-molecule the energy of the electron is lowered by two terms:

i) by G which is the Coulomb interaction energy of an electron, centred on proton "1", with proton "2" (G contains also the proton-proton repulsion; however, at large separation this repulsion is weak)

ii) by t as a result of the possibility to tunnel from a state centred at proton "1" to a state centred at proton "2".

To get some intuition about this problem we calculate the states corresponding to the two eigenvalues in Eq. II.32. For that we introduce

$$\varepsilon_+ = \varepsilon_{1s} + G - t \tag{II.33}$$

into Eq. II.28 or II.29 and find that $a = b$ and

$$\psi_+(\mathbf{r}) = \frac{1}{\sqrt{2}}(L+R) \tag{II.34}$$

For the high energy state we have similarly, with

$$\varepsilon_- = \varepsilon_{1s} + G + t \tag{II.35}$$

$$\psi_-(\mathbf{r}) \frac{1}{\sqrt{2}}(L-R) \tag{II.36}$$

This is a state with a node halfway between the two protons. The square root comes from the normalisation of the wave functions ψ_+ and ψ_-. In Fig. II.4 we indicate schematically the change in energy of the electron when another proton is added to a hydrogen atom to form an H_2^+-molecule. Important is that for the low energy state, the so-called **bonding state**, the wave function has a finite amplitude everywhere between the two protons, while for the high energy state, the so-called **anti-bonding state**, the wave function has zero amplitude between the two protons. This implies that the probability for the electron to tunnel from one proton to the other is smaller, or, in other words, that the electron is more localized than in the ground state. According to Heisenberg's uncertainty principle localisation implies a higher momentum and therefore a higher energy.

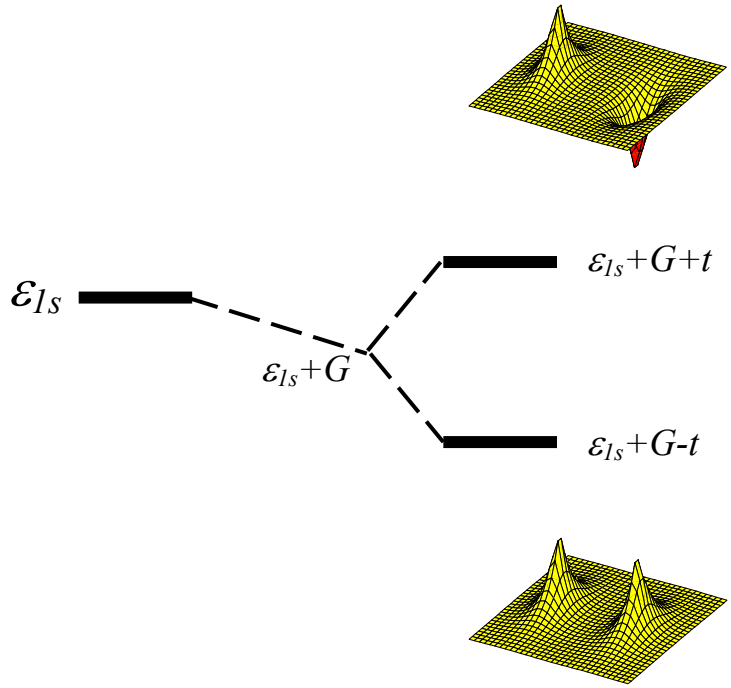


Fig. II.4: Effect of an approaching proton on the ground state of a hydrogen atom. The spatial spread of the wave functions ψ_+ and ψ_- is schematically indicated for the two levels. The lower state is called the bonding state. The upper state is called the antibonding state.

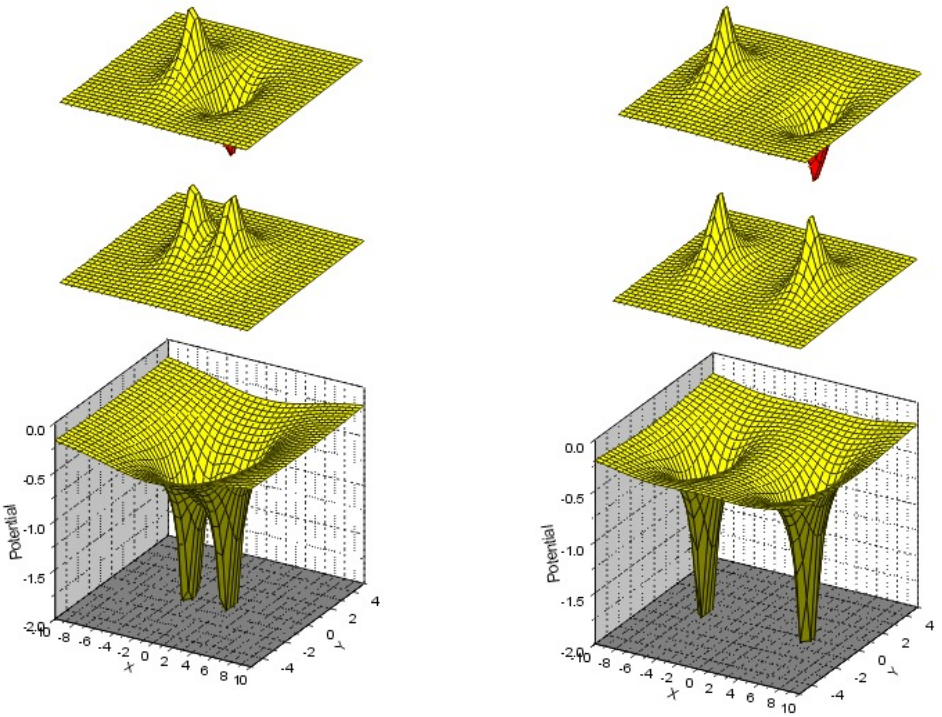


Fig. II.5: *left three panels)* Bonding (bottom) and antibonding (top) states in a situation where both protons (at x = -2 and x = +2) are close to each other. Their overlap is then much larger than in the right panels and the electron can easily tunnel from one proton to the other.; *(right three panels):* Bonding (bottom) and antibonding (top) states in a situation where both protons are far apart (at x = -5 and x = +5).As a function of separation the bonding state energy passes through a minimum, while the energy of the antibonding state increases steadily when the separation of the two protons decreases.

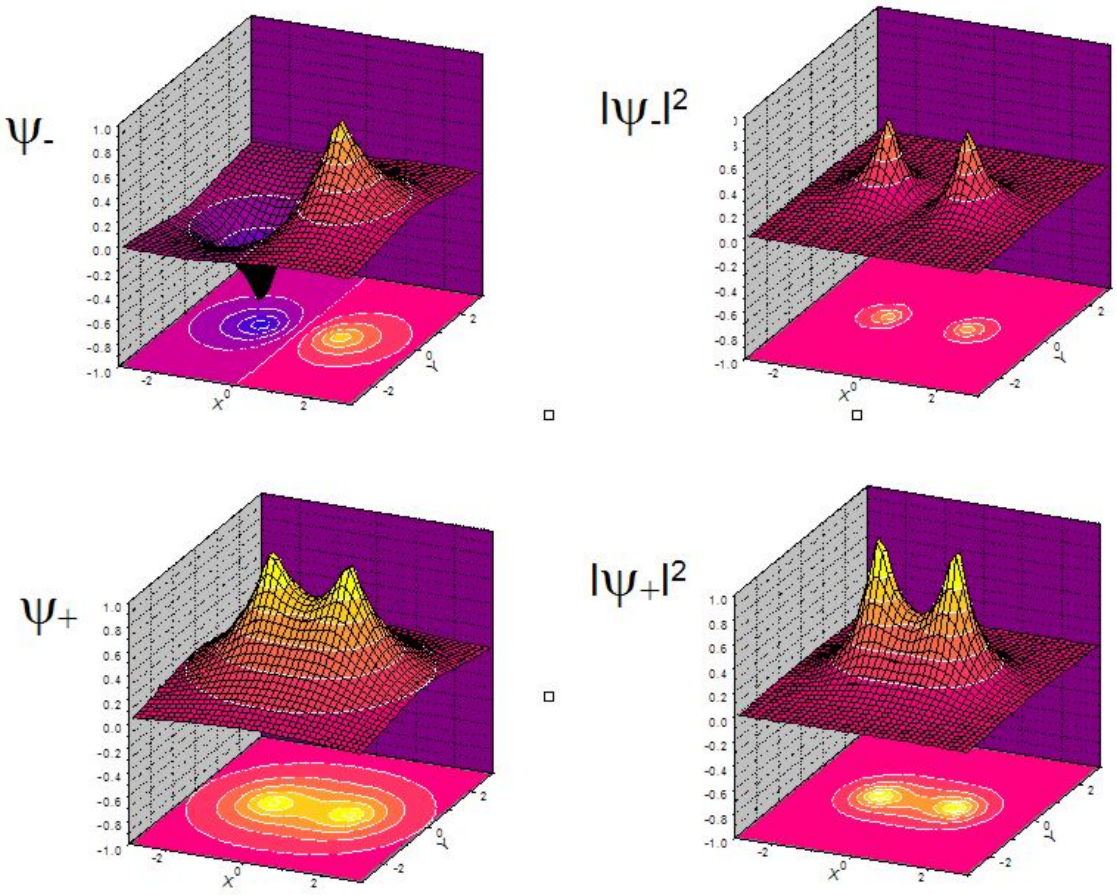


Fig. II.6: Antibonding (top) and bonding (bottom) states of the H_2^+ -molecule. On the left we indicate the wave functions and on the right the square of the norm of the wave functions.

II.3 The H_2 molecule (this part can be skipped in a first reading)

The H_2 molecule consists of two electrons orbiting around two protons at position **L** and **R, L** and **R** standing for left and right.

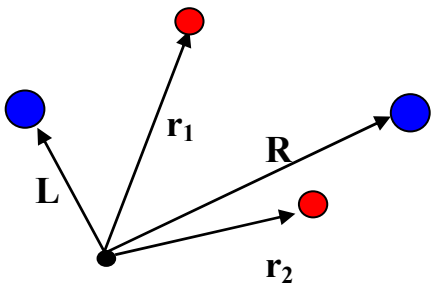


Fig. II.7: Definition of the coordinates chosen for the H_2 molecule. The protons are in blue and the electrons in red.

The Schrödinger equation for the two electrons is

$$-\frac{\hbar^2}{2m}\Delta_1\Psi-\frac{\hbar^2}{2m}\Delta_2\Psi+\left(\begin{array}{l}-\dfrac{e^2}{4\pi\varepsilon_0|\mathbf{L}-\mathbf{r}_1|}-\dfrac{e^2}{4\pi\varepsilon_0|\mathbf{R}-\mathbf{r}_1|}\\ -\dfrac{e^2}{4\pi\varepsilon_0|\mathbf{L}-\mathbf{r}_2|}-\dfrac{e^2}{4\pi\varepsilon_0|\mathbf{R}-\mathbf{r}_2|}+\dfrac{e^2}{4\pi\varepsilon_0|\mathbf{r}_2-\mathbf{r}_1|}\end{array}\right)\Psi=E\Psi \qquad (\text{II.37}$$

where the wave function Ψ depends both on $\mathbf{r_1}$ and $\mathbf{r_2}$. The Coulomb energy V_{pp} between the two protons will be taken into account at the very end of the calculation. For simplicity we write Eq.II.37 as

$$\left[T_1+V_L(1)+V_R(1)+T_2+V_R(2)+V_L(2)+V_{12}\right]\Psi=E\Psi \qquad (\text{II.38}$$

with

$$V_L(i)=-\frac{e^2}{4\pi\varepsilon_0|\mathbf{L}-\mathbf{r}_i|} \qquad V_R(i)=-\frac{e^2}{4\pi\varepsilon_0|\mathbf{R}-\mathbf{r}_i|} \qquad (\text{II.39}$$

and

$$V_{12}=-\frac{e^2}{4\pi\varepsilon_0|\mathbf{r}_2-\mathbf{r}_1|} \qquad (\text{II.40}$$

We construct a two-electron state from the atomic s-orbitals $\phi(\mathbf{r}_i\text{-}\mathbf{L})$ and $\phi(\mathbf{r}_i\text{-}\mathbf{R})$ which, for simplicity, shall be denoted below as L_i and R_i, respectively. There are six possible states

$$\begin{aligned}\Phi_0&=\frac{1}{\sqrt{2}}\left[L_1R_2+L_2R_1\right]\times\left|\uparrow\downarrow-\downarrow\uparrow\right\rangle\\ \Phi_1^1&=\frac{1}{\sqrt{2}}\left[L_1R_2-L_2R_1\right]\times\left|\uparrow\uparrow\right\rangle\\ \Phi_1^0&=\frac{1}{\sqrt{2}}\left[L_1R_2-L_2R_1\right]\times\left|\uparrow\downarrow+\downarrow\uparrow\right\rangle\\ \Phi_1^{-1}&=\frac{1}{\sqrt{2}}\left[L_1R_2-L_2R_1\right]\times\left|\downarrow\downarrow\right\rangle\end{aligned} \qquad (\text{II.41}$$

$$\begin{aligned}\Phi_L&=\left[L_1L_2\right]\times\left|\uparrow\downarrow-\downarrow\uparrow\right\rangle\\ \Phi_R&=\left[R_1R_2\right]\times\left|\uparrow\downarrow-\downarrow\uparrow\right\rangle\end{aligned} \qquad (\text{II.42})$$

The three states Φ_0, Φ_L, Φ_R have zero total spin (S=0) while the other three states have total spin 1. The solution of the Schrödinger equation will be seeked in the form of a linear combination of these six wave functions, i.e.

$$\Psi = c_0\Phi_0 + c_1\Phi_1^1 + c_2\Phi_1^0 + c_3\Phi_1^{-1} + c_4\Phi_L + c_5\Phi_R \qquad \text{(II.43}$$

In building up the matrix equation for the coefficients c_i we need to calculate matrix elements of the form

$$\begin{aligned}
&\langle L_1R_2 \pm L_2R_1 \,|\, L_1R_2 \pm L_2R_1 \rangle \\
&\langle L_1R_2 \pm L_2R_1 \,|\, L_1L_2 \rangle \\
&\langle L_1R_2 \pm L_2R_1 \,|\, R_1R_2 \rangle \\
&\langle L_1L_2 \,|\, R_1R_2 \rangle
\end{aligned} \qquad \text{(II.44}$$

and

$$\begin{aligned}
&\langle L_1R_2 \pm L_2R_1 \,|\, H | L_1R_2 \pm L_2R_1 \rangle \\
&\langle L_1R_2 \pm L_2R_1 \,|\, H | L_1L_2 \rangle \\
&\langle L_1R_2 \pm L_2R_1 \,|\, H | R_1R_2 \rangle \\
&\langle L_1L_2 \,|\, H | R_1R_2 \rangle
\end{aligned} \qquad \text{(II.45}$$

We assume here again that the overlaps between L and R orbitals are such that

$$\langle L_1 \,|\, R_1 \rangle = \langle L_2 \,|\, R_2 \rangle = 0 \qquad \text{and} \qquad \langle L_1 \,|\, L_1 \rangle = \langle R_1 \,|\, R_1 \rangle = 1 \qquad \text{(II.46}$$

In the spirit of the so-called **Hubbard** approximation we assume now that the Coulomb repulsion is only important when the two electrons are near the same proton. This implies that all matrix elements involving V_{12} vanish except

$$\langle L_1L_2 \,|\, V_{12} | L_1L_2 \rangle = \langle R_1R_2 \,|\, V_{12} | R_1R_2 \rangle = U \qquad \text{(II.47}$$

Introducing the notation

$$\begin{aligned}
&[T_i + V_R(i)]R_i = \varepsilon_0 R_i \\
&[T_i + V_L(i)]L_i = \varepsilon_0 L_i \\
&\\
&\varepsilon_H = \varepsilon_0 + \langle L_i \,|\, V_R(i) | L_i \rangle \\
&\varepsilon_H = \varepsilon_0 + \langle R_i \,|\, V_L(i) | R_i \rangle
\end{aligned} \qquad \text{(II.48}$$

and

$$W = \left\langle L_i \left| V_L(i) \right| R_i \right\rangle = \left\langle L_i \left| V_R(i) \right| R_i \right\rangle \qquad \text{(II.49)}$$

we obtain the following matrix

$$\begin{pmatrix} 2\varepsilon_H & 0 & 0 & 0 & \sqrt{2}W & \sqrt{2}W \\ 0 & 2\varepsilon_H & 0 & 0 & 0 & 0 \\ 0 & 0 & 2\varepsilon_H & 0 & 0 & 0 \\ 0 & 0 & 0 & 2\varepsilon_H & 0 & 0 \\ \sqrt{2}W & 0 & 0 & 0 & (2\varepsilon_H + U) & 0 \\ \sqrt{2}W & 0 & 0 & 0 & 0 & (2\varepsilon_H + U) \end{pmatrix} \begin{pmatrix} c_0 \\ c_1 \\ c_2 \\ c_3 \\ c_4 \\ c_5 \end{pmatrix} = E \begin{pmatrix} c_0 \\ c_1 \\ c_2 \\ c_3 \\ c_4 \\ c_5 \end{pmatrix} \qquad \text{(II.50)}$$

There exists a non-trivial solution if the following determinant vanishes,

$$\begin{vmatrix} 2\varepsilon_H - E & 0 & 0 & 0 & \sqrt{2}W & \sqrt{2}W \\ 0 & 2\varepsilon_H - E & 0 & 0 & 0 & 0 \\ 0 & 0 & 2\varepsilon_H - E & 0 & 0 & 0 \\ 0 & 0 & 0 & 2\varepsilon_H - E & 0 & 0 \\ \sqrt{2}W & 0 & 0 & 0 & (2\varepsilon_H + U) - E & 0 \\ \sqrt{2}W & 0 & 0 & 0 & 0 & (2\varepsilon_H + U) - E \end{vmatrix} = 0 \qquad \text{(II.51)}$$

There are three degenerate states with energy

$$E = 2\varepsilon_H \qquad \text{(II.52}$$

The other three states have an energy given by

$$\begin{vmatrix} (2\varepsilon_H - E) & \sqrt{2}W & \sqrt{2}W \\ \sqrt{2}W & (2\varepsilon_H + U - E) & 0 \\ \sqrt{2}W & 0 & (2\varepsilon_H + U - E) \end{vmatrix} = 0 \qquad \text{(II.53}$$

For a discussion of the behaviour of the roots of this equation we take the zero of energy as $2\varepsilon_H = 0$. Then,

$$\begin{vmatrix} (-E) & \sqrt{2}W & \sqrt{2}W \\ \sqrt{2}W & (U - E) & 0 \\ \sqrt{2}W & 0 & (U - E) \end{vmatrix} = 0 \qquad \text{(II.54}$$

with the secular equation

$$E(U-E)^2 + 4W^2(U-E) = 0 \qquad \text{(II.55}$$

The energy eigenvalues are

$$E_5 = \frac{U}{2} + \frac{1}{2}\sqrt{\left(U^2 + 16W^2\right)} \qquad (0.41, 0, 0, 0, 0.64, 0.64) \qquad \text{(II.56}$$

$$E_0 = \frac{U}{2} - \frac{1}{2}\sqrt{\left(U^2 + 16W^2\right)} \qquad (0.91, 0, 0, 0, -0.29, -0.29) \qquad \text{(II.57}$$

and

$$E_4 = U \qquad (0, 0, 0, 0, -0.71, 0.71) \qquad \text{(II.58}$$

Furthermore there are the three states at $E_1=E_2=E_3=0$ corresponding to Eq. II.49 with our new choice of the energy zero. The values given in the parentheses are the eigenvectors $(c_0, c_1, c_2, c_3, c_4, c_5)$ for a situation with U = 5 eV and W = $-\sqrt{2}$ eV. The corresponding energy levels are indicated in Fig. II.8. For clarity, we have also indicated the situation in absence of hybridisation, i.e. when W=0.
The ground state has a lower energy when W≠0 than for a situation where hybridisation vanishes. This is expected since W≠0 corresponds to a situation where tunnelling of an electron from one hydrogen to the other is possible. This weaker localisation of the electrons in space leads to a lowering of their energy as a result of Heisenberg's

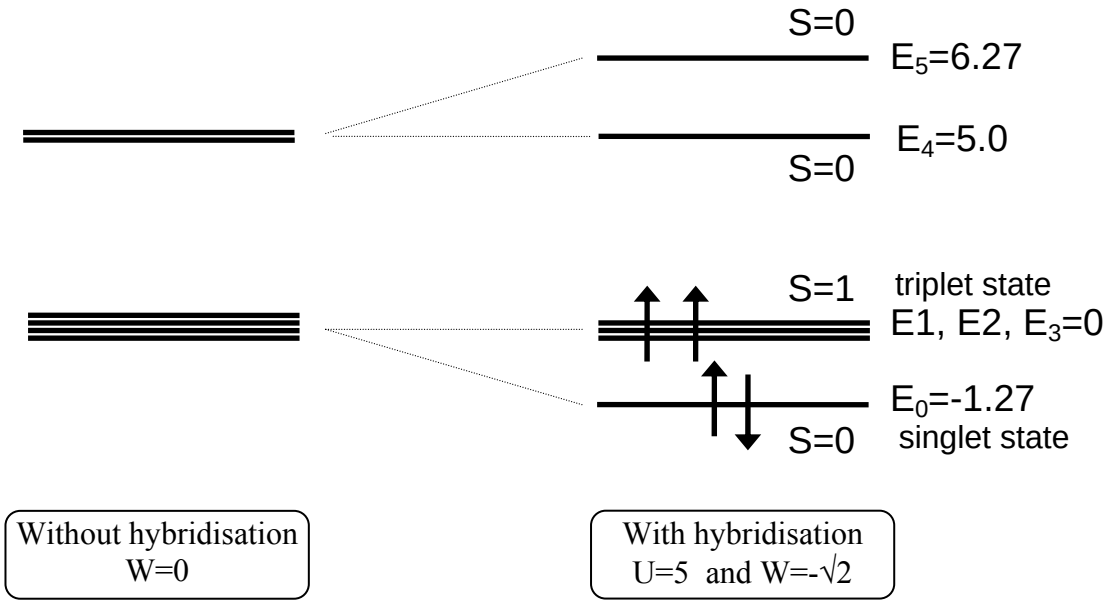


Fig. II.8: Influence of hybridisation on the total electronic energy of the H_2 molecule in the Hubbard approximation. The ground state is called the **bonding** state. Its total spin is *S*=0. The triplet state has *S*=1. The ground state is thus non-magnetic. The eigenvectors are given in Eqs.II.56-57.

uncertainty principle. The ground state having zero total spin is non-magnetic. The density of electrons does not vanish between the two protons as it does for the antisymmetric states with higher energies.

The dependence of the ground state energy (singlet state) as a function of the proton separation is indicated Fig. II.9. In contrast to the triplet state, the energy of the singlet state exhibits a minimum for a proton-proton separation of 0.74611 Å. The binding energy is then 4.52 eV. This implies that 2.26 eV are needed to break the H-H bond in the H_2 molecule. This corresponds to an energy of 218.1 kJ/molH since 1 eV=96.485 kJ/molH.

The different spin arrangements for the two states makes it possible to produce **atomic** hydrogen. For this one needs only to place hydrogen in a strong magnetic field that forces both spins to be parallel to each other. Silvera and Walraven showed experimentally that atomic H with a density of 1.8×10^{14} atoms/cm^3 could be kept for more than 9 minutes at a temperature of 0.27 K in a magnetic field of 7 T. There are two types of hydrogen molecules in the singlet state that differ only through the value of the proton nuclear spin. This a direct consequence of the requirement that the total wave

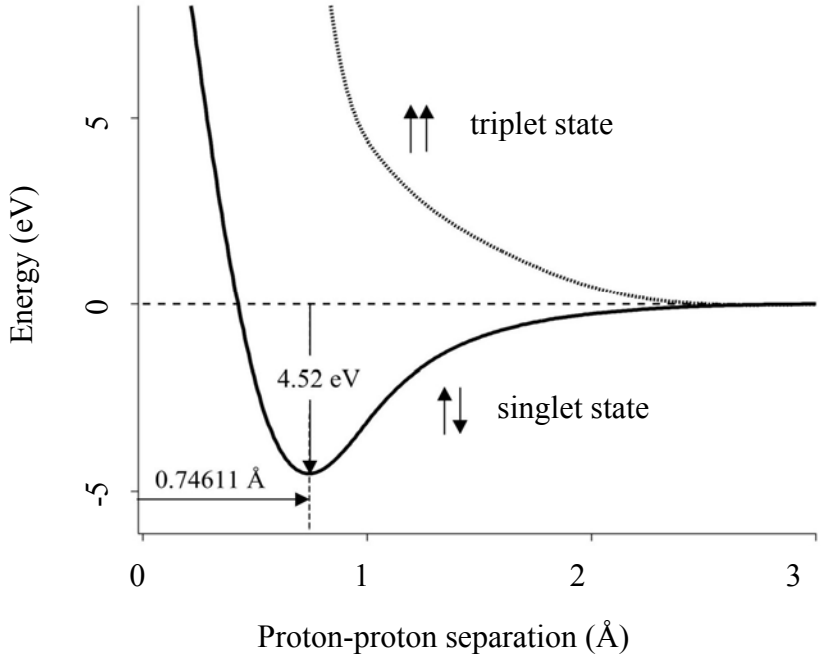


Fig. II.9:: Bonding and antibonding states of the H_2 molecule. At large separation W is very small and the singlet and triplet states are degenerate (see **Fig. II.8**). The large increase at small proton-proton separation is due to their Coulomb repulsion.

function of a system must be antisymmetric for the permutation of fermionic particles and symmetric for bosonic particles. This implies that the wave function of a H_2 (T_2) molecule must be antisymmetric for the permutation of the protons (tritons) and symmetric for the permutation of the deuterons in the D_2 molecule.

III A ONE DIMENSIONAL SOLID

Our next step in constructing a solid is to consider a linear chain of *N* identical atoms and to try to solve the corresponding Schrödinger equation. This problem cannot be solved exactly. We require a suitable approximation. In much the same way as we did for the H_2-molecule (we started by considering only one electron), we consider here the much simpler problem of **one** electron and *N*-protons. The separation between two adjacent protons is *a* and the total length of the chain is $L = (N-1)a$.

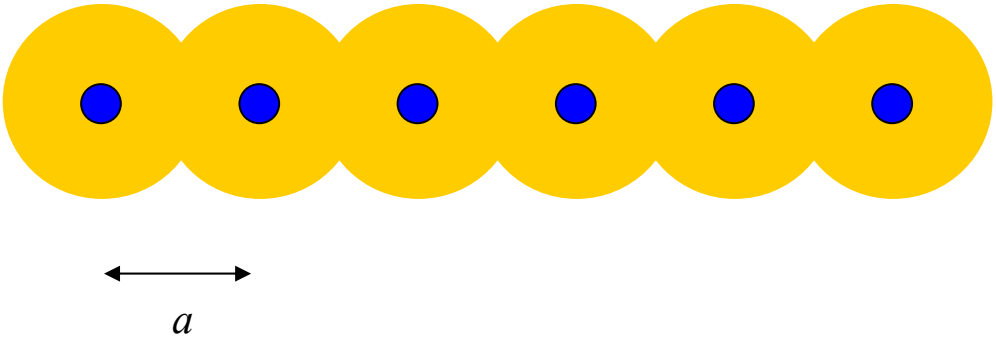


Fig. III.1: **:** A linear chain of N atoms. In solids *a* is typically 10^{-10} m.

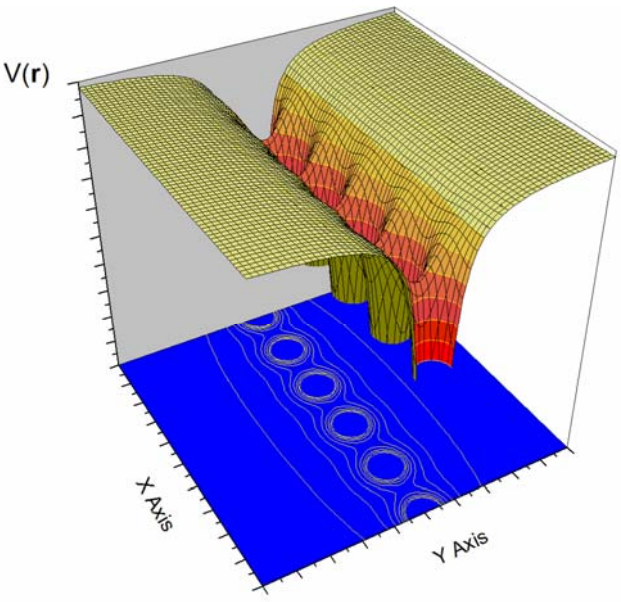


Fig. III.2: Periodic potential seen by one electron in a linear chain of positive ions.

The potential seen by the electron results from its Coulomb attraction with all protons. Writing the potential between the electron at position x and the proton at position νa as $V_{at}(x - \nu a)$ (with $0 \le \nu \le N-1$) we obtain for the Schrödinger equation

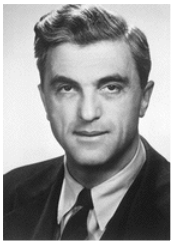
$$-\frac{\hbar^2}{2m}\frac{d^2\Psi(x)}{dx^2} + \sum_{\nu=0}^{N-1} V_{at}\,(x-\nu a)\,\Psi(x) = \varepsilon\,\Psi(x) \qquad \text{(III.1)}$$

The potential $V(x) = \Sigma\, V_{at}$ seen by the electron is obviously periodic as a result of the assumed regular arrangement of the atoms along the chain. The periodicity of the potential has an important implication for the form of the wave function $\Psi(x)$. This implication is known as **Bloch's theorem**.

III.1 Bloch's theorem

The eigenstates $\Psi_{nk}(x)$ of the one-electron Schrödinger equation with a periodic potential $V(x)$, i.e. with $V(x + \nu a) = V(x)$ for all integers ν, can be written as

$$\Psi_{nk}(x) = e^{ikx}\, u_{nk}(x) \qquad \text{(III.2)}$$



where u_{nk} is also a periodic function, i.e.

$$u_{nk}(x+\nu a) = u_{nk}(x) \quad \text{for all } \nu. \qquad \text{(III.3}$$

For reasons, which become obvious below, n is called the band index and k the wave-vector. This theorem is the key ingredient for the understanding of solids in general, and semiconductors, in particular.

III.2 The Born-von Karman boundary condition

So far we have not considered what happens to a quantum mechanical state at the two ends of the linear chain. To define Ψ_k we need to specify the boundary conditions. One possible choice would be $\Psi_k(0) = \Psi_k(L) = 0$. This would, however, lead to standing waves, which are neither appropriate nor appealing for the treatment of moving electrons. As we are primarily interested in the properties of a bulk sample, we are looking for boundary conditions, which do not emphasize the finiteness of the sample under consideration. One way to realize these objectives is to use **periodic boundary conditions** (so-called Born-Von Karman conditions) such that

$$\Psi_k\,(x+L) = \Psi_k\,(x) \qquad \text{(III.4)}$$

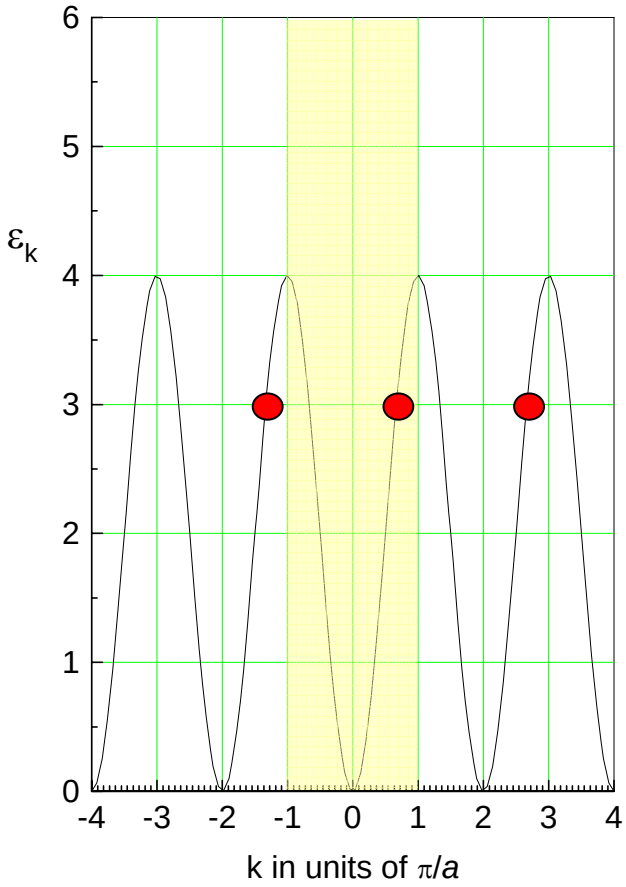


Fig. III.3: Schematic representation of ε_k showing that states separated by $2\pi/a$ (or a multiple of it) are equivalent. The Brillouin zone is indicated in light yellow, and equivalent electron states by red dots. The bottom of the band is arbitrarily set equal to zero.

This condition insures that when an electron travels, say from $x = 0$ to $x = L$, as soon as it leaves the chain at $x = L$ one replaces it by an electron with the same velocity at $x = 0$.

From Bloch's theorem follows that

$$\Psi_k(x+L) = e^{ikL}\Psi_k(x) \qquad \text{(III.5)}$$

and by comparison with Eq. III.4 that

$$e^{ikL} = 1 \qquad \text{(III.6)}$$

The possible values for k are

$$k = \frac{2\pi}{L} l \qquad \text{(III.7)}$$

where l is a positive or negative integer number.

One might at this point get the feeling that the infinite number of k-values leads to an infinite number of quantum states that satisfy Schrödinger's equation III.1 and the Born-von Karman boundary conditions. In fact, in the equation $\Psi_k(x) = e^{ikx}\, u_k(x)$, there is an ambiguity. One sees immediately that by replacing k by k' with

$$k' = k + \frac{2\pi}{a}\, l \qquad \text{(III.8)}$$

where l is an integer, the equation $\Psi(x + va) = e^{ikva}\, \Psi(x)$ remains unchanged since $e^{2\pi i} = 1$. The index k' is thus as legitimate a quantum number as k. In other words, the states Ψ_k and Ψ_{k+G} with

$$G = \frac{2\pi}{a}\, l \qquad l = 0, \pm 1, \pm 2, \ldots . \qquad \text{(III.9)}$$

are equivalent. This implies that the energy eigenvalues ε_k viewed as a function of k are periodic with a periodicity of $2\pi/a$. This is schematically indicated in Fig. III.3.

III.3 The Brillouin zone

As is evident from the redundancy in Fig. III.3, only a finite number of inequivalent quantum states are solutions of the one-electron problem in a periodic potential. Although any segment of length $2\pi/a$ along the k-axis would contain all the inequivalent states, it is more practical to consider the domain $[-\pi/a, \pi/a]$. This domain is called the Brillouin zone and is indicated by a yellow region in Fig. III.3. All the required information about the energy dispersion curve ε_k is contained in the Brillouin zone. Since from Eq. III.7 follows that the consecutive values of k are separated by $2\pi/L$, there are $(2\pi/a)/(2\pi/L) = (L/a) = N$ states in the Brillouin zone.

III.4 Energy bands in solids: The tight-binding approximation

The ε_k curve shown in Fig. III.3 has not been calculated. It merely serves as an illustration of a general property of ε_k. In this section we want to actually calculate the energy eigenvalues ε_k for the linear chain of atoms shown in Fig. III.1. The treatment described below resembles the method used in section II.2 for the H_2^+-molecule.

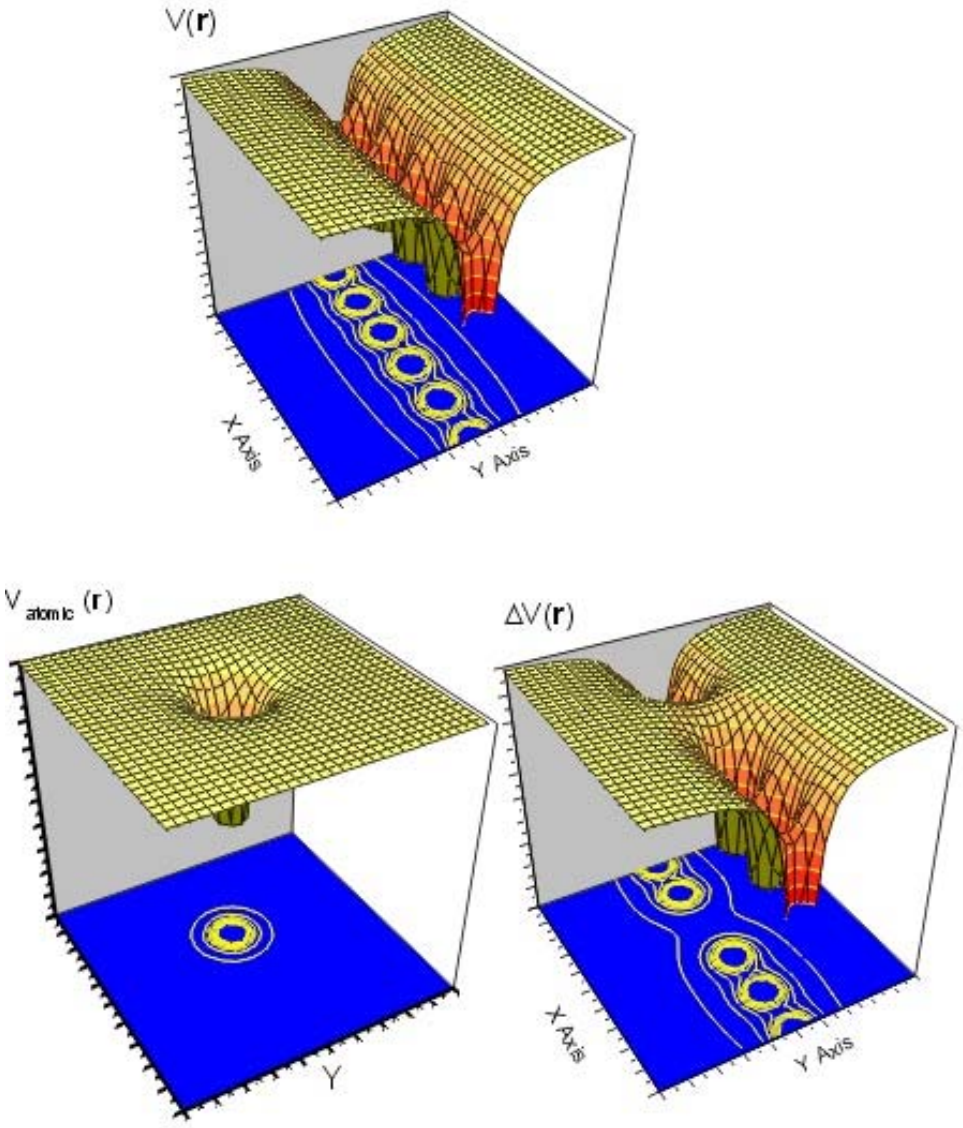


Fig. III.4: The periodic crystal potential *V(x)*, the atomic potential of a free atom at $x = R_0$ and the difference potential $\Delta V(x - R_0)$.

In the vicinity of an atom at R_0 we assume that the periodic crystal potential $V(x)$ can be approximated by the atomic potential $V_{at}(x - R_0)$ (see Fig. III.4). We then write the Schrödinger equation in the form

$$H\Psi(x) = H_{at}(R_0)\ \Psi(x) + \Delta V(x - R_0)\,\Psi(x) = \varepsilon\Psi(x) \qquad \text{(III.10)}$$

with

$$H_{at}(R_0) = -\frac{\hbar^2}{2m}\frac{d^2}{dx^2} + V_{at}(x - R_0) \qquad \text{(III.11)}$$

and

$$\Delta V(x - R_0) = \sum_{R \neq R_0} V_{at}(x - R) \qquad \text{(III.12)}$$

The wave function $\Psi(x)$ must satisfy Bloch's condition III.2. Furthermore we expect, if the atoms in the chain are not too close to each other, that $\Psi(x)$ will resemble the atomic wave function $\phi(x - R)$ in the vicinity of the atom at $x = R$.
A wave function that has these two properties is

$$\psi_k(x) = \frac{1}{\sqrt{N}} \sum_R e^{ikR}\ \phi(x - R) \qquad \text{(III.13)}$$

where

$$H_{at}(R)\,\phi(x - R) = E_{at}\,\phi(x - R) \qquad \text{(III.14)}$$

The factor $1/\sqrt{N}$ arises from the normalisation of $\Psi_k(x)$. As for the H_2^+-molecule we assume here that the overlap between neighbouring wave functions is so small that

$$\langle \phi(x - R)\ |\ \phi(x - R') \rangle \equiv I \cong 0 \qquad \text{if } R \neq R' \qquad \text{(III.15)}$$

We leave it as an exercise for the reader to show that $\Psi_k(x)$ satisfies Bloch's condition. Introducing Eq. III.13 into Schrödinger's equation and making use of the property [1]

---

[1] This property follows from the fact that for any two functions

$$\int_0^L \left(f\frac{d^2g}{dx^2} - g\frac{d^2f}{dx^2} \right) dx = \left(f\frac{dg}{dx} - g\frac{df}{dx} \right)\Big|_0^L$$

(Taking $g = \phi(x - R)$ which goes exponentially to zero for $|x - R| >> a$, we obtain Eq. III.16)

$$\left\langle \phi(x-R_0) \,\middle|\, H_{at}(R_0) \,\middle|\, \Psi_k \right\rangle = \left\langle \Psi_k \,\middle|\, H_{at}(R_0) \,\middle|\, \phi(x-R_0) \right\rangle \qquad \text{(III.16)}$$

we obtain after rearrangement of terms

$$(\varepsilon_k - E_{at}) \left\langle \phi(x-R_0) \,\middle|\, \Psi_k(x) \right\rangle = \left\langle \phi(x-R_0) \,\middle|\, \Delta V(x-R_0) \,\middle|\, \Psi_k(x) \right\rangle \qquad \text{(III.17)}$$

We consider now both integrals separately:

i) The integral on the left-hand-side is dominated by the contribution of one term so that

$$\left\langle \phi(x-R_0) \,\middle|\, \Psi_k(x) \right\rangle \cong \frac{1}{\sqrt{N}} e^{ikR_0} \qquad \text{(III.18)}$$

ii) In the other integral we have two different terms of comparable magnitude

$$\left\langle \phi(x-R_0) \,\middle|\, \Delta V(x-R_0) \,\middle|\, \Psi_k(x) \right\rangle = \frac{1}{\sqrt{N}} \left\langle \phi(x-R_0) \,\middle|\, \Delta V(x-R_0) \,\middle|\, \phi(x-R_0) \right\rangle e^{ikR_0} + \sum_{R \neq R_0} \frac{1}{\sqrt{N}} e^{ikR} \left\langle \phi(x-R_0) \,\middle|\, \Delta V(x-R_0) \,\middle|\, \phi(x-R) \right\rangle \qquad \text{(III.19)}$$

Taking $x = R_0$ as the origin of a new coordinate x' we find that

$$\varepsilon_k = E_{at} + \left\langle \phi(x') \,\middle|\, \Delta V(x') \,\middle|\, \phi(x') \right\rangle + \sum_{R \neq 0} \left\langle \phi(x') \,\middle|\, \Delta V(x') \,\middle|\, \phi(x'-R) \right\rangle e^{ikR} \qquad \text{(III.20}$$

Noting that in the summation only the nearest-neighbour contributions ($R = +a$ and $R = -a$) need to be retained because the wave function overlap with more distant atoms is negligible, we obtain

$$\varepsilon_k = E_{at} - \Delta V - t\left(e^{-ika} + e^{ika}\right) = E_{at} - \Delta V - 2t\cos(ka) \qquad \text{(III.21)}$$

with

$$t \equiv -\left\langle \phi(x) \,\middle|\, \Delta V(x) \,\middle|\, \phi(x-a) \right\rangle \qquad \text{(III.22)}$$

and

$$\Delta V \equiv -\left\langle \phi(x) \,\middle|\, \Delta V(x) \,\middle|\, \phi(x) \right\rangle \qquad \text{(III.23}$$

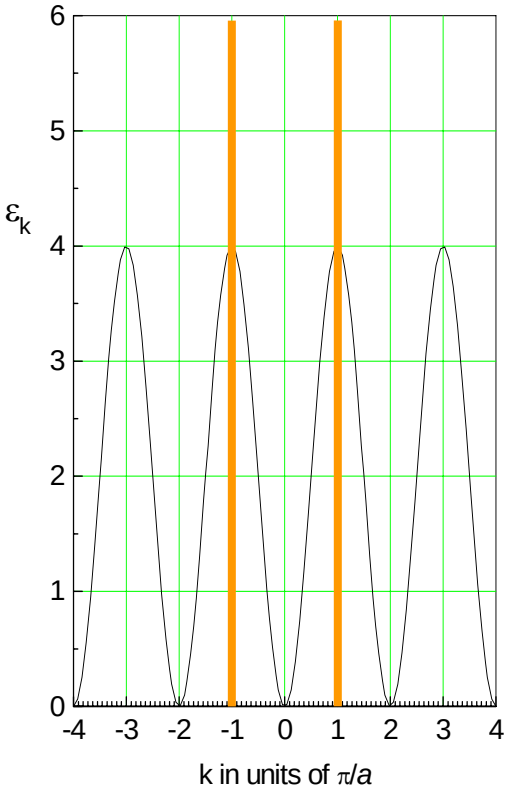


Fig. III.5: Energy dispersion curve for the linear chain in **Fig. III.1** calculated with the tight-binding approximation. The zero of energy is arbitrarily chosen at the bottom of the band. The width of the band is *4t* (with $t = 1$ for this example). The *k*-values allowed by the periodic boundary conditions are indicated by ticks on the *k*-axis. There are *N* different *k*-values in the Brillouin zone. In a real solid (~ 10^{23} atoms) the *k*-values form a quasi-continuum.

The periodicity of ε_k as a function of *k* is evident. The energy dispersion relation ε_k is shown in Fig. III.5 as a continuous function. Note, however, that the allowed *k*-values are given by Eq.III.7.

Until now we have only considered Bloch states originating from a given atomic level of energy E_{at}. Atoms have, however, many levels and, if they are well separated in energy, for each of them one can in principle apply the tight-binding method. In such a case one does not only obtain **one** dispersion curve ε_k but as many as the number of atomic levels. This leads to the formation of a set of so-called **energy bands** as shown in Fig. III.7. This explains why, besides *k*, we need a **band index** *n* to label unambiguously electronic states and energy eigenvalues, i.e. $\Psi_{nk}(x)$ and ε_{nk}. As we shall see later the existence of energy bands is one of the most fundamental results of solid state physics. It allows us to understand why some elements are metals, and other insulators or semiconductors.

To make contact with our treatment of the H_2^+-molecule let us come back to Eq. III.13 and consider two special cases.

- At the centre of the Brillouin zone $k = 0$ and $\varepsilon_k = E_{at} - \Delta V - 2t$. The Bloch wave is simply

$$\Psi_0(x) = \frac{1}{\sqrt{N}} \sum_R \phi(x - R)$$

(III.24

and does not have node if ϕ is a 1s atomic state (Fig. III.6).

- At the boundary of the Brillouin zone $k = \pi/a$ and the e^{ikR} term alternates sign. This leads to a wave function with nodes between each pair of atoms. The energy is $\varepsilon_k = E_{at} - \Delta V + 2t$

Both cases exhibit vividly the analogy with the H_2^+-molecule (see Fig. II.4).

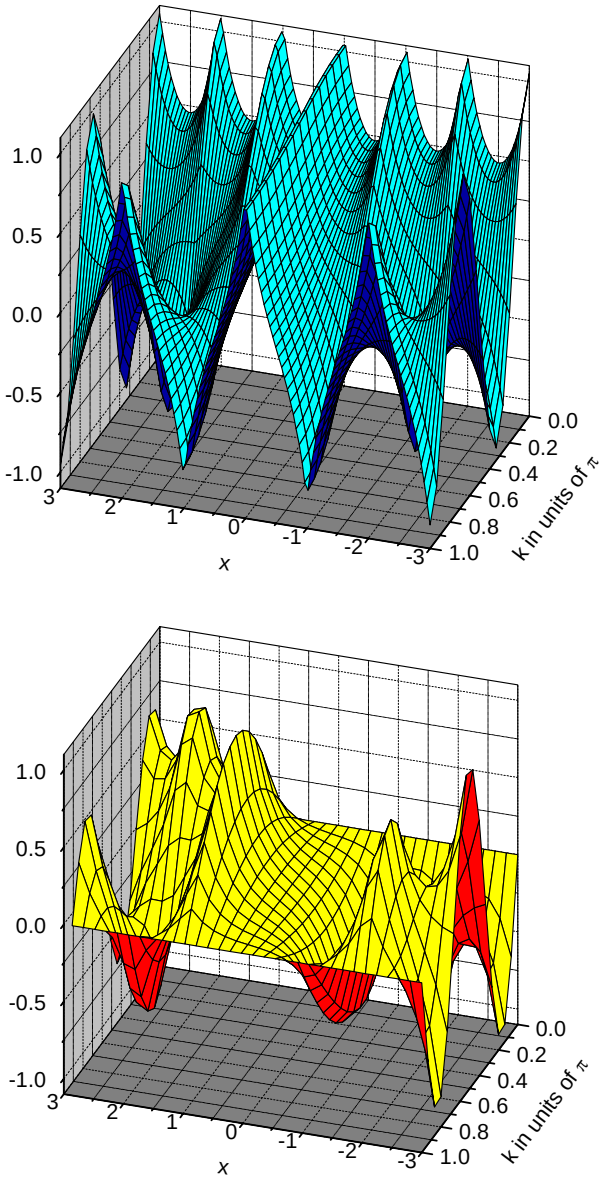


Fig. III.6: Real (top) and complex (bottom) part of the wave function of a Bloch electron as a function of its k quantum number. Note that k=0 corresponds to a state at the centre of the Brillouin zone while k=1 or -1 (in units of π/a) correspond to states at the boundary of the Brillouin zone. There is a strong resemblance with the states of the H_2^+ - molecule (see Fig. II.4)

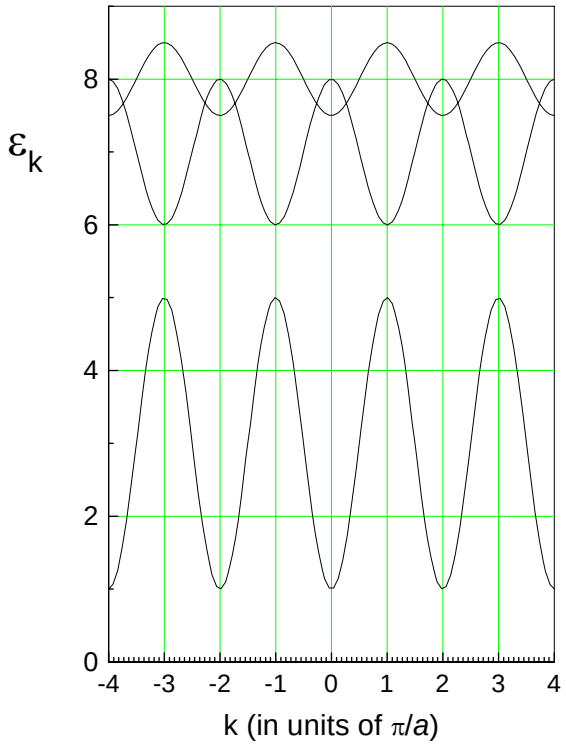


Fig. III.7: Energy bands originating from three different atomic energy levels. Each band contains N Bloch states. Note that the widths of the various bands are different as the overlap integrals depend on the spatial extent of the atomic wave functions $\phi_n(x)$.

III.5 The ground state

So far we have only considered **one** electron in the potential set up by N positive ions. The ground state of the N-electron system is obtained by simply filling all the one-electron levels, starting from the bottom of the lowest band and taking into account Pauli's principle. The occupancy probability of a Bloch state is given by the Fermi-Dirac distribution function shown in Fig. III.8.

$$f(\varepsilon) = \frac{1}{e^{((\varepsilon-\mu)/kT)}+1} \qquad \text{(III.25}$$

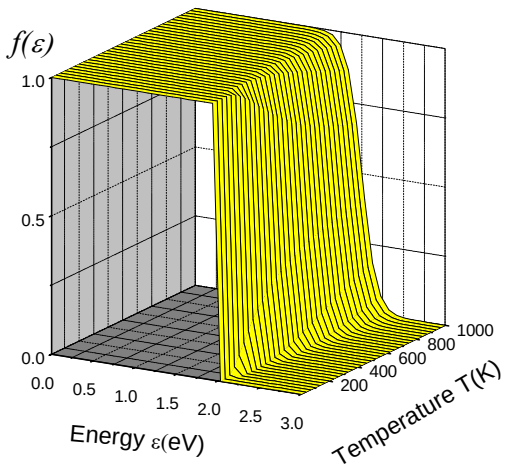


Fig. III.8: Fermi-Dirac distribution function for temperatures between 0 and 1000 K. For this example the chemical potential μ, the Fermi energy, is taken equal to 2 eV.

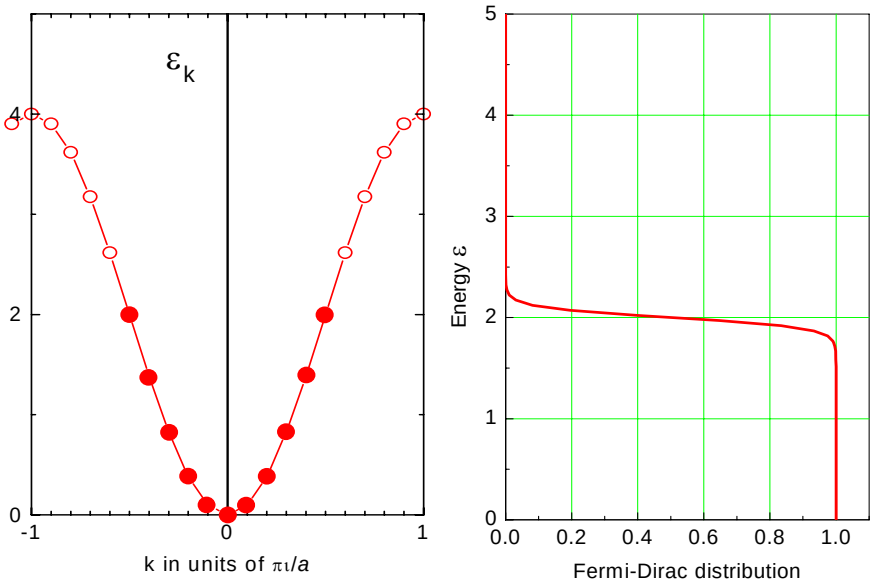


Fig. III.9: The ground state of the linear chain of hydrogen atoms. The degree of occupation of states (per spin) is given by the Fermi-Dirac function $f(\varepsilon)$. The Fermi energy E_F is set equal to 2 in this example.

Depending on the number of electrons per atom (until now we talked only about hydrogen with one electron per atom, but in all other elements we have more electrons), the energy of the highest occupied state may fall "within" a band or "between" two bands. The reason for this is simple. As seen above, there are N different k-values allowed by the periodic boundary conditions in a Brillouin zone. For each k-value within a given band n there are two states depending on the sign of the spin of the electrons. Each (nk)-state can thus accommodate at most two electrons in accordance with the Pauli principle (do not forget electrons have S = ½ and are consequently fermions). Each band provides space for $2N$ electrons (see Fig. III.9).

We consider now the following cases:

a) Hydrogen has one electron per atom. In a chain of N hydrogen atoms there are N electrons and consequently the lowest energy band is half-filled.

b) Lithium has two electrons in a 1s state and one in a 2s state. The lowest energy band is thus full while the second energy band is half-filled.

c) Helium has two electrons in a 1s-level; the corresponding energy band is thus full.

d) Aluminium has the electronic structure $1s^2 2s^2 2p^6 3s^2 3p$. The 1s, 2s and 2p-levels are so strongly localised near the nucleus, that the electrons cannot tunnel from one atom to the other. These are deep core levels. The only states with significant overlaps are the 3s and 3p levels. In these three elements, one can fill one band and half-fill the next one.

Lithium and aluminium are metals, while helium is an insulator. Under very high pressure, it is believed that hydrogen becomes metallic. These few examples suggest that there might be a relation between the metallic state and an uneven number of electrons.

IV CRYSTAL STRUCTURE

The suggestion given at the end of Chapter III can, however, not been drawn from our simple 1D-models since solids are obviously three dimensional objects with a highly organised atomic structure. This is evident from the photographs in Fig. IV.1.



Fig. IV.1: Natural crystals of pyrite (FeS_2) and quartz (SiO_2)

Pyrite and quartz are no exceptions. In fact most minerals have a very precise crystal structure. Much less evident is that all metals, on a sufficiently small scale are also crystalline. The macroscopic morphology of metals is, however, not representative of their intimate crystalline structure because of their great malleability, which makes it possible to shape them in virtually any form. The test of crystallinity is possible with X-rays or neutrons. As we shall see in Chapter VI a regular arrangement of ions leads to constructive interference patterns for scattered X-rays or neutrons which can easily be measured.

Beside crystalline solids there is a vast class of materials that are amorphous (e.g. polymers, liquids, etc.). Even metals can be made amorphous under certain extreme conditions. For example if molten alloys of zirconium and nickel, or palladium and silicon are solidified at a rate of ~ 10^6 degrees per second, the constituting atoms do not have time to form a regular lattice and they freeze into a solid without translation invariance. These amorphous metals, which are called **metallic glasses**, have very interesting elastic and magnetic properties. The theory of disordered systems is, however, difficult and for the time being, we shall therefore restrict our approach to perfectly ordered solids.

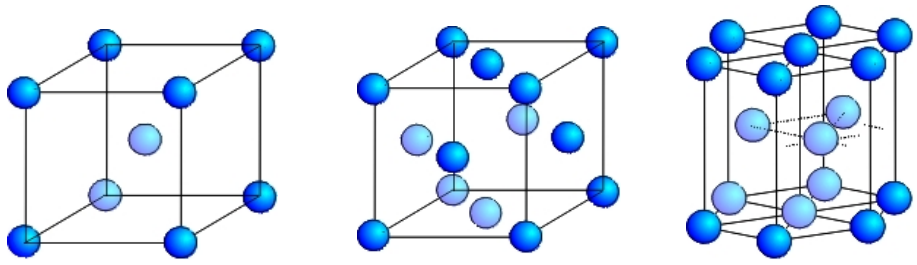


Fig. IV.2: Three common crystal structures of elements (BCC, FCC and HCP). For example, aluminium and copper crystallize in a face-centred cubic (FCC) structure, iron, niobium and chromium in a body-centred-cubic (BCC) structure and magnesium in a hexagonal-close-packed (HCP) structure.

IV.1 Bravais lattices and primitive cells

To introduce the concept of Bravais lattice let us consider the two-dimensional carpet in Fig. IV.3 . It is a periodic arrangement of building blocks, called **primitive cells.** There is no unique way to define a primitive cell as is evident from Fig. IV.4, which shows several possible primitive cells of the carpet in Fig. IV.3. Although the primitive cells are not uniquely defined their pilling up to form the carpet is uniquely defined. To see that, just choose a certain representative point of the primitive cells. These points form the regular lattice shown in Fig. IV.5.

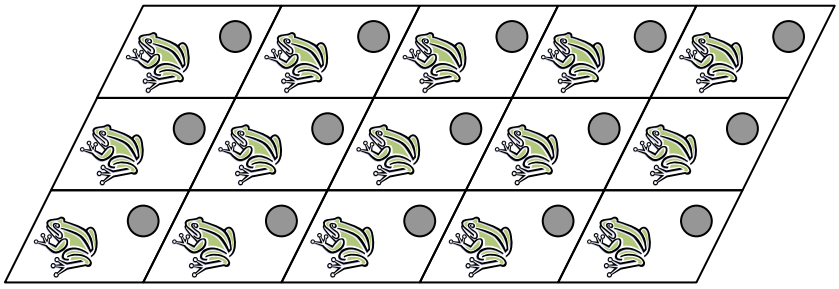


Fig. IV.3: A two dimensional carpet

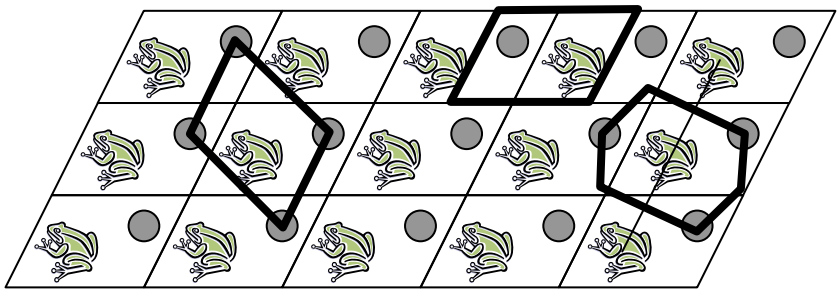


Fig. IV.4: Several primitive cells of the carpet shown in **Fig. IV.3**.

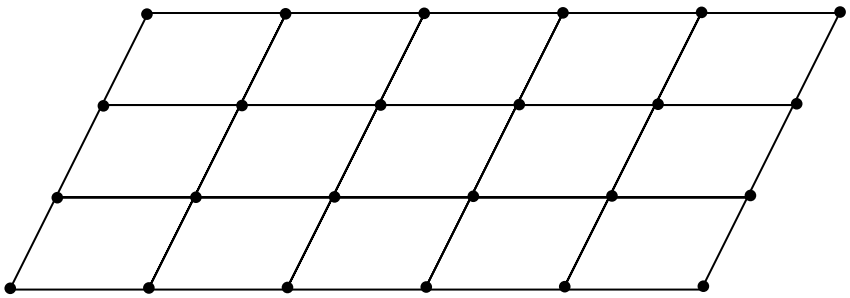


Fig. IV.5: Bravais lattice of the carpet in **Fig. IV.3**.

This lattice is called the **Bravais lattice**. It is spanned by the two primitive vectors $\mathbf{a}_1$ and $\mathbf{a}_2$ and the position vector $\mathbf{R}$ of each point of the lattice can be written as

$$\mathbf{R} = n_1\mathbf{a}_1 + n_2\mathbf{a}_2 \qquad (\text{IV.1}$$

In three dimensions we would have

$$\mathbf{R} = n_1\mathbf{a}_1 + n_2\mathbf{a}_2 + n_3\mathbf{a}_3 \qquad (\text{IV.2}$$

where n_i are integers. Here too we have to note that the choice of primitive vectors is not unique. Several possible choices are indicated in Fig. IV.6.

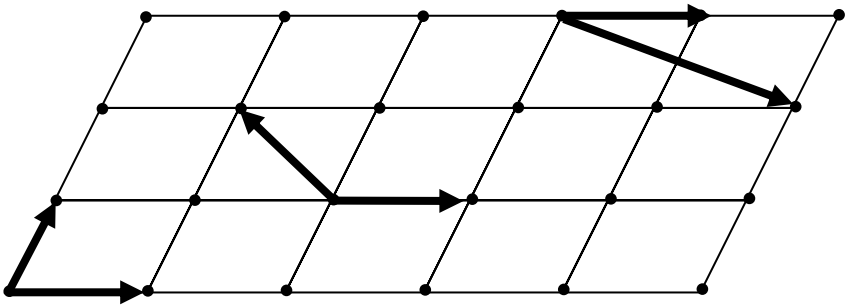


Fig. IV.6: Some possible choices of pairs of primitive vectors for the Bravais lattice in **Fig. IV.5**.

Some sets of primitive vectors are, however, more appropriate than others. In three dimensions there are only 14 different Bravais lattices. They are indicated in Fig. IV.7.

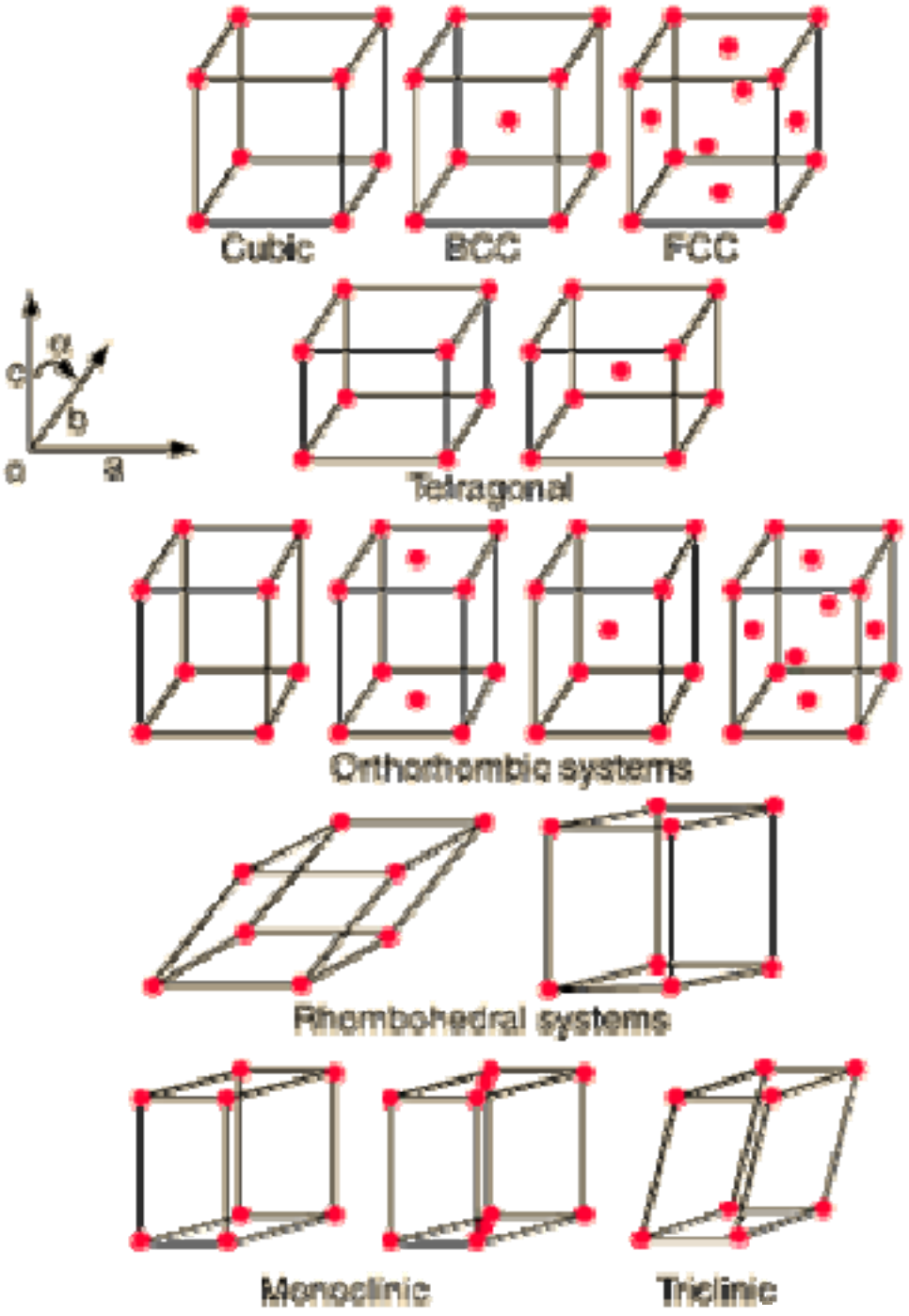


Fig. IV.7: The 14 Bravais lattices. For the cubic, tetragonal and orthorhombic lattices all the angles are 90°. In the monoclinic lattices only two of the angles at a given corner are 90°.

IV.2 Crystal structure of the elements

Most elements crystallize in relatively simple structures, such as the face-centred or body-centred cubic structure and the hexagonal closed-packed structure.

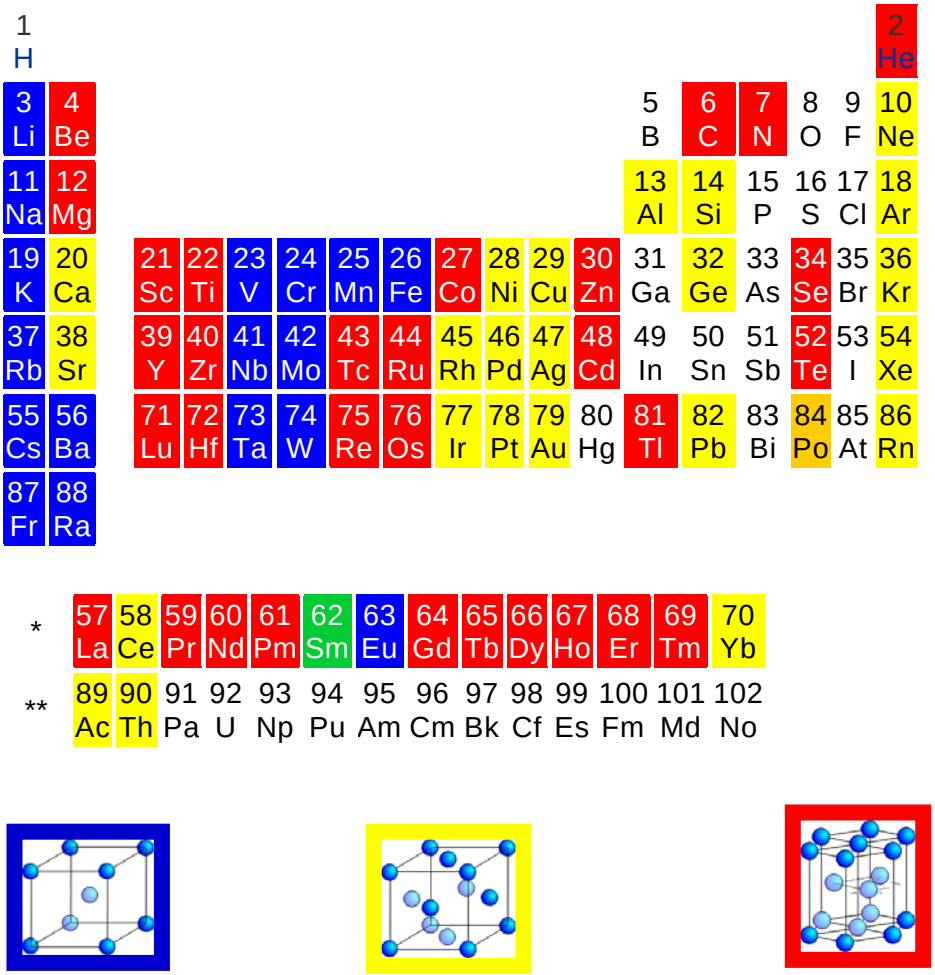


Fig. IV.8: Most of the elements crystallize in a BCC, FCC or HCP structure.

IV.2.1 Body-centered cubic structure (BCC)

Alkali metals, barium, transition metals such as V, Nb, Ta, Cr, Mo, W, Fe and some rare-earths crystallize in the structure shown in Fig. IV.10. To emphasize the cubic underlying structure one usually represents not only the **primitive unit cell** but also the **conventional unit cell** (normally called the unit cell).



Fig. IV.9: The atomium in Brussels represents the BCC lattice of iron (Fe).

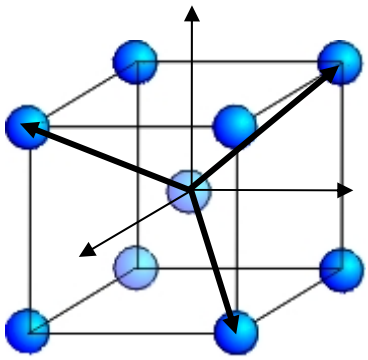


Fig. IV.10: Body centered cubic structure. The three vectors $\mathbf{a}_1$, $\mathbf{a}_2$, $\mathbf{a}_3$ span the primitive cell. The thin arrows indicate the *x, y* and *z*-axes.

The primitive translation vectors are

$$\mathbf{a}_1 = \frac{a}{2}\left(-\hat{\mathbf{x}}+\hat{\mathbf{y}}+\hat{\mathbf{z}}\right)$$
$$\mathbf{a}_2 = \frac{a}{2}\left(+\hat{\mathbf{x}}-\hat{\mathbf{y}}+\hat{\mathbf{z}}\right) \qquad \text{(IV.3}$$
$$\mathbf{a}_3 = \frac{a}{2}\left(+\hat{\mathbf{x}}+\hat{\mathbf{y}}-\hat{\mathbf{z}}\right)$$

where a is the lattice spacing $\hat{\mathbf{x}}, \hat{\mathbf{y}}$ and $\hat{\mathbf{z}}$ are unit vectors in the *x, y* and *z*-directions, respectively. The primitive cell contains exactly <u>one atom</u> while the cubic unit cell contains <u>two</u> (one at the center and 8 which belong only for 1/8 to the unit cell).

The BCC lattice gives us also the opportunity to see that the same arrangement of atoms (see Fig. IV.11) can be described in two different ways. One is simply the structure spanned by the three vectors $\mathbf{a}_1$, $\mathbf{a}_2$, $\mathbf{a}_3$. The other possibility is to take the BCC unit cell (not the primitive cell) as building block and pile these blocks up. The corresponding Bravais lattice is then simple cubic. The building block is more complicated (it contains 2 atoms), but the corresponding Bravais lattice is simpler. A building block with more than 1 atom is called a **unit cell with a basis**. The position of each atom in the building

block needs then to be specified.

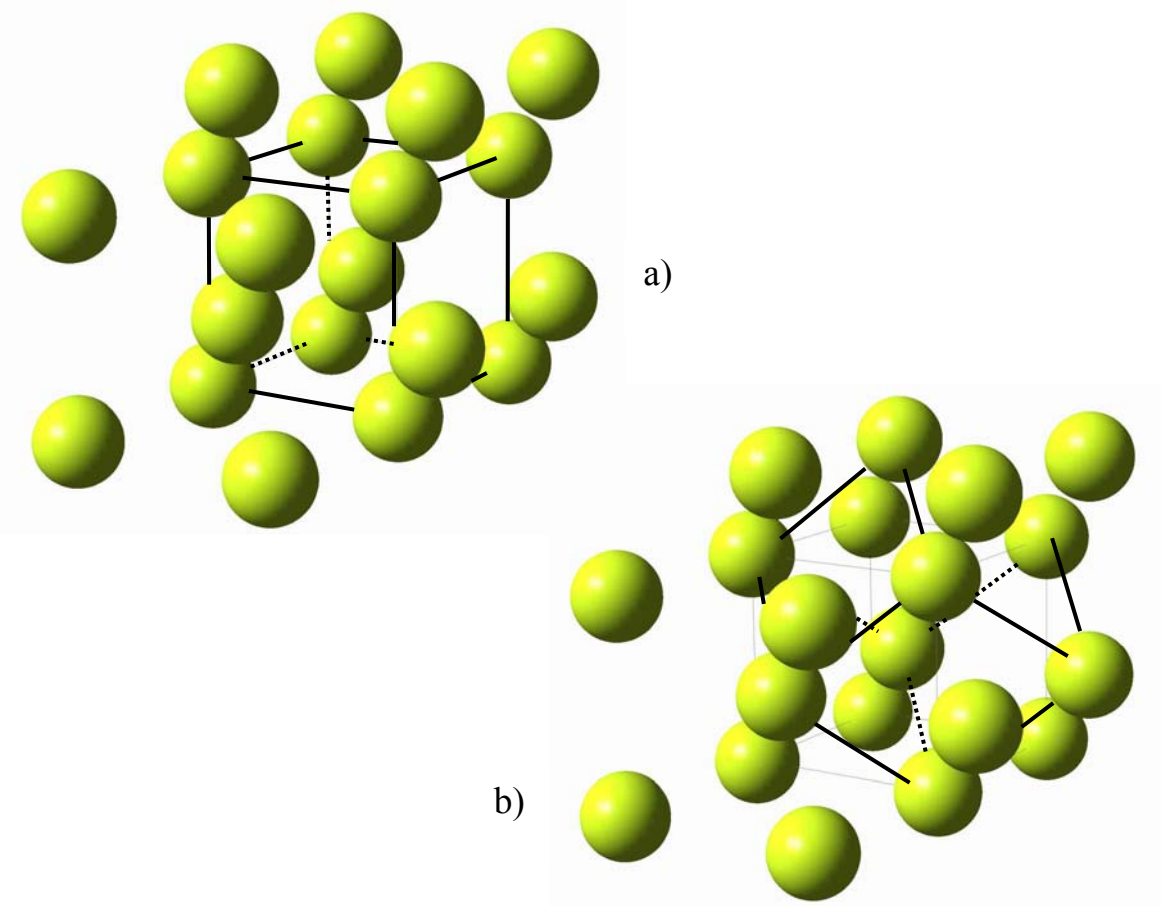


Fig. IV.11: The BCC-lattice structure can be constructed in two different ways:
a) BCC unit cells with **2** atoms per unit cell piled up on a simple cubic Bravais lattice
b) BCC primitive cells, each containing **one** atom, piled up on a BCC Bravais lattice

IV.2.2 Face centred cubic structure (FCC)

Elements that crystallize in this structure are for example calcium, strontium, copper, silicon, gold, aluminium and some transition metals such as Ni, Pd, Pt, Rb and Ir. Here again it is usual matter to consider the cubic unit cell rather than the primitive cell. Both are indicated in Fig. IV.12.

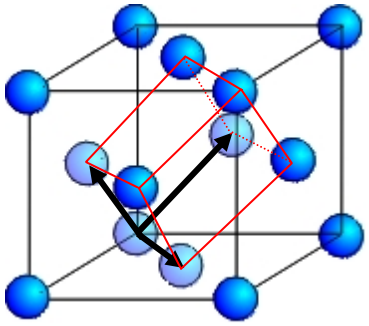


Fig. IV.12: Primitive (*red*) and cubic unit cell *(blue)* of the face centred cubic (FCC) crystal structure.

The three primitive vectors are

$$\mathbf{a}_1 = \frac{a}{2}(\hat{\mathbf{x}} + \hat{\mathbf{y}})$$
$$\mathbf{a}_2 = \frac{a}{2}(\hat{\mathbf{y}} + \hat{\mathbf{z}}) \qquad (\text{IV.4}$$
$$\mathbf{a}_3 = \frac{a}{2}(\hat{\mathbf{x}} + \hat{\mathbf{z}})$$

IV.2.3 Hexagonal close-packed structure (HCP)

Be, Mg, Cd, Ti, Zr, Hf, Re and many rare-earths (La, Pr, Gd, ...Lu) crystallize in the hexagonal structure shown in Fig. IV.13. It is not a Bravais lattice because it is not possible to find three primitive vectors $\mathbf{a}_1$, $\mathbf{a}_2$, $\mathbf{a}_3$ such that the position vector of all atoms can be written in the form of Eq.IV.2. The primitive cell contains two atoms and is thus a primitive cell with basis. Once the building block has been defined one sees that the total lattice is obtained by piling up primitive cells on the simple hexagonal Bravais lattice shown in Fig. IV.7

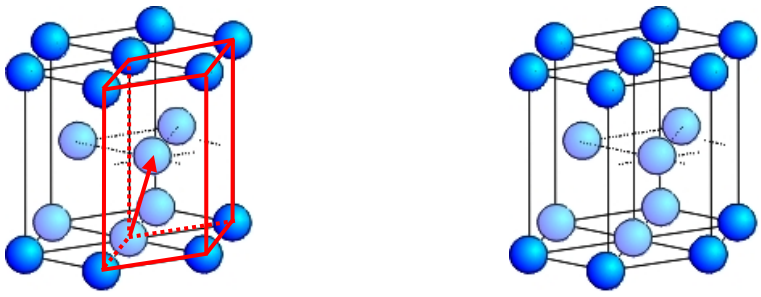


Fig. IV.13: Primitive cell (with basis) and unit cell of the hexagonal close-packed structure.

Both the HCP and FCC structures correspond to a close-packed arrangement of rigid balls. For the hexagonal arrangement the value of the lattice spacing *c* along the z-axis must then satisfy the following relation

$$c = \sqrt{\frac{8}{3}}a \;=\sim 1.633a \qquad (\text{IV.5}$$

For many elements, *c/a* is close, but not equal, to this ideal value

IV.2.4 Diamond structure

Diamond is the hardest material known presently. Other elements with the diamond structure are Silicon, Germanium and gray-tin. This structure can be viewed as consisting of a FCC-lattice with 4 extra atoms at position (a/4)(1,1,1), (a/4)((3,3,1), (a/4)((3,1,3), and (a/4)((1,3,3). The diamond structure is not a Bravais lattice.

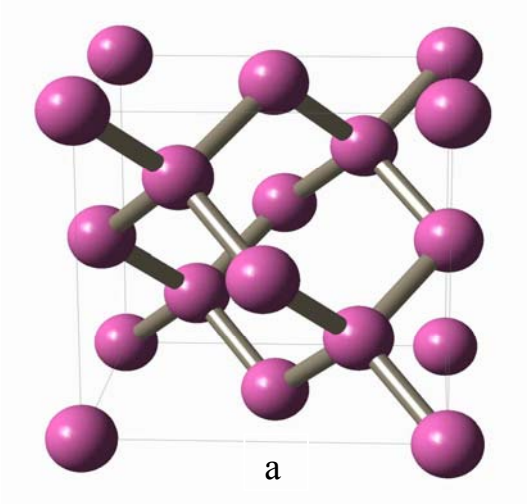
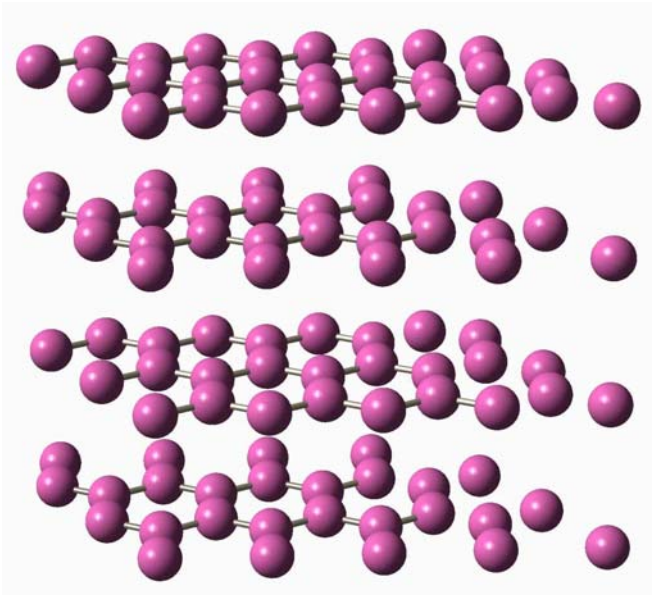




Fig. IV.14: Conventional unit cell of the diamond structure.

Graphite, which consists of the same carbon atom as diamond crystallizes in a simple hexagonal structure and is much softer, because the hexagonal planes can easily slide with respect to each other (this is the reason why pencils work).



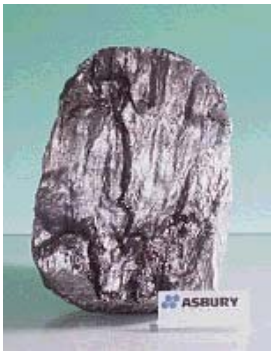


Fig. IV.15: The hexagonal planes of the crystal structure of graphite. Recently great interest has developed for grapheme, a material consisting of only **one** hexagonal plane of carbon atoms.

IV.2.5 Density of materials

So far we have only looked at the geometry of the regular arrangement of atoms in crystal structures. It is useful, in the light of our calculations of the band structures of solids (see for example Section III.4) to look at the actual value of typical interatomic separations in solids.

In the BCC-structure the smallest interatomic separation is $d = \sqrt{3}a/2 \cong 0.87a$. In Table IV.1 we indicate values of d for the BCC elements. For FCC metals $d = a/\sqrt{2} \cong 0.71a$ and one obtains the values indicated in Table IV.2.

Table IV.1: Smallest interatomic distance for BCC-elements (in Ångstroms = 10^{-10} m)

Ba	4.35	Li	3.02	Ta	2.87
Cr	2.49	Mo	2.73	Tl	3.36
Cs	5.24	Na	3.66	V	2.62
Fe	2.49	Nb	2.86	W	2.74
K	4.53	Rb	4.84		

Table IV.2: Smallest interatomic distance for FCC-elements (in Ångstrom).

Ag	2.89	Cu	2.55	Pt	2.77
Al	2.86	Ir	2.72	Rh	2.69
Au	2.88	La	3.75	Sc	3.21
Ca	3.95	Ni	2.49	Sr	4.30
Ce	3.65	Pb	3.50	Th	3.59
Co	2.51	Pd	2.75	Yb	3.88

These two tables show that neighbouring elements in the Periodic System have comparable values for d. Consider for example Fe (BCC, a = 2.87 Å) and Co (FCC, a = 3.55 Å) and Ni (FCC, a = 3.52 Å). The nearest-neighbour separation d is almost equal for all three elements.

Another point is that all transition metals have relatively small d-values. This is a direct influence of the d-electrons in these metals.

In our treatment of the H_2-molecule, as well as that of the linear chain of atoms, we discovered that tunneling of electrons from atom to atom contributed in lowering the total energy of the system. An important parameter in this context was the overlap integral t. In order to have a sizeable t it is necessary that the spatial extension of the wave functions of states near the Fermi energy is comparable to the interatomic spacing d. A way to estimate the extent of a wave function is to look at the so-called **radial probability density** $|rR(r)|^2$, where $R(r)$ is the solution of the radial part of the Schrödinger equation. The spatial extent of these densities is in all cases of the order several Ångstroms (see Fig. IV.16). This leads to overlap integral values t (see

Eq.III.22) of the order of 1 eV.

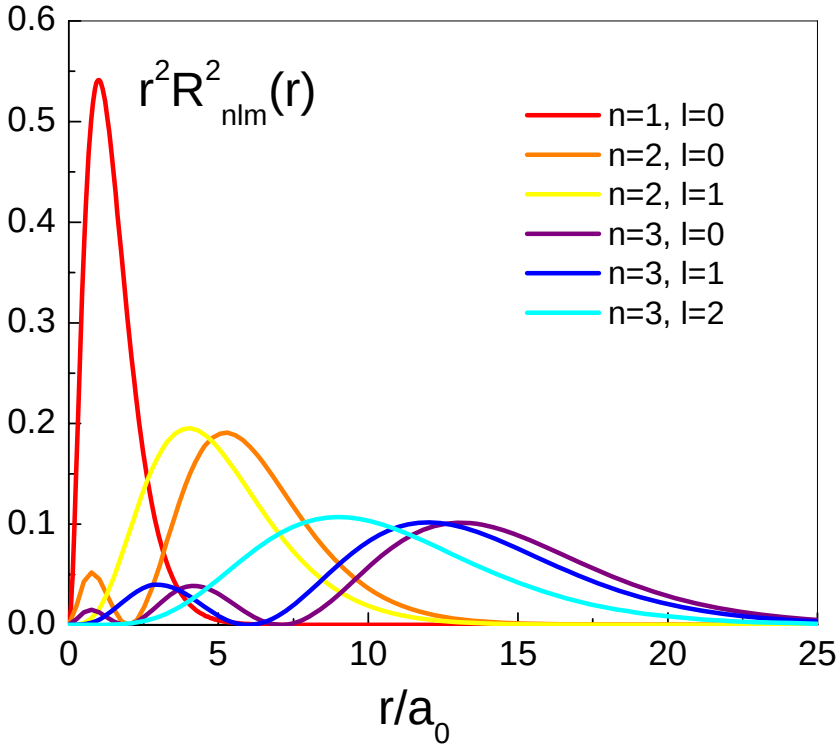


Fig. IV.16. Radial probability density $|rR(r)|^2$ of various states of the hydrogen atom (r is given in units of the Bohr radius a_0 = 0.5291 Å).

V THE RECIPROCAL LATTICE AND THE BRILLOUIN ZONE

In one dimension we arrived at the conclusion that the solutions $\psi_k(x)$ of Schrödinger's equation for an electron in a periodic potential $V(x)$ satisfied Bloch's theorem, i.e.

$$\psi_k(x) = e^{ikx} u_k(x) \qquad (V.1$$

where $u_k(x)$ is a periodic function or, what is equivalent, that

$$\psi_k(x + na) = e^{ikna} \psi_k(x) \qquad (V.2$$

for all integer values of n.

V.1 Bloch theorem in three dimensions

The generalization of Bloch's theorem to three dimensions is evident. Without demonstration, we indicate that

$$\psi_{\mathbf{k}}(\mathbf{r}) = e^{i\mathbf{k}.\mathbf{r}} u_{\mathbf{k}}(\mathbf{r}) \qquad (V.3$$

with $u_{\mathbf{k}}(\mathbf{r})$ a periodic function, or equivalently, that

$$\psi_{\mathbf{k}}(\mathbf{r} + \mathbf{R}) = e^{i\mathbf{k}.\mathbf{R}} \psi_{\mathbf{k}}(\mathbf{r}) \qquad (V.4$$

correspond to Eqs. V.1 and V.2, respectively. The quantum number k is replaced by a triple of quantum numbers (k_1, k_2, k_3) written as the vector **k** and **R** is any vector of the Bravais lattice, i.e.

$$\mathbf{R} = n_1\mathbf{a}_1 + n_2\mathbf{a}_2 + n_3\mathbf{a}_3 \qquad (V.5$$

V.2 The reciprocal lattice

In one dimension we had also found that the ambiguity in the definition of k led to the conclusion that the energy bands were periodic in k and that a finite domain of the k-axis (e.g. $-\pi/a \leq x \leq \pi/a$), the so-called **Brillouin zone**, was sufficient to specify ε_k entirely.
In three dimensions, one expects a similar situation, although probably more complicated. In analogy with the 1-dimensional case we look for vectors **G** such that

$$e^{i\mathbf{G}.\mathbf{R}} = 1 \qquad (V.6$$

for al vectors **R**. Once these vectors **G** are determined we will know that all states with wave vectors **k**' such that

$$\mathbf{k}' = \mathbf{k} + \mathbf{G} \qquad (V.7$$

are equivalent. So, what are the vectors **G**? They obviously must satisfy

$$\mathbf{G} \cdot \mathbf{R} = 2\pi n \qquad (V.8$$

where n is an integer. Writing

$$\mathbf{G} = q_1\,\mathbf{b}_1 + q_2\,\mathbf{b}_2 + q_3\,\mathbf{b}_3 \qquad (V.9$$

where $\mathbf{b}_i$ are yet unknown vectors it follows from Eqs. V.5, V.8 and V.9 that

$$(q_1\,\mathbf{b}_1 + q_2\mathbf{b}_2 + q_3\,\mathbf{b}_3) \cdot (n_1\mathbf{a}_1 + n_2\mathbf{a}_2 + n_3\mathbf{a}_3) = 2\pi n \qquad (V.10$$

This product contains nine terms and is in general not easily handled. One might thus, for practical reasons, wonder whether or not it would be possible to define the $\mathbf{b}_i$-vectors in such a way that

$$\mathbf{b}_i \cdot \mathbf{a}_j = 2\pi\delta_{ij} \qquad \text{for } i, j : 1,2,3 \qquad (V.11$$

where $\delta_{ij} = 0$ if $i \neq j$ and $\delta_{ii} = 1$. The factor 2π in Eq. V.11 is in fact completely arbitrary. However, by comparison with Eq. V.10 it is evident that inclusion 2π in Eq. V.11 "might" (we have not shown yet that V.11 is possible!) lead to integer values for the q_i's.
Consider now one of the vectors $\mathbf{b}_i$, say $\mathbf{b}_1$. According to Eq. V.11 it must be orthogonal to two $\mathbf{a}_i$ vectors, say $\mathbf{a}_2$ and $\mathbf{a}_3$. This implies that it must be parallel to $\mathbf{a}_2 \times \mathbf{a}_3$, i.e.

$$\mathbf{b}_1 = \alpha\mathbf{a}_2 \times \mathbf{a}_3 \qquad (V.12$$

However, from Eq. V.11 we must have

$$\mathbf{a}_1 \cdot \mathbf{b}_1 = 2\pi = \alpha\,\mathbf{a}_1 \cdot (\mathbf{a}_2 \times \mathbf{a}_3) \qquad (V.13$$

Consequently

$$\mathbf{b}_1 = 2\pi \frac{\mathbf{a}_2 \times \mathbf{a}_3}{\mathbf{a}_1 \cdot (\mathbf{a}_2 \times \mathbf{a}_3)} \qquad (V.14$$

and, similarly,

$$\mathbf{b}_2 = 2\pi \frac{\mathbf{a}_3 \times \mathbf{a}_1}{\mathbf{a}_1 \cdot (\mathbf{a}_2 \times \mathbf{a}_3)} \qquad (V.15$$

$$\mathbf{b}_3 = 2\pi \frac{\mathbf{a}_1 \times \mathbf{a}_2}{\mathbf{a}_1 \cdot (\mathbf{a}_2 \times \mathbf{a}_3)} \qquad (V.16$$

Herewith we have proven that three vectors $\mathbf{b}_1$, $\mathbf{b}_2$ and $\mathbf{b}_3$ can be constructed with the property V.11. For these vectors we find that Eq. V.10 is automatically satisfied. The space spanned by the reciprocal primitive lattice vectors $\mathbf{b}_1$ is called the **reciprocal lattice.**

Before exploring the reciprocal lattice let us come back to the 1-dimensional case considered in Chapter III. For this we take $\mathbf{a}_1$ = (a, 0, 0), $\mathbf{a}_2$ = (0, a, 0) and $\mathbf{a}_3$ = (0, 0, a). The last two vectors do not play any physical role but we need them to specialize Eqs. V.14 to 16 to the case of a linear solid. Then

$$\begin{aligned} \mathbf{b}_1 &= \frac{2\pi}{\mathrm{a}}(1,0,0) \\ \mathbf{b}_2 &= \frac{2\pi}{\mathrm{a}}(0,1,0) \\ \mathbf{b}_3 &= \frac{2\pi}{\mathrm{a}}(0,0,1) \end{aligned} \qquad (V.17$$

Since only one direction is relevant, say $\mathbf{b}_1$, the reciprocal lattice vectors **G** are then of the form

$$\mathbf{G} = \frac{2\pi}{\mathrm{a}} n(1,0,0) \qquad (V.18$$

This is exactly the periodicity of ε_k curves and $-\mathbf{G}/2$ and $+\mathbf{G}/2$ correspond to $-\pi/a$ and $+\pi/a$, the boundaries of the Brillouin zone. We now focus our attention on the reciprocal lattice of the FCC and BCC-crystal structures described in chapter IV.

V.2.1 Reciprocal lattice of the BCC-structure

From the definition of the primitive lattice vectors $\mathbf{a}_i$ in Eq.IV.3 and the definitions in Eqs. V.14 to 16 we calculate,

$$\begin{aligned} \mathbf{b}_1 &= \tfrac{2\pi}{a}\left(\hat{\mathbf{y}} + \hat{\mathbf{z}}\right) \\ \mathbf{b}_2 &= \tfrac{2\pi}{a}\left(\hat{\mathbf{x}} + \hat{\mathbf{z}}\right) \\ \mathbf{b}_3 &= \tfrac{2\pi}{a}\left(\hat{\mathbf{x}} + \hat{\mathbf{y}}\right) \end{aligned} \qquad (V.19$$

Here we find that the reciprocal lattice of the BCC-crystal structure is a FCC-lattice.

Note however that in real space the traditional unit cell of the BCC crystal structure has a side length a. That of the FCC reciprocal lattice is $4\pi/a$ (compare Eqs. V.19 to Eqs. IV.4).

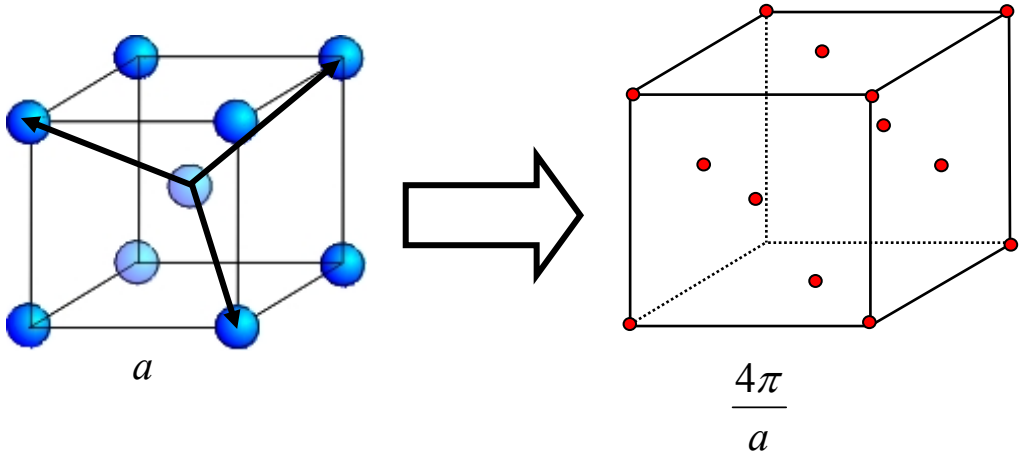


Fig. V.1: The reciprocal lattice of the BCC-structure is a FCC-lattice.

V.2.2 Reciprocal lattice of the FCC-structure

From the definition of the primitive lattice vectors $\mathbf{a}_i$ given in Eq. IV.4 and the definitions in Eqs. V.14 to 16, we find

$$\begin{aligned}\mathbf{b}_1 &= \tfrac{2\pi}{a}\left(-\hat{\mathbf{x}}+\hat{\mathbf{y}}+\hat{\mathbf{z}}\right)\\ \mathbf{b}_2 &= \tfrac{2\pi}{a}\left(+\hat{\mathbf{x}}-\hat{\mathbf{y}}+\hat{\mathbf{z}}\right)\\ \mathbf{b}_3 &= \tfrac{2\pi}{a}\left(+\hat{\mathbf{x}}+\hat{\mathbf{y}}-\hat{\mathbf{z}}\right)\end{aligned} \qquad \text{(V.20}$$

These vectors have exactly the same form as the primitive vectors of the BCC-lattice. The only replacement is a/2 → 2π/a. In other words the reciprocal lattice of the FCC-structure is a BCC-lattice with a cube dimension equal to 4π/a.

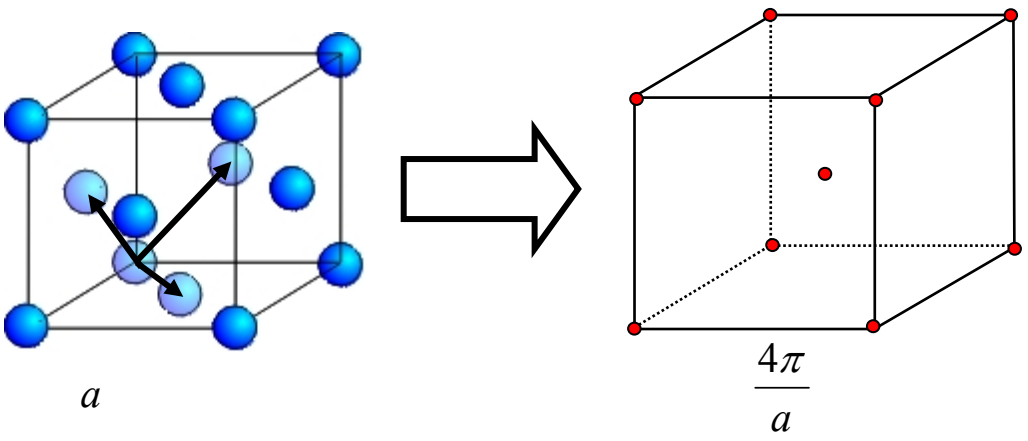


Fig. V.2: The reciprocal lattice of the FCC-crystal structure is a BCC-lattice.

V.3 The Brillouin zone

In the reciprocal space (spanned by the vectors $\mathbf{b}_i$) we have the same freedom as in the direct lattice (spanned by the $\mathbf{a}_j$ vectors) for the choice of a primitive unit cell. One could, for example, choose the same type of primitive unit cells as those shown in Fig. IV.4. In the reciprocal space, however, it is much more judicious to use another primitive unit cell. Our choice is essentially dictated by the following physical considerations.

Consider, for example, the special case of an electron in an infinitely weak periodic potential. Bloch's theorem is still valid and the equivalence of states $\psi_{\mathbf{k}}$ and $\psi_{\mathbf{k}-\mathbf{G}}$ where **G** is any reciprocal lattice vector, implies that

$$\varepsilon_{\mathbf{k}-\mathbf{G}} = \varepsilon_{\mathbf{k}} \qquad (\text{V.21}$$

However, since the electron is a "free" electron (i.e. $\varepsilon_{\mathbf{k}} = \frac{\hbar^2 |\mathbf{k}|^2}{2m}$) Eq.V.21 implies that

$$|\mathbf{k} - \mathbf{G}| = |\mathbf{k}| \qquad (\text{V.22}$$

Equation V.22 has a simple geometric interpretation. It implies that the **k**- and **k-G** vectors are as indicated in Fig. V.3.

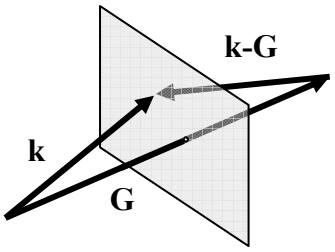


Fig. V.3: Locus of all the points that satisfy condition (V.22), the so-called Bragg condition.

The smallest volume of reciprocal space defined by all the planes obeying Eq. V.22 is called the **Brillouin zone of the reciprocal lattice**.

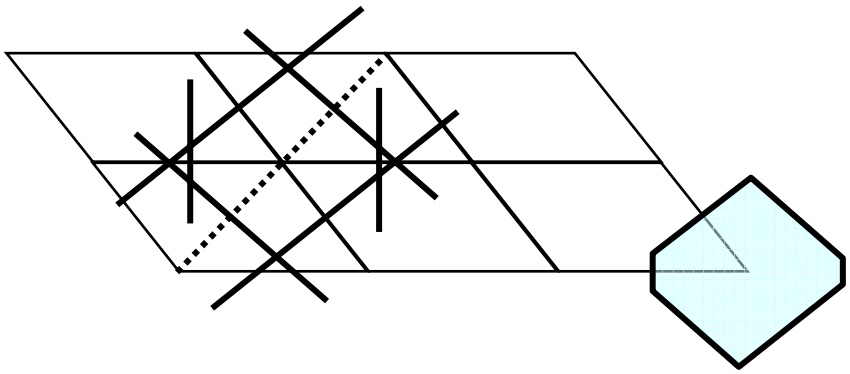
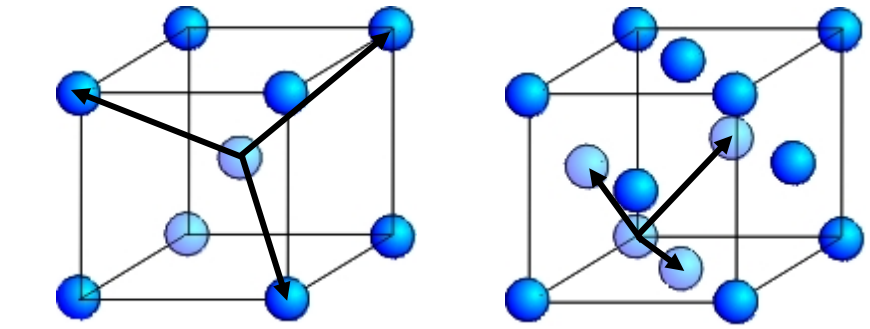
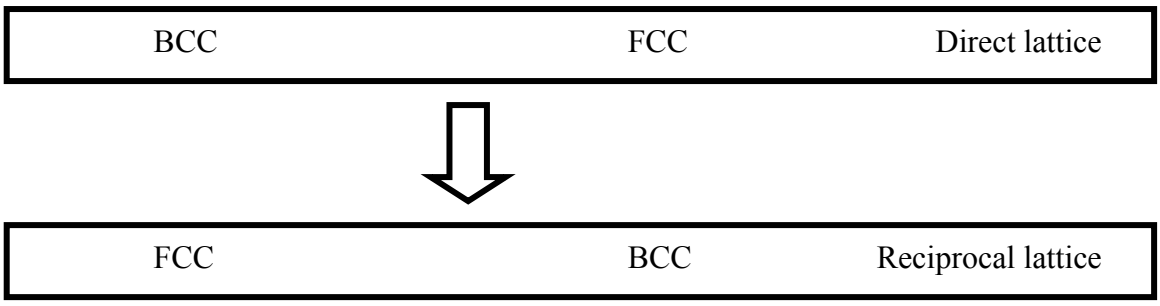


Fig. V.4: The Brillouin zone of a 2-dimensional reciprocal lattice is obtained by constructing the median planes for all the nearest-neighbour lattice vectors.

The Brillouin zone of a two-dimensional lattice is shown in Fig. V.4. In Chapter VI we shall show that condition (Eq.V.22) plays an essential role in the scattering of X-rays and neutrons by a crystal. There it is known as Bragg's condition. There are thus several good, physical reasons to use the Brillouin zone as the most appropriate primitive cell of the reciprocal lattice.
In Fig. V.5 we have drawn the Brillouin zones of the BCC and FCC reciprocal lattice (do not forget these are the reciprocal lattices of the FCC and BCC-structures, respectively).





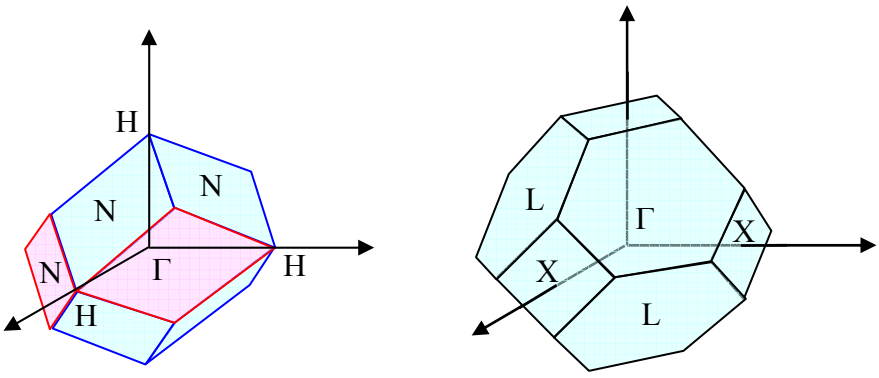


Fig. V.5: *(top panel):* BCC- and FCC-direct crystal lattices. *(bottom panel):* Brillouin zones in the corresponding reciprocal lattices

As it is maybe not obvious how the Brillouin zones in Fig. V.5 have been constructed we indicate below the various steps that have been followed for the specific case of a crystal with a BCC lattice.

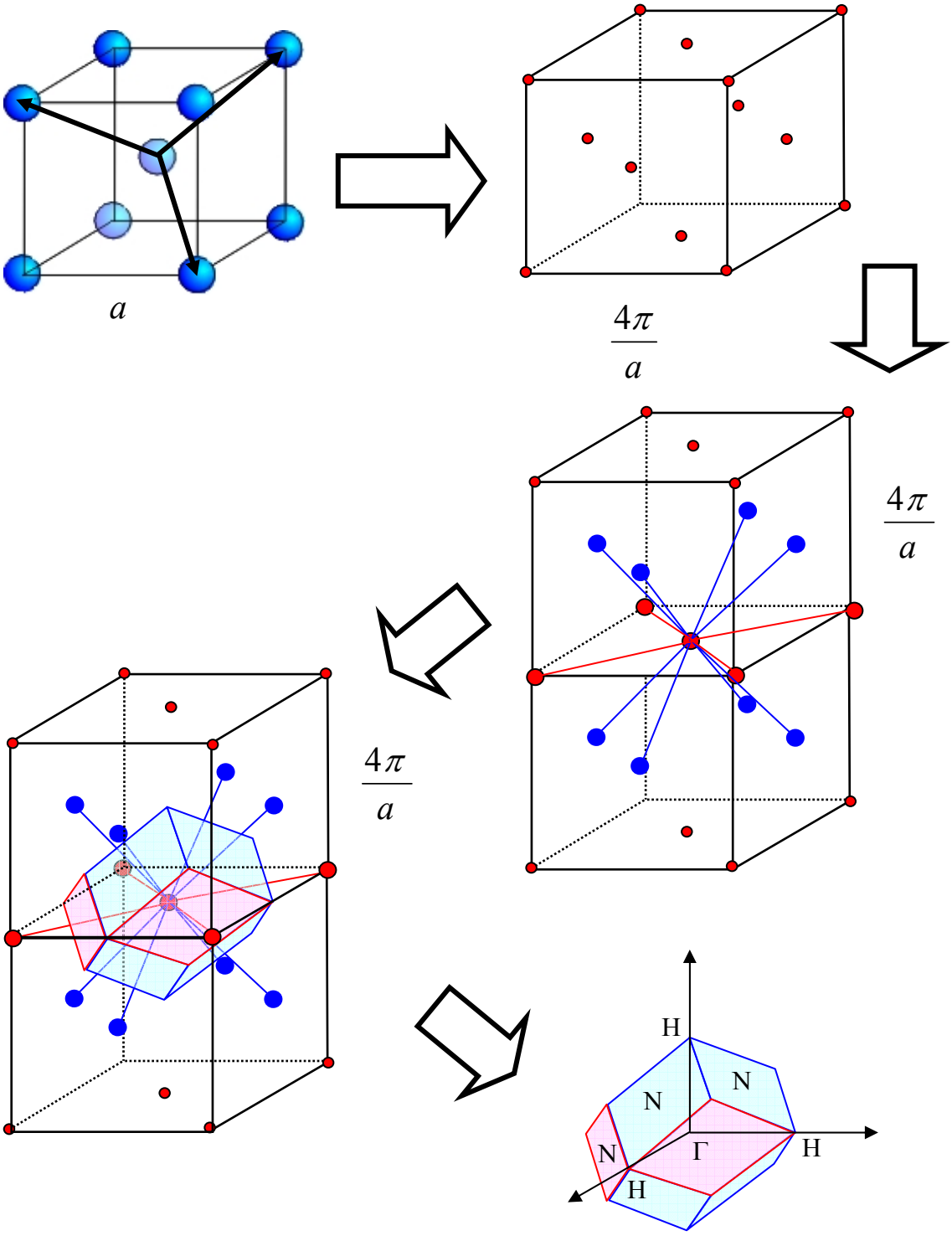


Fig. V.6: The various steps involved in constructing the Brillouin zone of the BCC crystal structure. The twelve faces of the Brillouin zone correspond to the twelve nearest-neighbour points of the FCC reciprocal lattice.

VI X-RAY AND NEUTRON SCATTERING IN SOLIDS

From the photographs in Fig. IV.1 it is obvious that atoms in quartz and pyrite are regularly arranged and form a crystal lattice. For many other materials, in particular for metals, this is far less evident. It is, however, nevertheless possible to determine their intimate crystalline structure by scattering "suitable" particles through them. Any interference effect will be the fingerprint of a regular internal structure on a microscopic scale. By "suitable" we mean particles whose de Broglie wavelength is comparable to typical interatomic distances in order to induce interference phenomena. Furthermore, the particles should not interact strongly with the solid in order to prevent excessive absorption. Two standard suitable particles for scattering experiments are photons and neutrons. We consider these two types of particles in more detail.

For photons to have a wavelength $\lambda = 10^{-10}$ m we need that $\hbar\omega = \hbar c/\lambda \cong 1.8 \times 10^{-15}$ J which corresponds approximately to 1.2×10^{4} eV. Such energetic photons are called X-ray photons. They can be produced by bombarding a target (e.g. copper) with electrons accelerated by several tens of keV.

For neutrons $E = \hbar^2 (2\pi/\lambda)^2/2m$ from which follows that $E \cong 10^{-20}$ J. This means that the energy of such neutrons is remarkably low, less than 1 eV. This is a great advantage since their energy is of the same order of magnitude as that of lattice vibrations (in Chapter X we will see that lattice vibrations have typically energies of the order of 0.03.....0.15 eV). Such neutrons can be obtained by thermalising the neutron beam of a reactor through a moderator.

VI.1 Simple theory of scattering

We consider the situation indicated in Fig. VI.1. The time dependent wave function $\Phi_{\mathbf{k}}$ of the incoming particle (for example, a photon or a neutron) is

$$\Phi_{\mathbf{k}} = Ae^{i\left(\mathbf{k}\cdot\mathbf{r}-\frac{E_{\mathbf{k}}}{\hbar}t\right)} \qquad (\text{VI.1}$$

and that of the scattered particle

$$\Phi_{\mathbf{k}'} = Ae^{i\left(\mathbf{k}'\cdot\mathbf{r}-\frac{E_{\mathbf{k}'}}{\hbar}t\right)} \qquad (\text{VI.2}$$

The probability of scattering the incident particle from its original state $\Phi_{\mathbf{k}}$ to the new state $\Phi_{\mathbf{k}'}$ by a crystal lattice is given by an expression of the form

$$P_{\mathbf{k}\mathbf{k}'} \propto \frac{1}{\hbar^2}\left|\int dt\, \langle \Phi_{\mathbf{k}}|\delta V|\Phi_{\mathbf{k}'}\rangle\right|^2 \qquad (\text{VI.3}$$

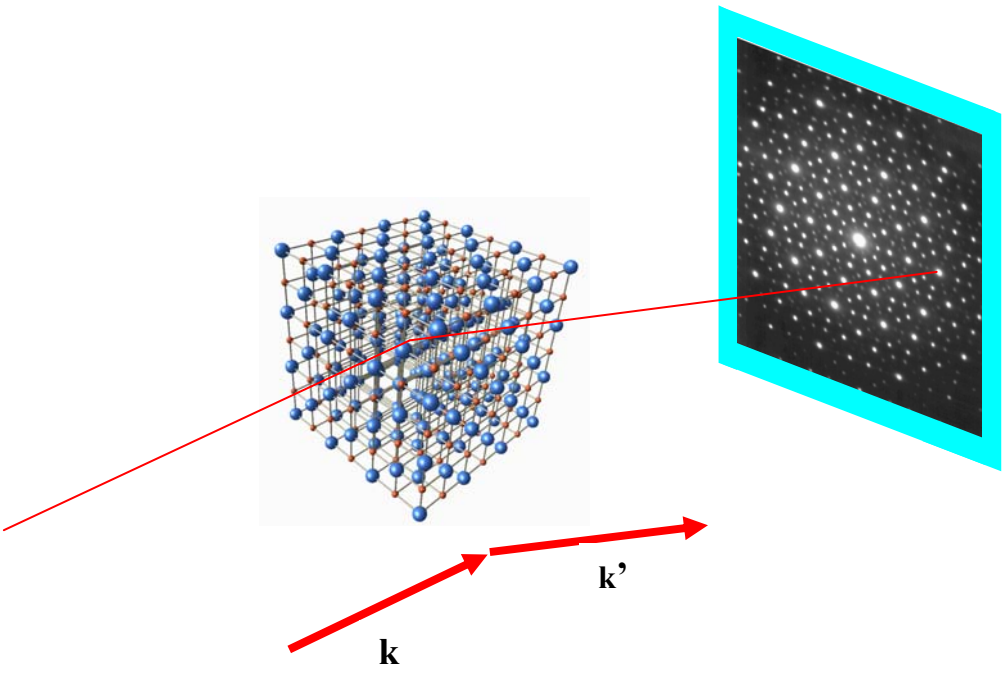


Fig. VI.1: Scattering of a particle by a lattice. The diffraction pattern reflects the periodicity of the lattice.

where δV is the perturbing potential, due to the periodic potential of the lattice. As the atoms in the lattice are always vibrating (they are also quantum particles !) the potential δV is the sum of the periodic potential

$$\delta V_{crystal} = \sum C_{\mathbf{G}} e^{i\mathbf{G}\cdot\mathbf{r}} \qquad \text{(VI.4}$$

where **G** are the reciprocal vectors defined in Section V.2 and the potential δV_{phonon} associated with a lattice vibration with wave vector **q**

$$\delta V_{phonon} = V_0 e^{-i(\mathbf{q}\cdot\mathbf{r}-\omega t)} \qquad \text{(VI.5}$$

The lattice vibrations are quantized and are called phonons (see Section X.4). We need then to evaluate a space and time integral of the form

$$P_{\mathbf{k}\mathbf{k}'} \propto \frac{1}{\hbar^2}\left|\int dt \,\langle \Phi_{\mathbf{k}} \left|\delta V\right| \Phi_{\mathbf{k}'}\rangle\right|^2 \propto$$

$$\propto \left|\sum C_{\mathbf{G}} \left(\int e^{-i\mathbf{k}\mathbf{r}} e^{i\mathbf{G}\mathbf{r}} e^{-i\mathbf{q}\mathbf{r}} e^{i\mathbf{k}'\mathbf{r}} d^3r\right)\left(\int e^{i\left(\frac{E_{\mathbf{k}}}{\hbar}-\frac{E_{\mathbf{k}'}}{\hbar}+\omega\right)t} dt\right)\right|^2 \qquad \text{(VI.6}$$

to calculate the scattering probability $P_{\mathbf{k}\mathbf{k}'}$. The integrals vanish except when

$$\mathbf{k}+\mathbf{q}=\mathbf{k}'+\mathbf{G} \qquad \text{(VI.7}$$

and

$$E_{\mathbf{k}}+\hbar\omega_{phonon}=E_{\mathbf{k}'} \qquad \text{(VI.8}$$

The first equation, which can be re-written as

$$\hbar\mathbf{k}+\hbar\mathbf{q}=\hbar\mathbf{k}'+\hbar\mathbf{G} \qquad \text{(VI.9}$$

means that the total momentum of the system is conserved. Before scattering the sample is at rest and there is a lattice vibration of wave vector **q** (later we will say that there is a phonon of wave vector **q**). The phonon is absorbed in the scattering process and, after scattering the particles has a momentum $\hbar\mathbf{k}'$. The term $\hbar\mathbf{G}$ represents the momentum acquired by the sample as a whole (mechanical momentum transfer) during the scattering process.

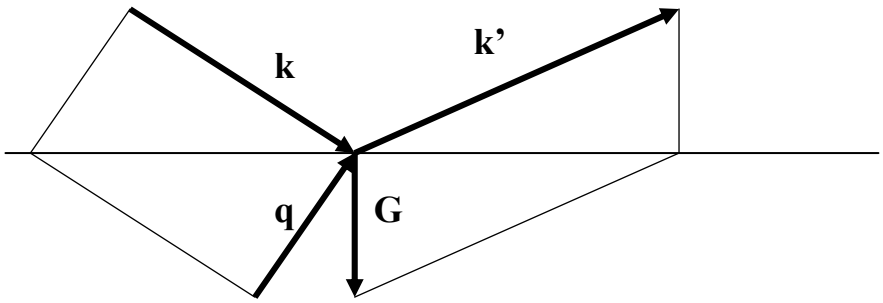


Fig. VI.2: Scattering of particle (neutron of photon) by a crystal in presence of a phonon. The wave vector of the incoming particle is **k**, that of the scattered particle is **k’** and that of the phonon **q**. The reciprocal lattice vector involved in the scattering process is **G**.

The second equation corresponds to conservation of energy. For a photon Eq. VI.8 takes the form

$$\hbar\omega+\hbar\omega_{\text{phonon}}=\hbar\omega' \qquad \text{(VI.10}$$

and for a neutron

$$\frac{\hbar^2\mathrm{k}^2}{2\mathrm{M}}+\hbar\omega_{\text{phonon}}=\frac{\hbar^2\mathrm{k}'^2}{2\mathrm{M}} \qquad \text{(VI.11}$$

On the right hand side of Eqs. VI.8 and 10 there is no energy term corresponding to $\hbar\mathbf{G}$. This is due to the well-known fact that a very light particle can transfer momentum to a heavy one but almost no energy. For a photon or a neutron interacting with a sample with a mass of the order of grams, the energy transfer is thus completely negligible.

So far, we have assumed that the incident particle was scattered by a phonon that induces a perturbing potential

$$\delta V_{phonon} = V_0 e^{-i(\mathbf{qr}-\omega t)} \qquad (\text{VI.12}$$

We could of course also have written

$$\delta V_{phonon} = V_0 e^{+i(\mathbf{qr}-\omega t)} \qquad (\text{VI.13}$$

In the integrals corresponding to Eq. VI.6 the signs of **q** and ω are changed and we find the following conditions for a non-vanishing scattering probability $P_{\mathbf{kk}'}$.

$$\hbar\mathbf{k} = \hbar\mathbf{k}' + \hbar\mathbf{q} + \hbar\mathbf{G} \qquad (\text{VI.14}$$

and

$$E_{\mathbf{k}} = E_{\mathbf{k}'} + \hbar\omega_{phonon} \qquad (\text{VI.15}$$

These two equations can be interpreted as the conservation of momentum and energy in a process where an incoming particle with momentum $\hbar\mathbf{k}$ and energy $E_{\mathbf{k}}$ is scattered to a state with momentum $\hbar\mathbf{k}'$ and energy $E_{\mathbf{k}'}$, after having created a phonon of momentum $\hbar\mathbf{q}$ and energy $\hbar\omega_{\text{phonon}}$. At low temperatures, the number of equilibrium phonons is very small and scattering by existing phonons is rather infrequent.

We consider now two different types of scattering: **elastic** scattering and **inelastic** scattering. By elastic we mean that the scattering process leaves the energy of the scattered particles unchanged. By inelastic we mean the opposite: the energy of the incident particle is different from that of the scattered particle.

VI.2 Elastic scattering

A scattering process is called “elastic” if the energy of the outgoing particle is equal to that of the incoming particle. In this case no phonons are involved and we have simply

$$\mathbf{k} = \mathbf{k}' + \mathbf{G} \qquad (\text{VI.16}$$

and

$$E_{\mathbf{k}} = E_{\mathbf{k'}} \qquad \text{(VI.17}$$

The conservation of energy implies (both for the photon and the neutron) that |**k**| = |**k'**|. Equation VI.16 together with Eq. VI.17 define thus a plane perpendicular to **G** passing through its midpoint (see Fig. V.3). To give a more "crystallographic" interpretation of these equations consider the situation indicated in Fig. VI.3. The length | **k'** - **k**| is equal to 2| **k**| sin θ where θ is the angle between the incident particle and the crystallographic plane. Writing | **k**| = 2π/λ and| **G** | = 2πn/a where a is the separation between crystal planes (see Eq. V.18) we find from Eq. VI.16 that

$$n\lambda = 2a \sin\theta \qquad \text{(VI.18}$$

which is the well-known **Bragg's law**.

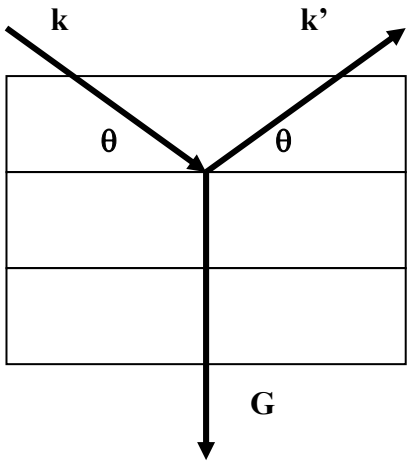


Fig. VI.3: Wave vector of the incoming particle (**k**) and of the outgoing (scattered) particle (**k'**) in an elastic scattering process involving the reciprocal lattice vector **G**.

An elementary derivation of Bragg's law can also be obtained by assuming that the photons are light waves that are partially reflected by the internal crystal planes. As shown in Fig. VI.4, in order to have a constructive interference of the outgoing light waves the path length difference $2a\ sin\theta$ of the wave reflected by consecutive planes must be equal to an integer number of wavelengths. Thus $2a\ sin\theta = n\lambda$. In contrast to the treatment described at the beginning of this Chapter, Bragg's simple interference model is not able to make predictions about the scattering probability as a function of **G**. That this probability is not the same for all **G** vectors is evident from diffraction pattern shown in Fig. VI.1. The central white halo is due to the incident particles. The symmetry is immediately apparent. From the position of the spots on can determine the position and the lattice parameters of the crystal structure of the sample. A similar diffraction pattern (though with different intensities) could be obtained by looking at the elastic scattering of neutrons.

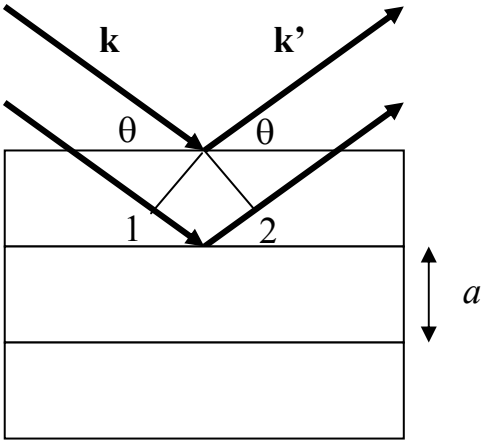


Fig. VI.4: Bragg scattering of light waves by crystallographic planes. For constructive interference the light path difference (1→2) should be equal to an integer number of wavelengths.

VI.3 Inelastic scattering of neutrons

As discussed in Section VI.1 the energy of neutrons with a wavelength comparable to the lattice spacing of typical solids is low and in fact comparable to that of phonons (i.e. lattice vibrations). There is therefore a rather large probability for a neutron to be scattered inelastically. By measuring **k** and **k'**, and the energies $E_{\mathbf{k}}$ and $E_{\mathbf{k}'}$ it is possible to determine the frequency ω_{phonon} and wave vector **q** of phonons and to construct point by point their dispersion law $\omega = \omega(\mathbf{q})$. An example of such measurements will be given in Fig.X.6.

VII ELECTRON STATES IN THREE DIMENSIONS

After a long excursion to crystal structures and the reciprocal space we return now to the problem of the electronic structure of a 3D-solid. The Schrödinger equation for an electron in a three dimensional periodic potential is

$$-\frac{\hbar^2}{2m}\Delta\Psi_{\mathbf{k}} + V(\mathbf{r})\Psi_{\mathbf{k}} = \varepsilon_{\mathbf{k}}\Psi_{\mathbf{k}} \qquad (\text{VII.1}$$

As indicated earlier, in three dimensions Bloch's theorem is

$$\psi_{\mathbf{k}}(\mathbf{r}) = e^{i\mathbf{k}.\mathbf{r}}u_{\mathbf{k}}(\mathbf{r}) \qquad (\text{VII.2}$$

with $u_{\mathbf{k}}(\mathbf{r})$ a periodic function, or, equivalently,

$$\psi_{\mathbf{k}}(\mathbf{r}+\mathbf{R}) = e^{i\mathbf{k}.\mathbf{R}}\psi_{\mathbf{k}}(\mathbf{r}) \qquad (\text{VII.3}$$

for any Bravais lattice vector **R.**

VII.1 Periodic boundary conditions

In analogy with Eq.III.4 we have for a cube of side L the following periodic conditions

$$\begin{aligned}\psi_{\mathbf{k}}(x+L) &= \psi_{\mathbf{k}}(x)\\ \psi_{\mathbf{k}}(y+L) &= \psi_{\mathbf{k}}(y)\\ \psi_{\mathbf{k}}(z+L) &= \psi_{\mathbf{k}}(z)\end{aligned} \qquad (\text{VII.4}$$

which implies that the possible values of **k** are

$$\mathbf{k} = \frac{2\pi}{L}(n_1, n_2, n_3) \qquad (\text{VII.5}$$

where n_i are positive or negative integers. Equation VII.5 implies that the space "occupied" by a **k**-point is $(2\pi/L)^3$, as indicated in Fig. VII.1. The number of states contained in a given

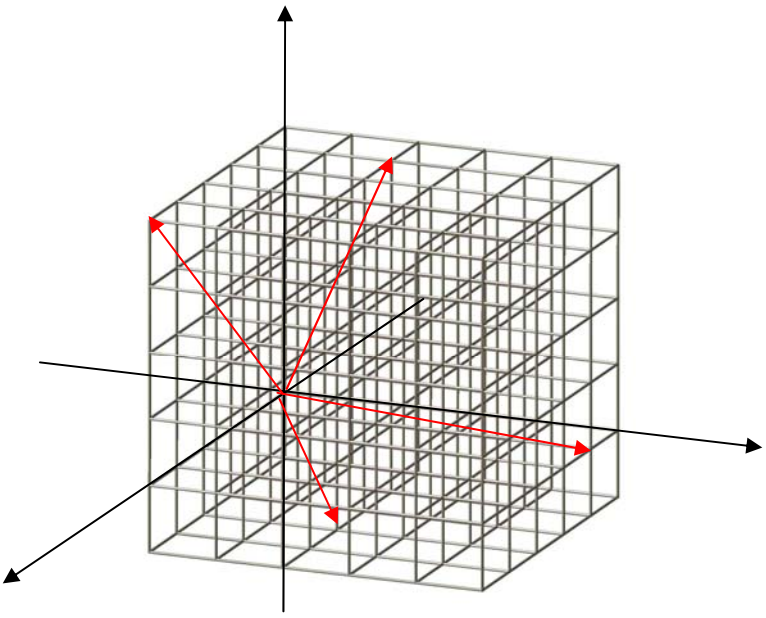


Fig. VII.1: Possible **k**-vectors allowed by the Born-von Karman periodic boundary conditions (only a few of them are indicated, of course).

volume Ω of **k**-space is thus simply obtained by dividing Ω by $(2\pi/L)^3$. With this method we can, for example, calculate the number of Bloch-states contained in a primitive unit cell of volume

$$\Omega = \mathbf{b}_1 \cdot \mathbf{b}_2 \times \mathbf{b}_3 = (2\pi)^3 \frac{(\mathbf{a}_2 \times \mathbf{a}_3) \cdot [(\mathbf{a}_3 \times \mathbf{a}_1) \times (\mathbf{a}_1 \times \mathbf{a}_2)]}{[\mathbf{a}_1 \cdot (\mathbf{a}_2 \times \mathbf{a}_3)]^3}$$
$$= (2\pi)^3 \frac{1}{\mathbf{a}_1 \cdot (\mathbf{a}_2 \times \mathbf{a}_3)} \qquad (\text{VII.6}$$

However, $\mathbf{a}_1 \cdot (\mathbf{a}_2 \times \mathbf{a}_3)$ is the volume L^3 of the primitive unit cell of the direct lattice for which

$$L^3 = N \cdot \mathbf{a}_1 \cdot (\mathbf{a}_2 \times \mathbf{a}_3) \qquad (\text{VII.7}$$

if N atoms are contained in a sample of volume L^3 (we assume here that we have a lattice structure without basis and that consequently each primitive unit cell contains one atom). The number of Bloch-states in the primitive unit cell of the reciprocal lattice is

$$\frac{\Omega}{(2\pi / L)^3} = N \qquad (\text{VII.8}$$

It is also the number of Bloch states contained in the Brillouin zone as Brillouin zone and primitive cell have the same volume. This is exactly what we already had in one dimension: a band can accommodate at most $2N$ electrons (the factor 2 comes from the spin of electron).

VII.2 Band structure and ground state

In Section III.5 we showed that the ground state of an N-electron system could be obtained by simply filling up all the Bloch states starting at the bottom of the band until all N electrons have been accommodated in a quantum state. To do this one needs, of course, to know the function $\varepsilon_{\mathbf{k}}$, i.e. one needs to know how the energy depends on the three quantum numbers k_1, k_2 and k_3 that define the vector **k.**
As an illustration of a simple band structure calculation in three dimensions we generalize our treatment of the linear chain of hydrogen atoms to a 3D-crystal structure. To keep everything as simple as possible we consider again hydrogen atoms and seek a solution of the Schrödinger equation in the form

$$\psi_{\mathbf{k}}(\mathbf{r}) = \frac{1}{\sqrt{N}} \sum_{\mathbf{R}} e^{i\mathbf{kR}} \, \phi(\mathbf{r}-\mathbf{R}) \qquad \text{(VII.9}$$

By following exactly the same steps as in Section III.4, we arrive at the following relation for $\varepsilon_{\mathbf{k}}$

$$\varepsilon_{\mathbf{k}} = E_{atomic} - \Delta V - t \sum_{\mathbf{R}_{nn}} e^{i\mathbf{k}\cdot\mathbf{R}} \qquad \text{(VII.10}$$

with

$$t \equiv -\left\langle \phi(\mathbf{r}) \middle| \Delta V(\mathbf{r}) \middle| \phi(\mathbf{r}-\mathbf{R}) \right\rangle \qquad \text{(VII.11}$$

and

$$\Delta V \equiv -\left\langle \phi(\mathbf{r}) \middle| \Delta V(\mathbf{r}) \middle| \phi(\mathbf{r}) \right\rangle \qquad \text{(VII.12}$$

The summation in Eq. VII.10 is over all nearest neighbour atoms.
The band structure of a BCC solid is readily evaluated since the position of the nearest neighbour atoms are given by

$$\mathbf{R} = \frac{a}{2}(\pm \hat{\mathbf{x}} \pm \hat{\mathbf{y}} \pm \hat{\mathbf{z}}) \qquad \text{(VII.13}$$

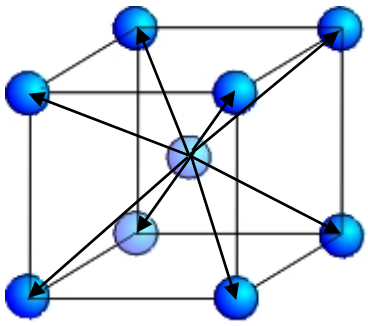


Fig. VII.2: The 8 nearest neighbour atoms in a BCC crystal structure.

Equation VII.10 is then for $\mathbf{k} = (k_1, k_2, k_3)$

$$\varepsilon_{\mathbf{k}} = E_{atomic} - \Delta V - t\left[e^{i\frac{a}{2}(k_1+k_2+k_3)} + e^{i\frac{a}{2}(k_1-k_2+k_3)} + e^{i\frac{a}{2}(-k_1+k_2+k_3)} + e^{i\frac{a}{2}(-k_1-k_2+k_3)} \right] \quad \text{(VII.14}$$
$$- t\left[e^{-i\frac{a}{2}(k_1+k_2+k_3)} + e^{-i\frac{a}{2}(k_1-k_2+k_3)} + e^{-i\frac{a}{2}(-k_1+k_2+k_3)} + e^{-i\frac{a}{2}(-k_1-k_2+k_3)} \right]$$

and can be more compactly written as

$$\varepsilon_{\mathbf{k}} = E_{atomic} - \Delta V - 8t\cos\left(\frac{k_1 a}{2}\right)\cos\left(\frac{k_2 a}{2}\right)\cos\left(\frac{k_3 a}{2}\right) \quad \text{(VII.15}$$

As it is not possible to represent directly $\varepsilon_{\mathbf{k}}$ as a function of the three components of the **k-** vector various "partial" representations have been chosen in the literature to visualize the band structure of a solid.

VII.2.1 Band structure for a particular choice of k

For example we can choose k_3=0 in Eq.VII.15. One obtains then

$$\varepsilon_{\mathbf{k}} = E_{atomic} - \Delta V - 8t\cos\left(\frac{k_1 a}{2}\right)\cos\left(\frac{k_2 a}{2}\right) \quad \text{(VII.16}$$

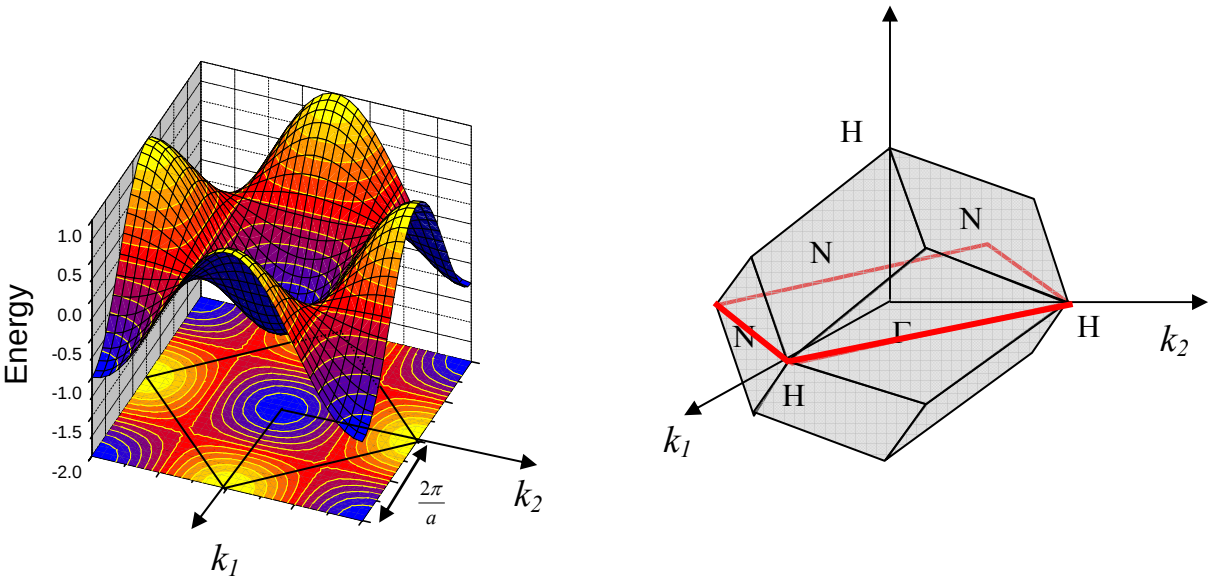


Fig. VII.3: *(left panel):*Band structure of a BCC solid for k_3=0. For this example we have chosen t=1/8 eV, E_{atomic} and ΔV equal to zero; *(right panel):* Brillouin zone of the BCC crystal structure. The black square in the left panel corresponds to the red square in the Brillouin zone.

VII.2.2 Following a path in k-space

Instead of showing a two-dimensional representation of the band structure as in Fig. VII.3 one can also plot the energy along a chosen path in *k*-space. For example, along a path Γ-H-H-Γ the band structure looks as indicated in Fig. VII.4. In a real metal the band structure can look quite complicated since many bands exist. We give in Fig. **VII.5** a typical example of the band structure of a transition metal: tungsten (W).

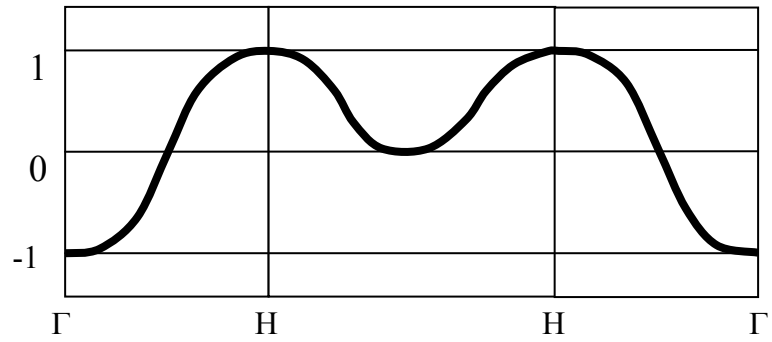


Fig. VII.4: Band structure of a BCC solid along the path Γ-H-H-Γ in *k*-space (see Fig. VII.3)

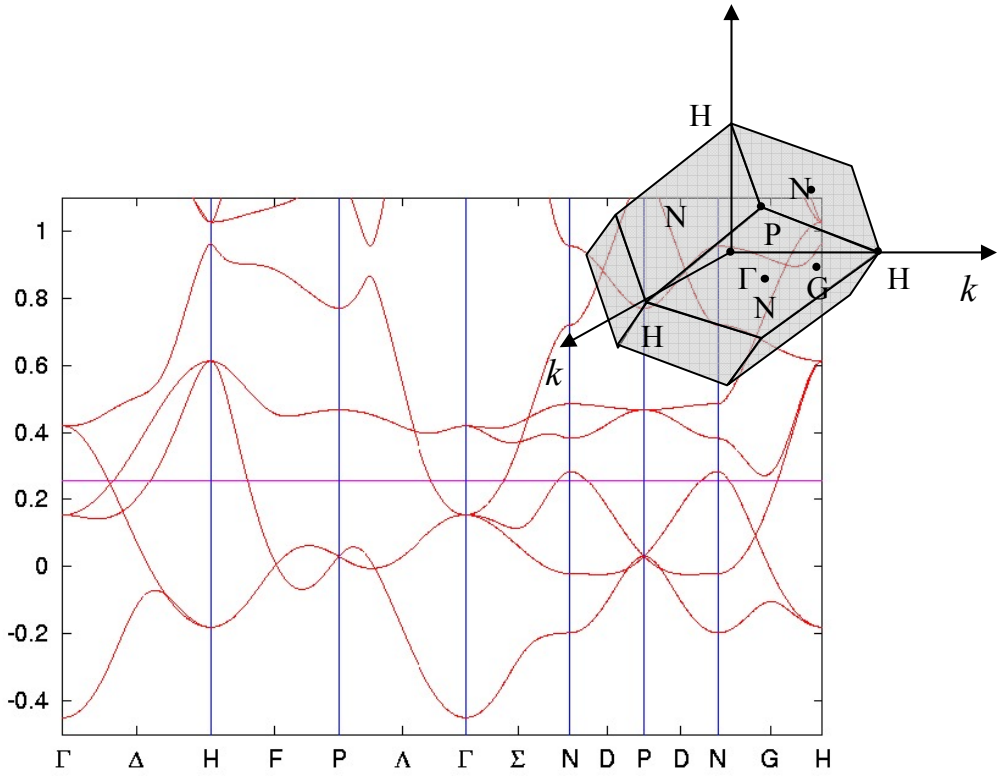


Fig. VII.5: Band structure of Tungsten (W). The relatively flat bands originate from the atomic *d*-states. The path chosen for the representation of the energy bands can be followed on the schematic Brillouin zone.

VII.2.3 Surfaces of constant energies.

Another way to visualize the function in Eq.VII.15 is to set $\varepsilon_{\mathbf{k}}$ equal to a constant. For the examples given in Fig. VII.6 we have written Eq.VII.15 in the form

$$\eta = \frac{\varepsilon_{\mathbf{k}} - E_{atomic} + \Delta V}{8t} = -\cos\left(\frac{k_1 a}{2}\right)\cos\left(\frac{k_2 a}{2}\right)\cos\left(\frac{k_3 a}{2}\right) \qquad \text{(VII.17}$$

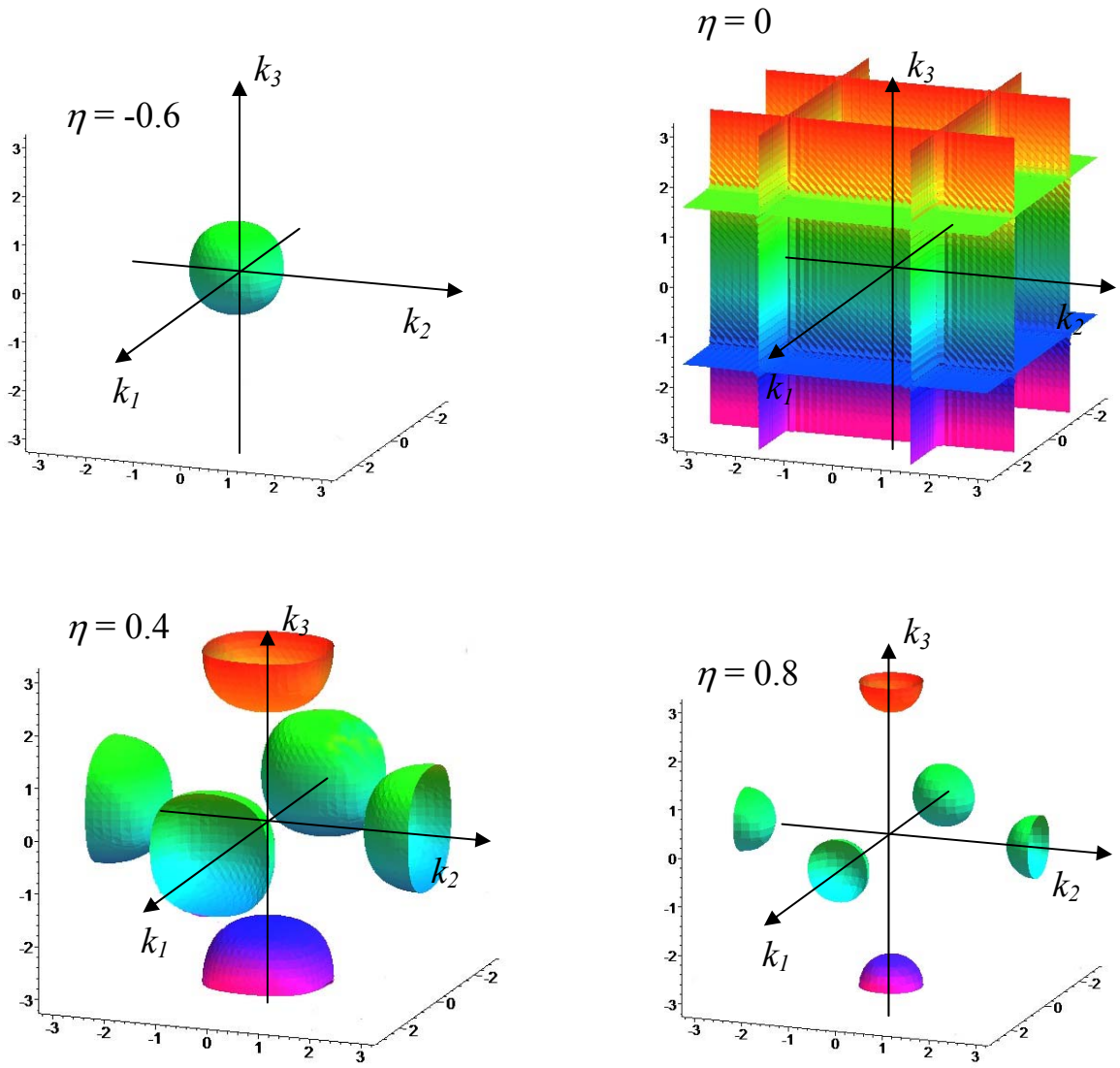


Fig. VII.6: Surfaces of constant energy for various values of the parameter η defined in Eq.VII.17. For negative energies of η the constant energy surface is nearly a sphere. At half filling of the band the surface is a cube. For positive values of η the surface consists of spheroidal portions that decrease in size when η approaches 1.

VII.3 The Fermi surface

By definition, the **Fermi surface is the constant energy surface within which all Bloch states are occupied**. For a solid made of atoms with 1 valence electron per atom the band is half-filled and the Fermi surface is in the case of a BCC structure simply a cube (see Fig. VII.6). For atoms with 2 valence electrons the Fermi surface fills the whole Brillouin zone, since all the states are occupied.
For real metals, the situation is more complicated since there is not only one energy band. For example for the transition metal tungsten (W) the Fermi surface consists of the two sheets shown in Fig. VII.7.

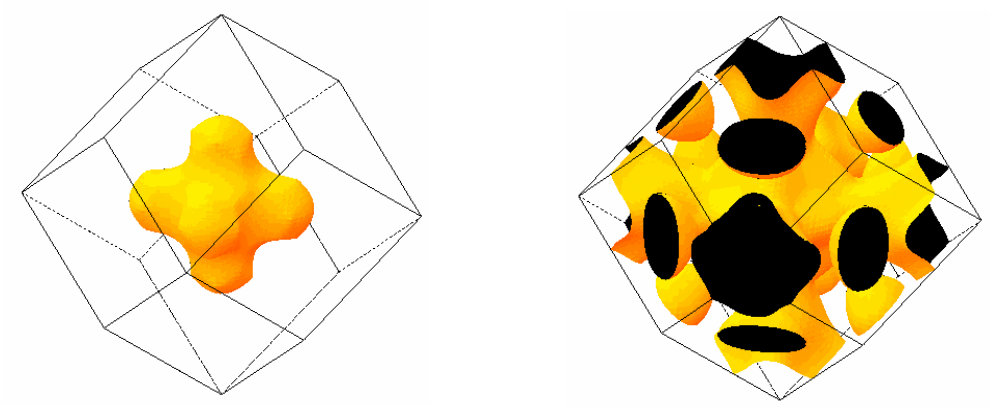


Fig. VII.7: The two sheets of the Fermi surface of Tungsten.

For the alkali metals on the other hand, the Fermi surface is very simple. It is essentially a perfect sphere as shown in

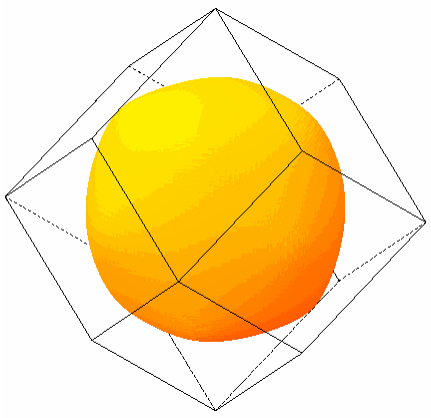


Fig. VII.8: The Fermi surface of Lithium. Li has only one valence electron. This electron is so weakly bound to the Li-nucleus that it is essentially free to move through the whole crystal lattice. For such a case the tight-binding approximation is not adequate. The nearly-free-electron model works much better.

Finally, for the noble metals Cu, Ag and Au that have also only one valence electron per atom, the Fermi surface has a shape intermediate between that of a sphere and that of a cube. What is absolutely remarkable is that the Fermi surface can actually be measured experimentally by means of the so-called De Haas-van Alphen effect. It is thus not merely a mathematical construction.

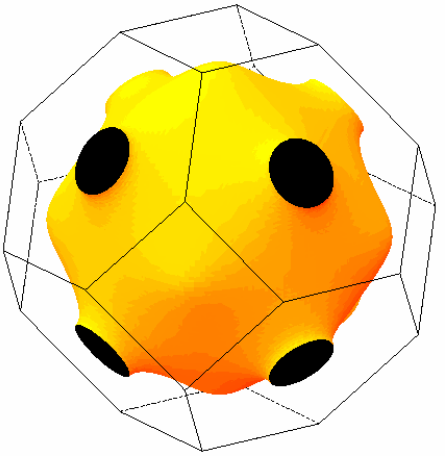


Fig. VII.9: Fermi surface of Copper. The Fermi surface is approximately spherical with protuberances that touch the hexagonal faces of the Brillouin zone. Note that Copper has a face-centered-cubic crystal structure (see **Fig. V.5**).

VII.4 The density of states

Although easily explained in words, the construction of the ground state of a real material is numerically cumbersome. It requires an accurate determination of the volume of the constant energy surface as a function of the number of electrons until the correct number of electron states is reached. An efficient way to present the results of such calculation is in the form of the **density-of-states** g(ε) which is defined as follows:

$$g(\varepsilon)d\varepsilon = \frac{\text{Number of Bloch states with energy in the range } \varepsilon \text{ and } \varepsilon + \mathrm{d}\varepsilon}{\text{volume of the sample}} \qquad (\text{VII.18}$$

From this definition follows immediately that

$$\int_{E_b}^{\varepsilon_F} g(\varepsilon)d\varepsilon = n \qquad (\text{VII.19}$$

and

$$\int_{E_b}^{E_t} g(\varepsilon)d\varepsilon = 2(N/V) \qquad \text{(VII.20}$$

where n is the number of electrons per unit volume and N the number of atoms in the volume V. E_b and E_t are respectively, the energy at the bottom and at the top of a given energy band. In Eq. VII.20 we have assumed that there is no overlap with another band. The density of states function can in general not be expressed analytically.

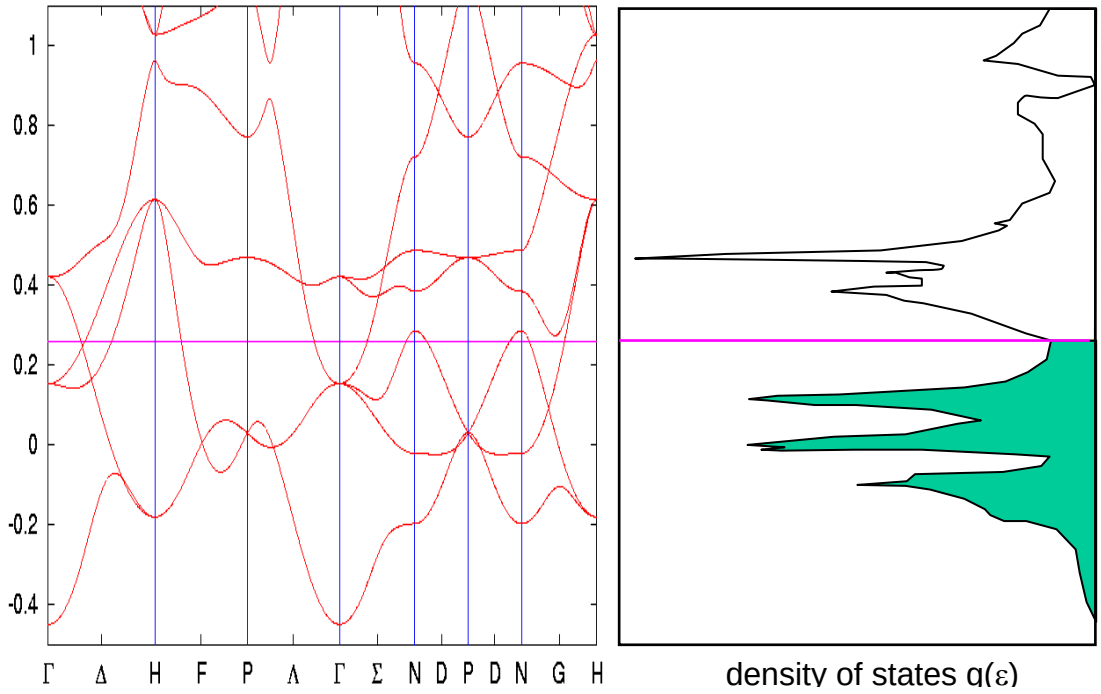


Fig. VII.10: (*left*) Density of states corresponding to the energy band structure of tungsten given in Fig.VII.7. Note that there are peaks in the density of states (*right panel*) whenever the electronic bands are relatively flat. The occupied part of the density of states is indicated in green. The Fermi energy is indicated in violet.. The integral of g(ε) up to ε_F is equal to 5 since W has 5 valence electrons (conduction electrons).

VII.5 The free electron gas

Although band structures and density of states functions can be very complicated, it is often useful to use the simplest possible model, the **free electron model**, for an order-of-magnitude evaluation of relevant parameters. We indicate here the relevant relations without explicit derivations (which are left as an exercise to the reader).

Band structure $\varepsilon_k = \frac{\hbar^2 k^2}{2m}$ (VII.21

Fermi energy $\varepsilon_F = \frac{\hbar^2}{2m}(3\pi^2 n)^{2/3}$ (VII.22

Fermi surface radius k_F $k_F = (3\pi^2 n)^{1/3}$ (VII.23

Fermi velocity $v_F = \frac{\hbar k_F}{m}$ (VII.24

Density of states $g(\varepsilon) = \frac{m}{\hbar^2 \pi^2}\sqrt{\frac{2m\varepsilon}{\hbar^2}}$ (VII.25

Density of states at ε_F $g(\varepsilon_F) = \frac{3n}{2\varepsilon_F}$ (VII.26

Typical values of ε_F, k_F and $g(\varepsilon_F)$, the density of states at the Fermi energy ε_F are given in Table VII.1 for various metals. (NB. the values listed are obtained by assuming that the electrons are completely free which is not true. These values are thus at best orders of magnitude). What you should remember is that $\varepsilon_F \cong 10$ eV, $v_F \cong 10^6$m/s (the electrons are thus moving almost 2000 times faster than the supersonic Concord-jet), $k_F \cong 10^{10}$ m^{-1} which is comparable to the dimension of the Brillouin zone, and $g(\varepsilon_F) \cong 10^{28}$ states per eV per m^3 (very approximately 1 state per eV per atom).

Table VII.1: Density of electron n, valence Z, Fermi energy ε_F, Fermi wave vector k_F and density of states g (ε_F) of metals in the free electron approximation. (1eV ≅ 1.602 * 10^{-19}J).

Metal	N $\left(\frac{10^{28}}{m^3}\right)$	Z	ε_F (eV)	v_F $(10^6 \frac{m}{s})$	k_F $(\frac{10^{10}}{m})$	$g(\varepsilon_F)$ $\left(\frac{10^{28}}{eVm^3}\right)$
Li	4.70	1	4.74	1.29	1.12	1.49
Cu	8.47	1	7.00	1.57	1.36	1.82
Be	24.7	2	14.3	2.25	1.94	2.59
Mg	8.61	2	7.08	1.58	1.36	1.82
Nb	27.8	5	15.6	2.34	2.02	2.67
Al	18.1	3	11.7	2.03	1.75	2.32
Pb	13.2	4	9.47	1.83	1.58	2.09
Bi	14.1	5	9.90	1.87	1.61	2.14

The relations indicated above for a free electron gas are readily derived. We give therefore only details for one particular quantity, the density of states g(ε) . It is best calculated from the following expression

$$g(\varepsilon)d\varepsilon = \frac{1}{L^3}\frac{4\pi k^2 dk}{(2\pi/L)^3}\cdot 2 \qquad (\text{VII.27}$$

where

i) $\frac{1}{L^3}$ = (volume)$^{-1}$

ii) $4\pi k^2$ = area of sphere of radius k

iii) $4\pi k^2 dk$ = volume of a shell of thickness dk at the surface of the sphere of area $4\pi k^2$

iv) 2 = spin-up and spin-down

As for free electrons

$$\varepsilon = \frac{\hbar^2 k^2}{2m} \qquad (\text{VII.28}$$

we have

$$d\varepsilon = \frac{\hbar^2}{m} k dk \qquad (\text{VII.29}$$

combining Eqs.VII 27 to 29 we obtain finally

$$g(\varepsilon) = \frac{m}{\hbar^2\pi^2}\sqrt{\frac{2m\varepsilon}{\hbar^2}} \qquad (\text{VII.30}$$

The density of states of a free electron gas varies thus as the square root of the energy and the 3/2-power of the mass of the electron.

VII.6 Effective mass of the electron

To introduce the concept of electron effective mass we consider the explicit expression given in Eq.VII.15 for the electronic band of a BCC metal. At the bottom of the band the cosines can be expanded to give

$$\varepsilon_{\mathbf{k}} = E_{atomic} - \Delta V - 8t + a^2 t|\mathbf{k}|^2 = E_b + a^2 t|\mathbf{k}|^2 \qquad (\text{VII.31}$$

Comparing this expression with that for a free electron gas in Eq.VII.28 we conclude that the k-dependence is quadratic in both cases. The only difference is in the curvature of the band. One defines the effective mass m^* of a Bloch electron in the following way

$$\frac{\hbar^2}{2m^*} = a^2 t \qquad \text{(VII.32}$$

The effective mass is small when the overlap t is large and vice versa. This is quite intuitive since a large overlap means a large velocity and, therefore, an easily (=light) moving electron.
The free electron model is despite its great simplicity quite useful for the analytical description of electron states at the bottom or at the top of a tight-binding band.
From the fact, that at the bottom and the top of the band given by Eq.VII.28 $\varepsilon_{\mathbf{k}}$ varies quadratically with $|\mathbf{k}|$ or $|\mathbf{k}-\mathbf{k}_0|$ follows that, in analogy with Eq. VII.30,

$$g(\varepsilon) \cong \frac{m^*}{\hbar^2 \pi^2} \sqrt{\frac{2m^*(\varepsilon - E_b)}{\hbar^2}} \quad \text{for } \varepsilon > E_b \qquad \text{(VII.33}$$

and

$$g(\varepsilon) \cong \frac{m^*}{\hbar^2 \pi^2} \sqrt{\frac{2m^*(E_t - \varepsilon)}{\hbar^2}} \quad \text{for } \varepsilon < E_t \qquad \text{(VII.34}$$

These relations will be used to model the band structure of semiconductors in Chapter IX.

VIII METALS, SEMICONDUCTORS AND INSULATORS

The considerations in Section III.5suggest that the degree of filling of an energy band is related to the electrical properties of a material, in the sense that a half-filled band is favourable for electric conduction and the material is consequently a metal. A full band on the contrary seems to lead to a non-conducting material, which can be a semiconductor or an insulator. Here we show that this can qualitatively be understood by considering the movement of a Bloch electron in an electric field.

VIII.1 The crystal momentum

We consider an electron of energy ε_k in a Bloch state Ψ_k that satisfies the Schrödinger equation in one dimension

$$H\Psi_k = \varepsilon_k \Psi_k \qquad \text{(VIII.1)}$$

with

$$H = -\frac{\hbar^2}{2m}\frac{d^2}{dx^2} + V(x) \qquad \text{(VIII.2)}$$

where *V(x)* is the periodic potential of the crystal lattice. Assume now for the moment that *V(x)* is so weak that it may be neglected altogether. The solutions of Eq.VIII.1 are then simply plane waves

$$\Psi_k = \frac{1}{\sqrt{L}} e^{ikx} \qquad \text{(VIII.3)}$$

where L is the length of the linear chain of atoms shown in Fig. III.1. The energy eigenvalues are

$$\varepsilon_k = \frac{\hbar^2 k^2}{2m} \qquad \text{(VIII.4)}$$

and the expectation value of the momentum of the electron

$$p_k = \left\langle \Psi_k \left| -i\hbar \frac{d}{dx} \right| \Psi_k \right\rangle = \int \frac{1}{\sqrt{L}} e^{-ikx} \left(-i\hbar \frac{d}{dx} \right) \frac{1}{\sqrt{L}} e^{ikx} dx = \hbar k \qquad \text{(VIII.5}$$

This special example suggests that the quantum number k appearing in Bloch's theorem is simply related to the momentum of the electron. This is, however, only true for the special case of **free electrons.** For electrons in a periodic potential it is **certainly not true** since

$$p_k = \left\langle \Psi_k \left| -i\hbar \frac{d}{dx} \right| \Psi_k \right\rangle = \int e^{-ikx} u_k^*(x) \left(-i\hbar \frac{d}{dx} \right) e^{ikx} u_k(x) dx = \hbar k - i\hbar \int u_k^* \frac{du_k}{dx} dx \neq \hbar k \qquad \text{(VIII.6}$$

For this reason $\hbar \times$(the quantum number k) appearing in Bloch's theorem

$$\Psi_k(x) = e^{ikx} u_k(x) \qquad \text{(VIII.7}$$

is called the **crystal momentum** to distinguish it from the **true momentum** of the electron. As we shall see later, however, the crystal momentum is a very useful quantity as it appears in conservation laws for the total momentum that are very similar (at least formally) to classical conservation laws.

VIII.2 The true momentum of an electron

The true momentum of an electron in a Bloch state k given by Eq.VIII.6 that can also be written as

$$p_k = \left\langle \Psi_k \left| -i\hbar \frac{d}{dx} \right| \Psi_k \right\rangle = \int u_k^* \left(\hbar k - i\hbar \frac{d}{dx} \right) u_k dx \qquad \text{(VIII.8)}$$

This expression has the disadvantage that it requires the knowledge of the Bloch wave function $u_k(x)$. The question arises therefore whether it would be possible to find a more practical relation. For a free electron, we see immediately that

$$p_k = m v_k = \frac{d}{dv_k} \left(\frac{1}{2} m v_k^2 \right) = \frac{md}{\hbar dk} \left(\frac{\hbar^2 k^2}{2m} \right) = \frac{m}{\hbar} \frac{d\varepsilon_k}{dk} \qquad \text{(VIII.9)}$$

This is a nice relation since it allows to calculate the true momentum (or equivalently, the true velocity) of an electron in a Bloch state Ψ_k simply from the dispersion relation ε_k .To check whether or not this relation is still valid in the general case of Bloch electrons we calculate now $d\varepsilon_k / dk$. Since Ψ_k is normalised, we have

$$\varepsilon_k = \left\langle \Psi_k \left| H \right| \Psi_k \right\rangle \qquad \text{(VIII.10}$$

Replacing Ψ_k by $e^{ikx}u_k(x)$ and H by the expression in Eq.VIII.2 we obtain

$$\varepsilon_k = \langle u_k | \frac{\hbar^2}{2m}\left(k^2 - 2ik\frac{d}{dx} - \frac{d^2}{dx^2}\right) + V(x) | u_k \rangle \qquad \text{(VIII.11}$$

which implies that ε_k is also an eigenvalue of the following problem

$$H_k u_k = \varepsilon_k u_k \qquad \text{(VIII.12}$$

with

$$H_k = \frac{\hbar^2}{2m}\left(k^2 - 2ik\frac{d}{dx} - \frac{d^2}{dx^2}\right) + V(x) \qquad \text{(VIII.13}$$

Since $u_k(x)$ is a function of x only, we find from Eq.VIII.11 that

$$\frac{d\varepsilon_k}{dk} = \langle u_k | \frac{\hbar^2}{m}\left(k - i\frac{d}{dx}\right) | u_k \rangle \qquad \text{(VIII.14}$$

which according to Eq.VIII.8 can be written as

$$\frac{d\varepsilon_k}{dk} = \frac{\hbar}{m} p_k = \hbar v_k \qquad \text{(VIII.15}$$

and, consequently, the expectation value of the velocity of a Bloch electron in state Ψ_k is given by the remarkably simple relation

$$v_k = \frac{1}{\hbar}\frac{d\varepsilon_k}{dk} \qquad \text{(VIII.16}$$

This expression implies that a Bloch electron in state Ψ_k moves with a **constant** velocity v_k as if it would not "see" the atoms in the linear chain. This is completely different from the classical picture where the electron is scattered by the atoms and deflected in all directions. In our quantum mechanical picture the electron tunnels from one atom to the other without ever slowing down.

Equation VIII.16 is very useful as it allows calculating very simply the velocity of an electron once the band structure ε_k is known. For example, for the tight-binding band considered in Section III.4, where

$$\varepsilon_k = E_{atomic} - \Delta V - 2t\cos(ka) \qquad \text{(VIII.17}$$

we obtain

$$v_k = \frac{2}{\hbar} ta \sin(ka) \qquad \text{(VIII.18}$$

This function is shown in Fig. VIII.1. The velocity v_k vanishes at the centre and at the boundary of the Brillouin zone. The two curves in this figure show also clearly the difference between the **crystal momentum** $\hbar k$ and the **true momentum** mv_k.

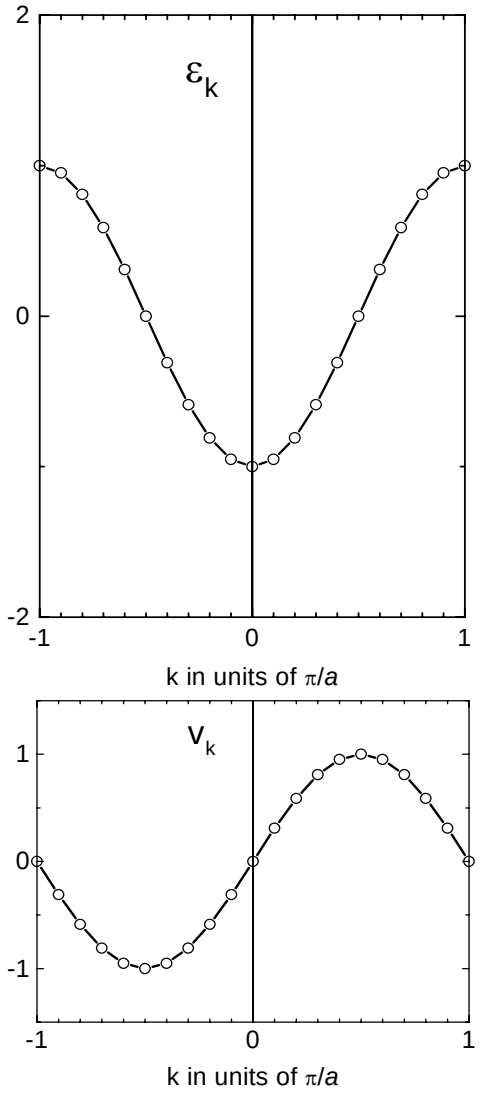


Fig. VIII.1: Electron energy ε_k and electron true velocity v_k for a tight-binding band. Note that the true momentum (or, equivalently, true velocity) is a sinusoidal function while the crystal momentum would simply be a straight line $p_k = \hbar k$. For this illustration we have chosen t=1/2

VIII.3 Bloch electron in an electric field

When an external electric field **E** is applied to an electron it is accelerated by the force

$$\mathbf{F} = -e\mathbf{E} \qquad \text{(VIII.19}$$

where $e \cong 1.602 \times 10^{-19}$ C is the elementary charge. The work ΔW done by the electric field during the time interval Δt is

$$\Delta W = \mathbf{F} \cdot \mathbf{v}_{\mathbf{k}} \Delta t = \Delta \varepsilon_{\mathbf{k}} \qquad \text{(VIII.20}$$

and is equal to the change $\Delta\varepsilon_{\mathbf{k}}$ in the energy of the electron. As $\varepsilon_{\mathbf{k}}$ depends only on **k**

$$\Delta \varepsilon_k = \frac{d\varepsilon_{\mathbf{k}}}{d\mathbf{k}} d\mathbf{k} = \hbar \mathbf{v}_{\mathbf{k}} \cdot \Delta \mathbf{k} \qquad \text{(VIII.21}$$

By comparison of Eqs.VIII.20 and 21 we arrive at another very remarkable relation,

$$\mathbf{F} = \frac{d(\hbar \mathbf{k})}{dt} \qquad \text{(VIII.22}$$

Although it has the same form as Newton's equation **F**=*m***a** its meaning is **completely different**. It says that the force associated with the **external** field (i.e. **not the total force** that also includes the forces between electron and ions in a solid **!**) is equal to the time derivative of the **crystal momentum** (i.e. **not the true momentum of the electron)**. Although we have considered specifically a force generated by an electric field Eq.VIII.22 is true also for an electron subjected to the Lorentz force in a magnetic field.

Equation VIII.22 tells us how a quantum mechanical state $\Psi_{\mathbf{k}}$ evolves as a function of time. For example, for an electric field pointing in the negative direction of the x-axis, the force **F** points in the positive x-axis direction and after a time Δt the state $\Psi_{\mathbf{k}}(x)$ has changed into the state $\Psi_{\mathbf{k}+\Delta\mathbf{k}}(x)$ with

$$\Delta \mathbf{k} = -\frac{e\mathbf{E}}{\hbar} \Delta t \qquad \text{(VIII.23}$$

As **k** depends linearly on time *t* it will grow forever with time. At a certain time, it will reach the boundary of the first Brillouin zone and continue into the second Brillouin zone. However, the second Brillouin zone is equivalent to the first one. This implies that $\Psi_{k=-\pi/a} = \Psi_{k=\pi/a}$. We can thus shift the Bloch state from A to B in Fig. VIII.2.

Then the crystal momentum $\hbar\mathbf{k}$ starts again to increase until it reaches point A and the whole process repeats itself indefinitely. This leads to an oscillatory movement (Bloch oscillations) of an electron although the applied electric field generates a constant force! This funny behaviour is due to the periodic potential that modifies the dynamics of an electron in a rather unusual way. This behaviour is so much contra-intuitive that one might question the validity of the approach followed so far. However, there are many phenomena that confirm the picture we have developed here. The best-known examples of such phenomena are the existence of "holes" in metals (i.e. "electrons" that seem to have a positive charge) and Bloch oscillations in nanosized samples. These Bloch oscillations however are not observed in macroscopic samples. The reason is quite simple: in macroscopic samples there are defects that disturb the periodicity of the lattice. Bloch's theorem is then not valid anymore and **k** is not a good quantum number anymore.

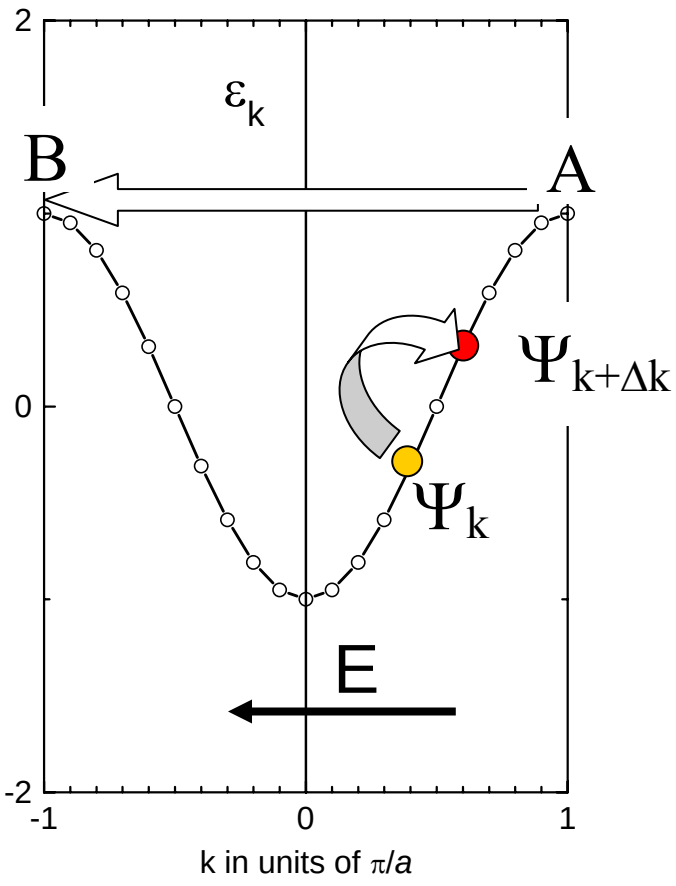


Fig. VIII.2: Time evolution of a Bloch state in an applied electric field E. The change Δk is given by Eq.VIII.23.

VIII.4 The relaxation time

The simplest way to incorporate the scattering of electrons (due to collisions with impurities) is to assume that during a certain time, the electron states evolve as described in Section VIII.3 but that at a time $t=\tau$ the electrons relax to their original states (i.e. the states they occupied at t=0). In other words, we assume that every τ-

seconds the electrons forget completely that they have been previously accelerated. The overall effect is that in presence of an electric field E all the $\Psi_{\mathbf{k}}$ states change into $\Psi_{\mathbf{k}+\Delta\mathbf{k}}$ states with

$$\Delta\mathbf{k} = -\frac{e\mathbf{E}}{\hbar}\tau \qquad \text{(VIII.24}$$

The time τ is called the **relaxation time**. In presence of defects the quantum numbers of all the states are therefore displaced by the **same** $\Delta\mathbf{k}$ which, in contrast to Eq.VIII.23 is no longer a function of time. The relaxation time mimics the effect of all scattering processes and is thus difficult to calculate theoretically. At the level of this introductory course we shall treat it as a characteristic, material dependent parameter that needs to be determined experimentally. In a perfect system τ would be infinite. In a disordered system τ is limited by impurity atoms, crystalline defects and the vibration of atoms at finite temperatures. In relatively pure metals τ is of the order of 10^{-14} s. For an electric field of 1 V/m one obtains thus

$$|\Delta k| = \frac{eE}{\hbar}\tau = \frac{1.6\times10^{-19}\,C\times1\frac{V}{m}}{1.06\times10^{-34}\,Js}\times10^{-14}\,s \cong 15\,m^{-1} \qquad \text{(VIII.25}$$

This value must be compared to the dimension of the Brillouin zone which is typically 10^{10} m^{-1}. The change in *k* is thus **9 orders of magnitude smaller** than the Brillouin zone.

VIII.5 The electric current

Consider the situation of a half-filled band as indicated in Fig. VIII.3. The occupied states are given by red dots and the unoccupied states by open circles. Independently of its occupation a state $\Psi_{\mathbf{k}}$ is displaced by a certain amount Δk given by Eq.VIII.24. There is then unbalance between electrons flowing to the right and those flowing to the left. This unbalance leads to an electric current *I* given by

$$I = -2e\sum_{\substack{occupied\\states}} v_k \qquad \text{(VIII.26}$$

where the summation is taken over all occupied states in the Brillouin zone. The factor 2 arises from the fact that each Bloch state is occupied by two electrons: a spin-up and a spin-down electron. This expression suggests that the more electrons are in a system the higher the electric current. This is, however, wrong: a completely filled band is **not** able to carry any current ! This is easily understood by looking at Fig. VIII.4. As for the half-filled band all the k-states are displaced to the right. The states that were close to the top of the band on the right side of the Brillouin zone are forced to move into the second Brillouin zone. As explained before these states are, however, equivalent to the states indicated by arrows. The net result is that the number of electrons flowing to the right remains equal to that flowing to the left and no net current flows through the sample.

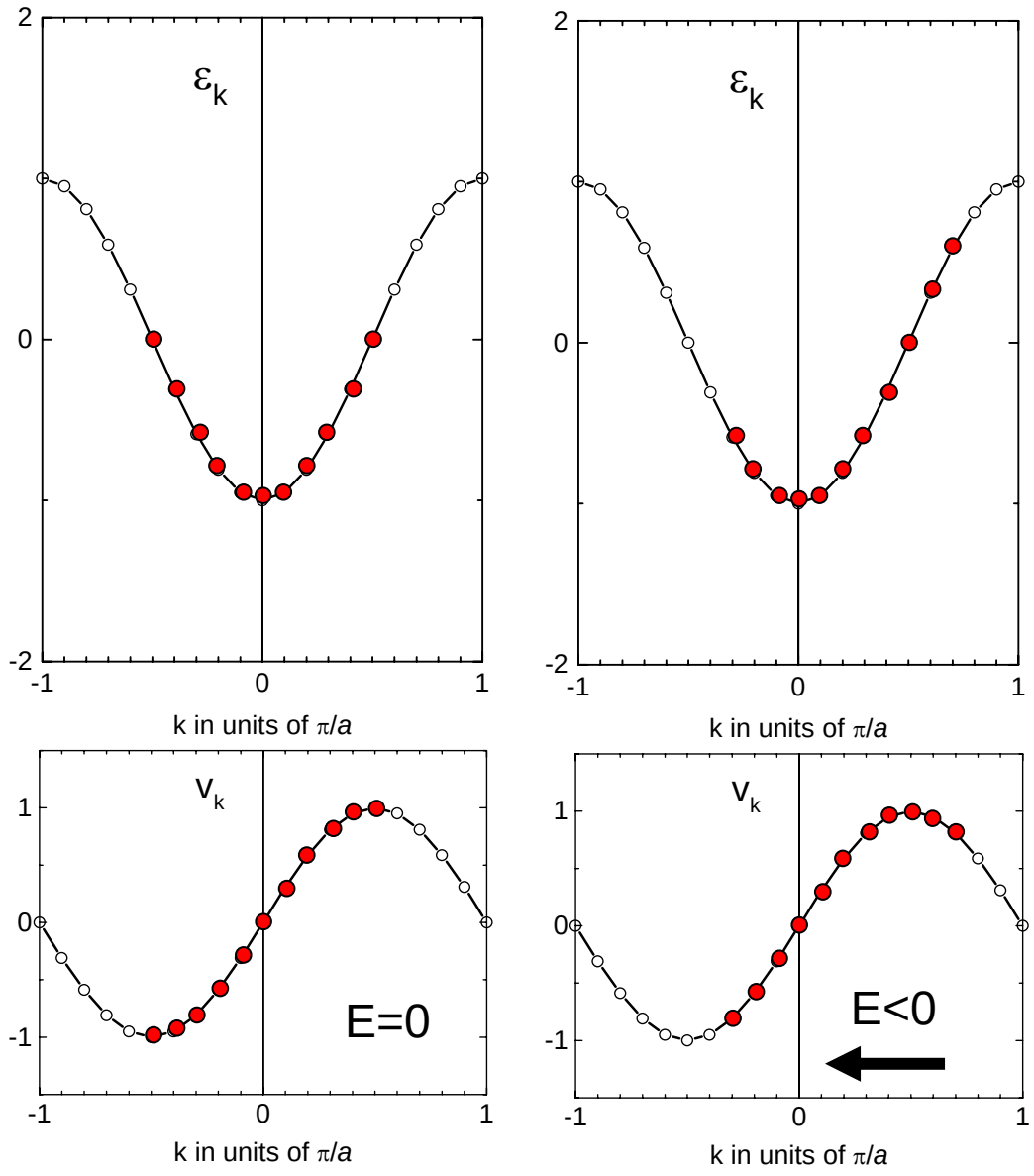


Fig. VIII.3: Effect of an electric field on the occupation of Bloch states in a **half-filled** band in the relaxation time approximation. a) *Left panel*: a half-filled band in the absence of an electric field. b) *Right panel*: the same band in presence of an electric field directed in the direction of the negative x-axis. There are clearly more electrons moving to the right than electrons moving to the left. Consequently an electric current is flowing in the sample in presence of an electric field. The separation between allowed k-values is grossly exaggerated for clarity (see Section VIII.4)

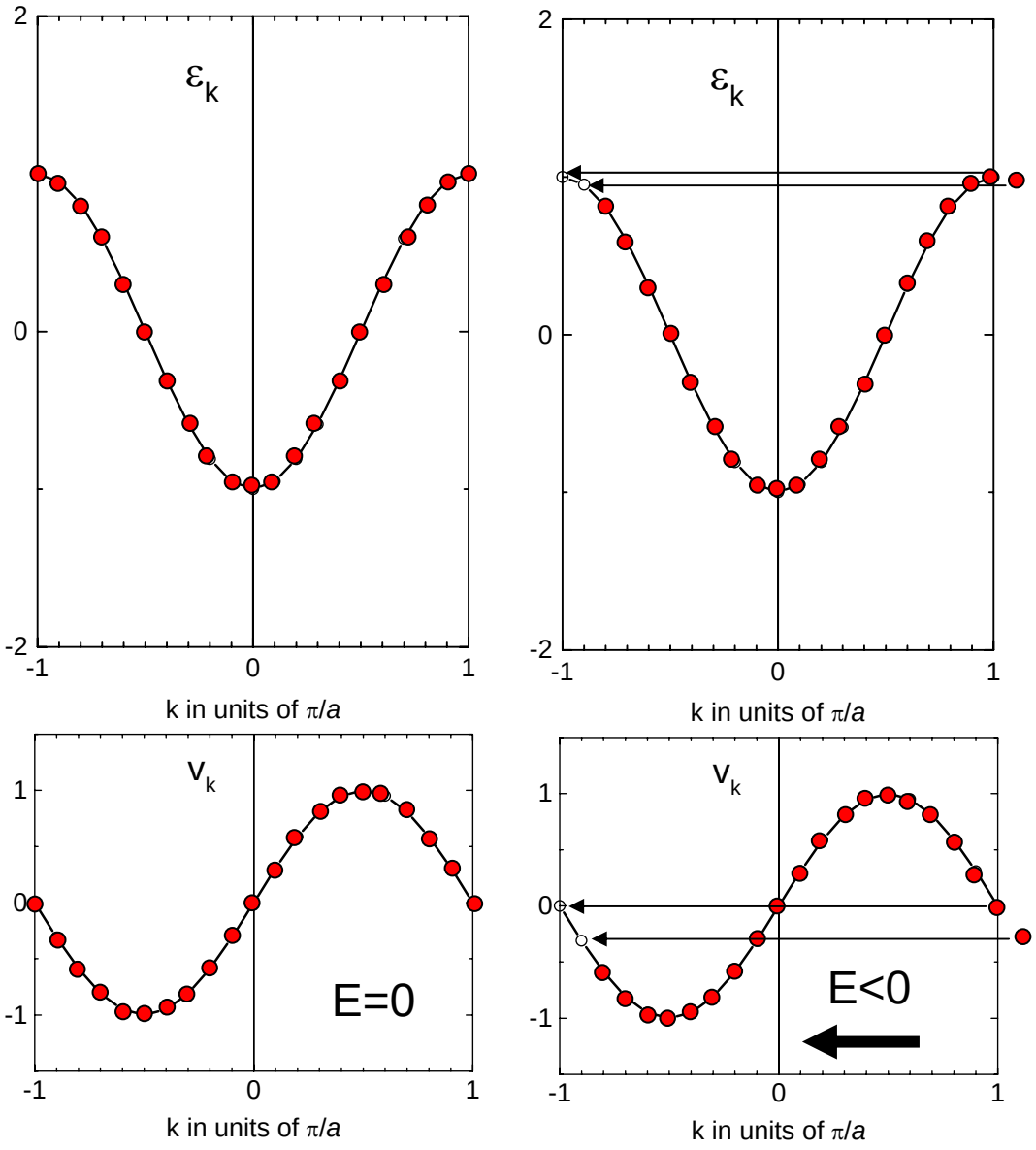


Fig. VIII.4: Effect of an electric field on the occupation of Bloch states in a **full** band in the relaxation time approximation. a) Left panel: a completely filled band in the absence of an electric field. b) Right panel: the same band in presence of an electric field directed in the direction of the negative x-axis. There are therefore as many electrons moving to the right as electrons moving to the left. Consequently, there is **no** electric current flowing in the sample in presence of an electric field. The separation between allowed k-values is grossly exaggerated for clarity.

VIII.6 Various types of materials

The results derived above lead to a natural classification of solids. Although all solids contain electrons, their electric properties may be very different. Solids with full electronic bands are, for example, not able to conduct electricity. At T=0 K they are

therefore **insulators**. Materials with not completely filled bands can conduct electricity and are therefore **metals.** For materials with only one electron band, or materials with well separated electronic bands (i.e. not overlapping) we expect then that

- materials made of atoms with 1,3,5… electrons are **metals**
- materials made of atoms with 2,4,6… electrons are **insulators**

since each band can accommodate 2 electrons per atom. This explains why the alkali metals (Li, Na, K, Rb, Cs) and the noble metals (Cu, Ag and Au), which all have one electron per atom, are metals. Similarly materials with three electrons per atom (e.g. Al, Ga, In, Tl) are also metals. It also "explains" why diamond (C) with four electrons is an insulator. However, it seems to be in contradiction with the fact that divalent materials such as Zn and Cd are metals. The reason is that in these materials the electronic bands overlap. One has then a situation as shown in Fig. VIII.5.
At finite temperature one can distinguish between insulators and semiconductors. Although both materials have full and non-overlapping bands a semiconductor is able to conduct somewhat electricity when electrons are excited across the energy gap (see Fig. VIII.6). This is only possible if the gap is sufficiently small (say of the order of 1 eV as in Si and Ge). If the gap is large (say 5 eV) then thermal energy is too small to excite

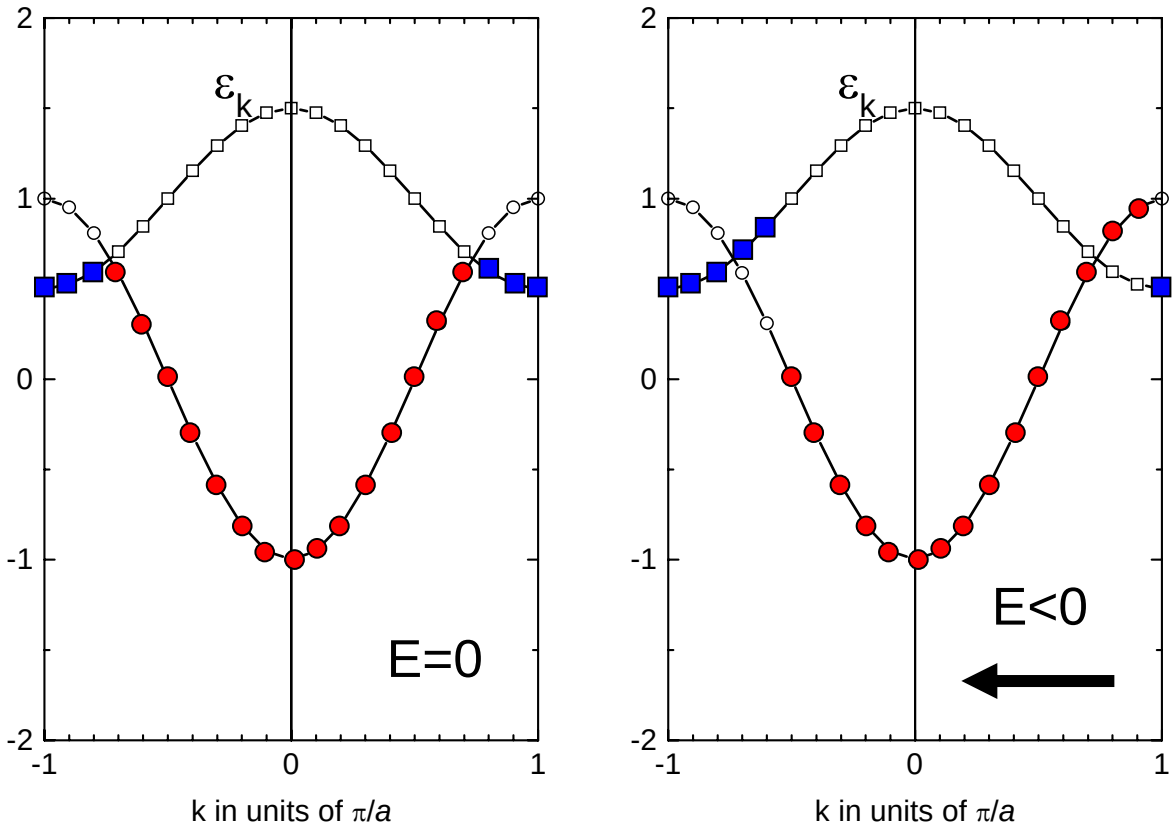


Fig. VIII.5: If two electronic bands overlap, a material made of atoms with two valence electrons is a metal as each band is not full. Therefore, each band can carry an electric current.

electrons in the upper band and conductivity remains negligible at all practical temperatures. This is for example the case of diamond.

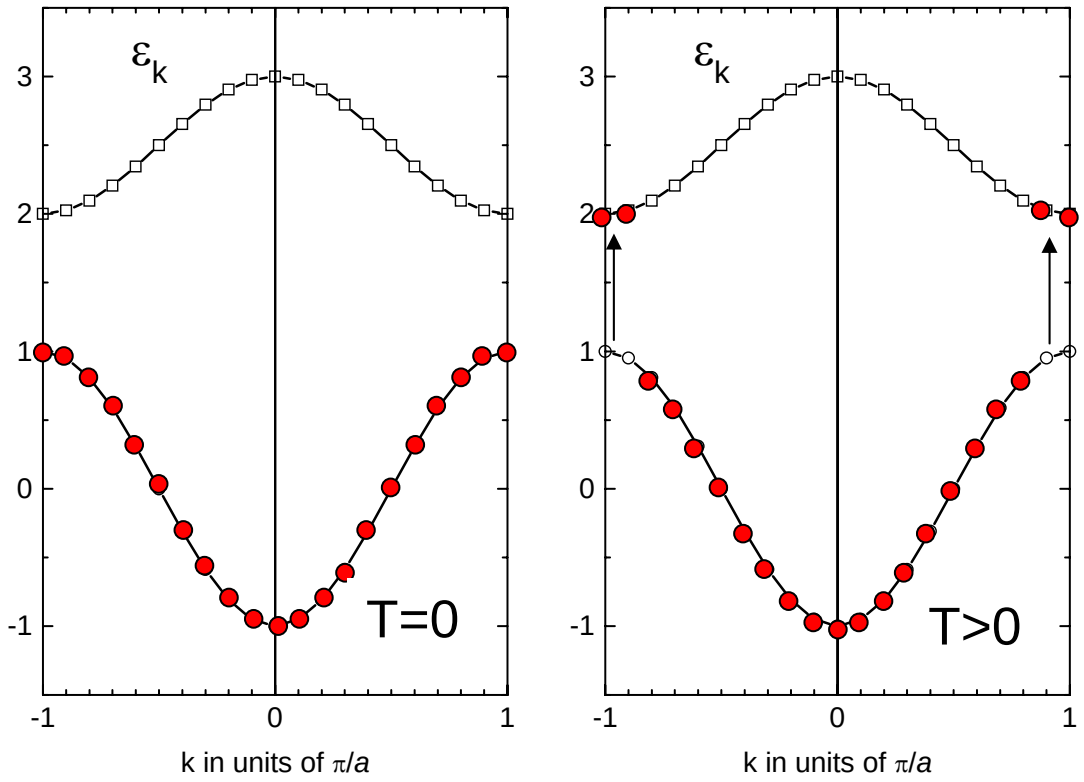


Fig. VIII.6: Excitation of electrons across the energy gap of a semiconductor. With increasing temperature, more and more electrons are thermally excited and the semiconductor becomes gradually a better conductor.

IX SEMICONDUCTORS

IX.1 Properties

Already in the 19th century it was well known that a certain class of materials, the semiconductors, exhibited rather anomalous properties such as:

- **Increase of conductivity** with increasing temperature (For metals, in the free electron approximation, the conductivity is given by $\sigma = ne^2\tau/m$. The only temperature dependence is in the relaxation time τ. Since an increase in temperature corresponds to an increase of disorder in the crystal lattice the conductivity decreases when T increase).

- **Photoconductivity**: Electrical conductivity is greatly increased by shining light of appropriate wavelength on a semiconductor.

- **Temperature dependent Hall effect**: in sharp contrast, for metals $R_H = -1/ne$ in the free electron model; R_H is thus constant.

We show in this Chapter that all these mysterious properties may be understood within an energy band theory. Later on, we shall also explain a technically extremely important property of semiconductors: the rectification of an electrical current by junctions of two different semiconductors. To get some insight into the nature of semiconducting materials let us look at the electrical resistivity ρ and the Hall constant R_H as a function of temperature for relatively pure Si (see Fig. IX.1). Both curves exhibit a linear dependence of the form $log\rho \propto 1/T$ or $logR_H \propto 1/T$ above approximately 500 K. We shall restrict ourselves now to this temperature range which is called the **intrinsic** region.

Although the free electron results

$$\rho = \frac{m}{ne^2\tau} \quad \text{and} \quad R_H = \frac{1}{(-e)n} \qquad (\text{IX.1}$$

cannot really be used here let us nevertheless see what Fig. IX.1 is telling us. From the fact that ρ is decreasing with increasing temperature we see that n (the concentration of charge carriers) should increase with temperature.

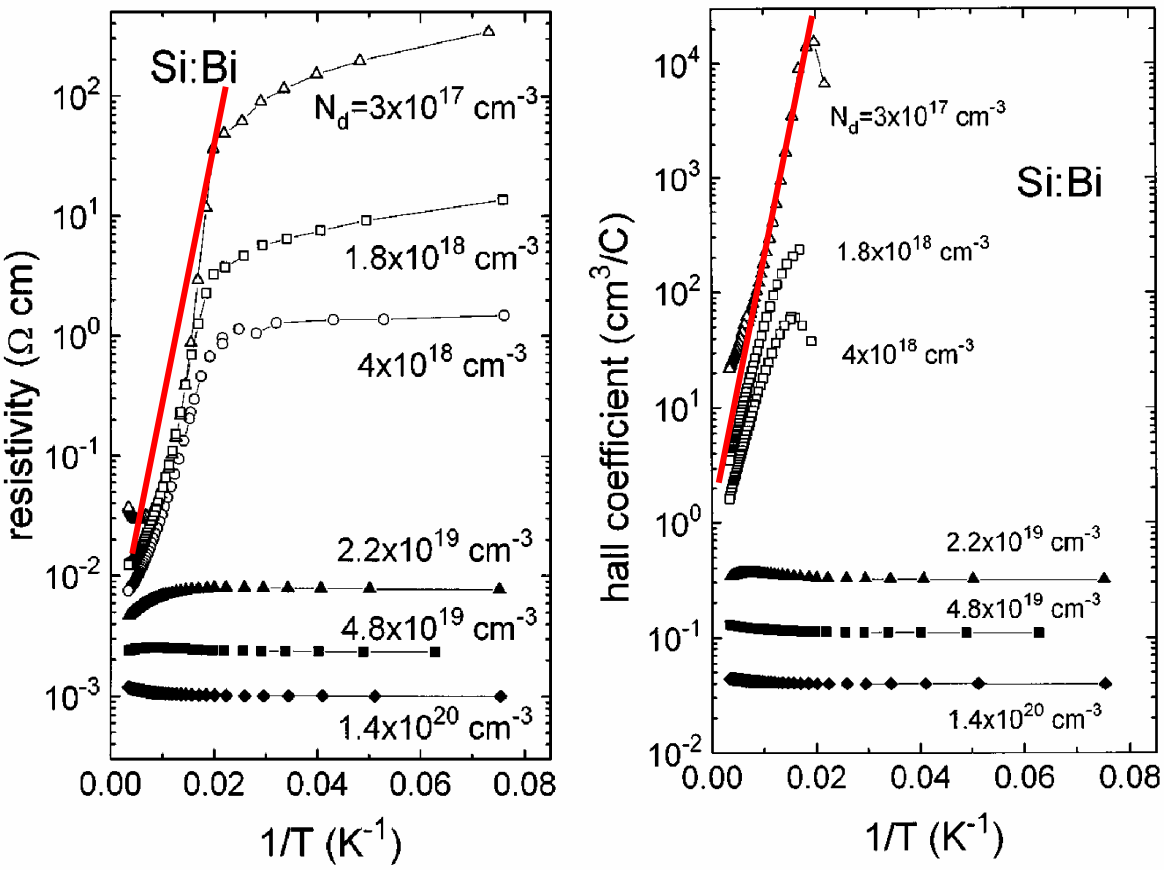


Fig. IX.1: Electrical resistivity ρ and Hall coefficient R_H as a function of temperature for Silicon (Si) containing various amounts of impurities (Bi: bismuth). Note the log-scale for ρ and R_H and the inverse temperature scale *1/T*. Above about 500 K we see (red curves) that $\rho \propto \exp(T_o/T)$ and $R_H \propto \exp(T_o/T)$ where T_o is a characteristic temperature (we shall see later that it is proportional to the energy gap. Below approximately 500 K, both ρ and R_H exhibit a significant departure from a straight line. This is due to impurity conduction (see Section IX.3).

This conclusion is confirmed by the Hall effect measurements that show that R_H is decreasing with temperature (because of the proportionality to *1/n*). The presence of an exponential relationship between ρ or R_H and *1/T* suggests very strongly that we have a population of energy levels according to a Boltzmann-type of statistics. How does it come that we do not have a Fermi-Dirac statistical distribution?
From the standard expression for the Fermi-Dirac distribution we see that

$$f(\varepsilon) = \frac{1}{e^{\frac{\varepsilon-\mu}{kT}} + 1} \cong e^{-\left(\frac{\varepsilon-\mu}{kT}\right)} \qquad \text{(IX.2}$$

if $\varepsilon\text{-}\mu >> kT$.

This means that in this regime the Fermi-Dirac distribution reduces to a Boltzmann distribution.

IX.2 Band structure of a semiconductor

The considerations made above suggest that a semiconductor can be modelled in the following way: A semiconductor is a material with two bands separated by an energy gap, so that

a) the first band is completely full at 0 K

b) the second band is completely empty at 0 K,

c) the true energy gap is small enough to make an excitation of an electron from the first band to the second band possible, the true energy gap is, however, large enough so that $f(\varepsilon) \cong e^{-\left(\frac{\varepsilon-\mu}{kT}\right)}$.This is shown schematically in Fig. IX.2 and a list of typical semiconductors is given in Table IX.1 together with their energy gaps E_g (measured at room temperature; note that due to both thermal expansion of the lattice and to lattice vibrations, E_g is a function of temperature).

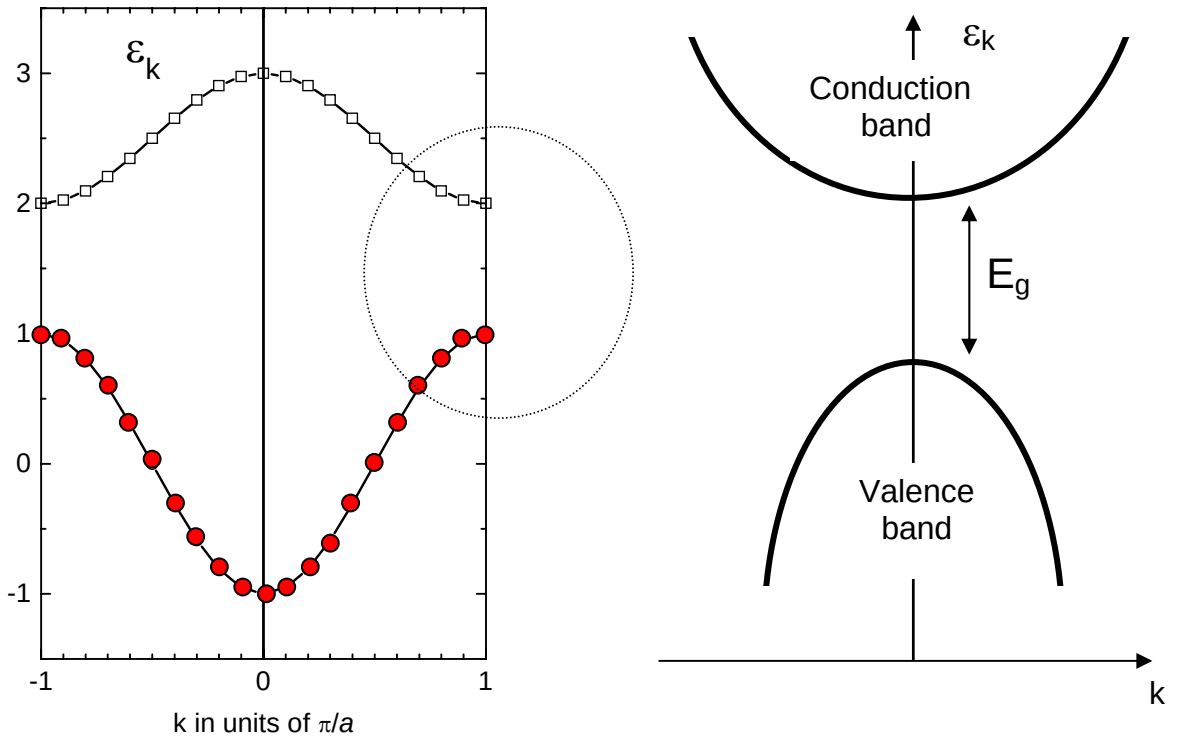


Fig. IX.2: Band structure of a semiconductor. The lowest band is called the **valence band** and the upper band is called the **conduction band**. At T = 0 K, all the states of the valence band are occupied and the conduction band is empty. The material is thus a perfect insulator. At T > 0 K both bands give a contribution to the electrical conductivity: hole conduction in the valence band and electron conduction in the conduction band. In the right panel we show the idealized model of the band structure of a semiconductor. In all the relations given in the text, we take the zero of energy at the top of the valence band.

All the action takes place in the encircled region indicated in Fig. IX.2. For the simplicity of the calculations let us further simplify the model of a semiconducting solid: we assume that the top of the **valence band** can be approximated by a dispersion relation of the form

$$\varepsilon_k = -\frac{\hbar^2 k^2}{2m_h} \qquad \text{(IX.3}$$

where m_h is the effective mass of a hole in the valence band, and that for the **conduction band**

$$\varepsilon_k = E_g + \frac{\hbar^2 k^2}{2m_e} \qquad \text{(IX.4}$$

where m_e is the effective mass of an electron in the second band. This model is shown in Fig. IX.2. The corresponding density of states are

$$g_h(\varepsilon) = \frac{m_h}{\hbar^2 \pi^2}\sqrt{\frac{2m_h(-\varepsilon)}{\hbar^2}} \qquad \text{(IX.5}$$

and

$$g_e(\varepsilon) = \frac{m_e}{\hbar^2 \pi^2}\sqrt{\frac{2m_e(\varepsilon - E_g)}{\hbar^2}} \qquad \text{(IX.6}$$

The position of the chemical potential μ is determined by the condition that the total number of electrons is conserved and thus independent of the temperature of the semiconductor. For a semiconductor without impurities this condition is equivalent to the condition that the number of holes in the valence band is equal to the number of the electrons in the conduction band i.e.

$$n_h = \int_{-\infty}^{0} [1 - f(\varepsilon)] g_h(\varepsilon) d\varepsilon = n_e = \int_{E_g}^{\infty} f(\varepsilon) g_e(\varepsilon) d\varepsilon \qquad \text{(IX.7}$$

Using the fact that the energy E_g (typically 1 eV) of the gap is much larger than the thermal energy, we find for the **valence band**

$$n_h = \alpha m_h^{3/2} \int_{-\infty}^{0} e^{(\varepsilon-\mu)/kT}\sqrt{(-\varepsilon)}\, d\varepsilon = \frac{(m_h kT)^{3/2}}{\sqrt{2\pi^3}\hbar^3} e^{-\mu/kT} \qquad \text{(IX.8}$$

Table IX.1: Experimental values for the energy gap E_g between the valence and the conduction band of typical semiconductor. Note that diamond is a limiting case between semiconductor and insulator. The values for E_g are for $T = 300$ K.

Material	E_g (eV)	Material	E_g (eV)
C (Diamond)	5.33	PbS	0.34
Si	1.14	PbSe	0.27
Ge	0.67	PbTe	0.30
InSb	0.23	CdS	2.42
InAs	0.33	CdSe	1.74
InP	1.25	CdTe	1.45
GaAs	1.4	Zn0	3.2
A1Sb	1.6-1.7	ZnS	3.6
GaP	2.25	ZnSe	2.60
SiC	3	AgCl	3.2
Te	0.33	AgI	2.8
ZnSb	0.56	Cu_20	2.1
CaSb	0.78	Ti02	3

and for the **conduction band**

$$n_e = \alpha m_e^{3/2} \int_{E_g}^{\infty} e^{-(\varepsilon-\mu)/kT} \sqrt{(\varepsilon - E_g)}\, d\varepsilon = \frac{(m_e kT)^{3/2}}{\sqrt{2\pi^3}\hbar^3} e^{(\mu - E_g)/kT} \qquad \text{(IX.9}$$

where $\alpha = \sqrt{2}/\pi^2\hbar^3$

From Eqs.IX.8 and 9 we obtain

$$m_h^{3/2} e^{(-\mu)/kT} = m_e^{3/2} e^{(\mu - E_g)/kT} \qquad \text{(IX.10}$$

which leads to

$$\mu = \frac{1}{2} E_g + \frac{3}{4} kT \ln\left(\frac{m_h}{m_e}\right) \qquad \text{(IX.11}$$

At T=0 K the chemical potential lies thus exactly in the middle of the gap. If m_e=m_h then μ=*(1/2)* E_g at all temperatures.
Inserting μ from Eq.IX.11 into Eq.IX.9 we can now calculate the number of electrons in the conduction band. We obtain

$$n_e = \frac{(kT)^{3/2}}{\sqrt{2\pi^3}\hbar^3} (m_e m_h)^{3/4} e^{-E_g/2kT} \qquad \text{(IX.12}$$

This means that the number of electrons is increasing in the way one expected from the experimental data shown in Fig. IX.1. The characteristic temperature T_o used to parameterise the experimental data is thus $k_B T_o = E_g/2$.
Since we have postulated parabolic energy bands, we can immediately write down the conductivity of our model-semiconductor (using the so-called Drude model)

$$\sigma = \sigma_e + \sigma_h = \frac{n_e e^2 \tau}{m_e} + \frac{n_h e^2 \tau}{m_h} \qquad \text{(IX.13}$$

Except at very low temperatures (but certainly in the so-called **intrinsic** region T > 300 K, see Fig. IX.1) the conductivity σ is entirely dominated by the exponential in Eq.IX.12. It is interesting to point out that the expression Eq.IX.12 can also be derived without calculating explicitly the temperature dependence of the chemical potential, since the expressions for n_e and n_h (Eqs.IX.8 and 9) lead to the very interesting property that

$$n_e n_h = \frac{(kT)^3}{2\pi^3 \hbar^6} (m_e m_h)^{3/2} e^{-E_g/kT} \qquad \text{(IX.14}$$

and consequently to

$$n_e \propto (kT)^{3/2} e^{-E_g/2kT} \qquad \text{and} \qquad n_h \propto (kT)^{3/2} e^{-E_g/2kT} \qquad \text{(IX.15}$$

The result in Eq. IX.14 (which is known under the **law of mass action**) is remarkable for two reasons

a) it does not depend on the chemical potential and

b) it does not depend on the number of atoms in the crystal. Note that this result (Eq.IX.14) was not established by requiring $n_e = n_h$. lt is valid also in the general case where n_e is different from n_h. How is it possible that $n_e \neq n_h$?

IX.3 Impurity states

It is a well-known experimental fact that the electrical properties of semiconductors are drastically modified by the presence of impurities. For example, an additional 10 ppm boron (B) in Si increases the conductivity of Si by a factor of 1000. Si has four valence electrons and crystallizes in the so-called diamond structure (see CD). The lines between ions represent covalent bonds (each bond accommodating 2 electrons). If one of the Si atoms is replaced by a Boron atom of valence 3 (in place of B one can also use Al, Ga or In) then one of the bonds will have a hole in which a valence electron could jump. If one electron is accepted by the Boron atom (which is called an **acceptor)** then a hole is created in the valence band. However, from Eq.IX.14 we see that if n_h increases then n_e should decrease and it is not clear at this point why impurities should increase drastically the conductivity of a semiconductor. We can also consider the

inverse case: if P, As or Sb is added to Si, then there is one electron in excess which moves around the pentavalent impurity (since 4 electrons are occupying bond states). The Coulomb field seen by the electron is that of a (+*e*) charge). One must not forget here that the excess electron is moving in a polarizable medium and that it does not see the bare vacuum Coulomb potential

$$V(r) = \frac{-e^2}{4\pi\varepsilon_0 r} \qquad \text{(IX.16}$$

but the screened potential

$$V(r) = \frac{-e^2}{4\pi\varepsilon_0 \varepsilon r} \qquad \text{(IX.17}$$

where ε is the dielectric constant of the material under consideration.

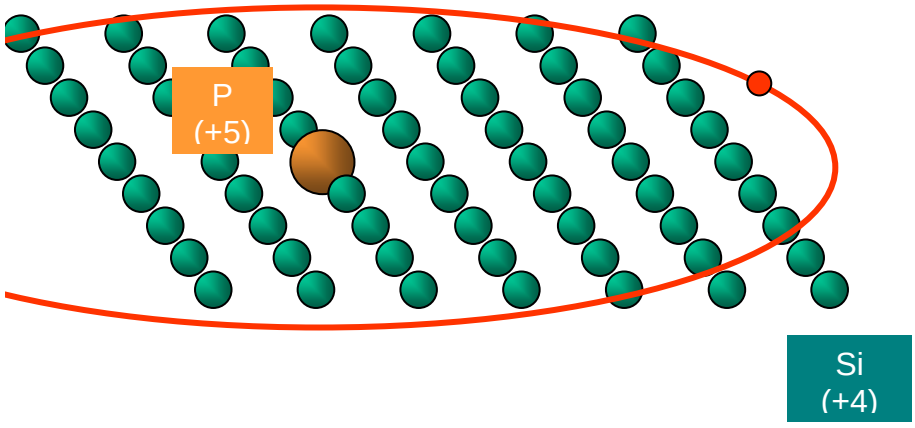


Fig. IX.3: Phosphorous (P; valence 5) impurity in silicon (valence 4). The extra electron of P is very loosely bound to the +1 effective charge of the Phosphorous. Its effective Bohr radius is of the order of 10 nm.

This approximation is only valid for large orbits and has to be justified a posteriori. The problem of an electron in a central potential of the form Eq.IX.17 is in fact that of the hydrogen atom if we replace e^2 by e^2/ε. Thus,

$$[\varepsilon_n]_{donor} = -\frac{m_e e^4}{8\varepsilon_0^2 \varepsilon^2 h^2}\frac{1}{n^2} = \frac{m_e}{m\varepsilon^2}[\varepsilon_n]_{H-atom} \qquad \text{(IX.18}$$

where ε= 15.8 for Ge and 11.7 for Si and m_e /m is typically of the order of 0.1. We see that therefore the ionization energy of the electron around a donor impurity is more than 10^3 times smaller than that of hydrogen (ε_I = - 13.6 eV) and is just a few 0.01 eV. This means that if this energy is provided to the electron it will leave the As atom and travel through the crystal as a **free conduction electron**. In presence of donor impurities we have to modify Fig. IX.2 as indicated in Fig. IX.4. One sees now which mechanism is going to enhance the conductivity so dramatically: due to the very small gap (E_d

between the donor levels and the bottom of the conduction band, it will be possible to excite many impurity electrons into the conduction band already at modest temperatures (i.e. below room temperature).

At low temperatures all donor levels are occupied with one electron. The chemical potential is then exactly at E_g-(1/2)E_d. With increasing temperature more and more of these electrons are excited into the conduction band. At high temperatures electrons from the valence band start to be excited and the chemical potential (Fermi energy) drops to approximately the middle of the intrinsic gap E_g. This is illustrated in the lowest panel of Fig. IX.5.

The same arguments can be developed for the **holes** in the valence band. If one dopes Si with a trivalent impurity, say In, then this impurity can capture an electron from the Si host. This captured electron orbits then around the In impurity and cannot contribute to conductivity. However, it leaves a hole in the valence band that is now no longer filled, and that is now able to transport electricity

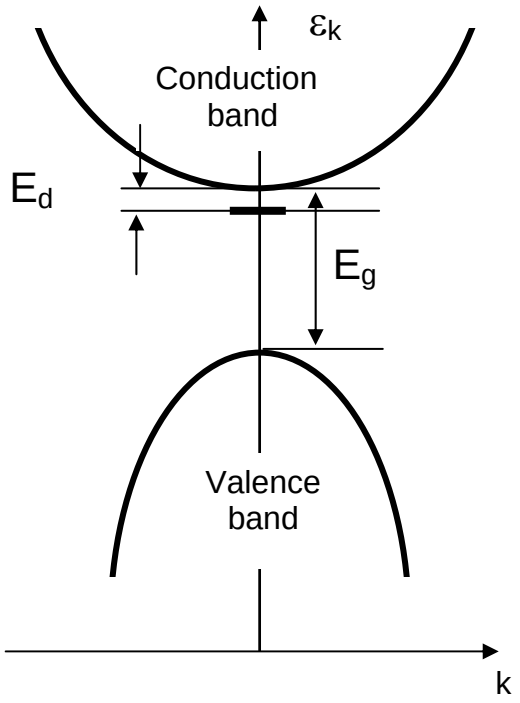


Fig. IX.4: Donor levels in a semiconductor with impurities of higher valence (e.g. P or As in Si). In equations below we write E_d for $|\varepsilon_{donor}|$.

.

In real semiconductors there are always acceptors and donors as the starting material is never completely free of impurities. However, by appropriate doping it is, for example, possible to have many more donors than acceptors. One speaks then of a **n-type material.** In the opposite case, when there are more acceptors than donors one speaks of a **p-type semiconductor**. One can calculate the temperature dependence of the density of electrons in the conduction band and the density of holes in the valence band. The results of such a calculation are shown in Fig. IX.6 for a n-type semiconductor with a density of donors $N_d = 10^{14}\ cm^{-3}$ and a 100 times lower density N_a of acceptors. The gap is 0.6 eV and the donors are 0.015 eV below the conduction band. The results are compared with measurements on *n*-type Si.

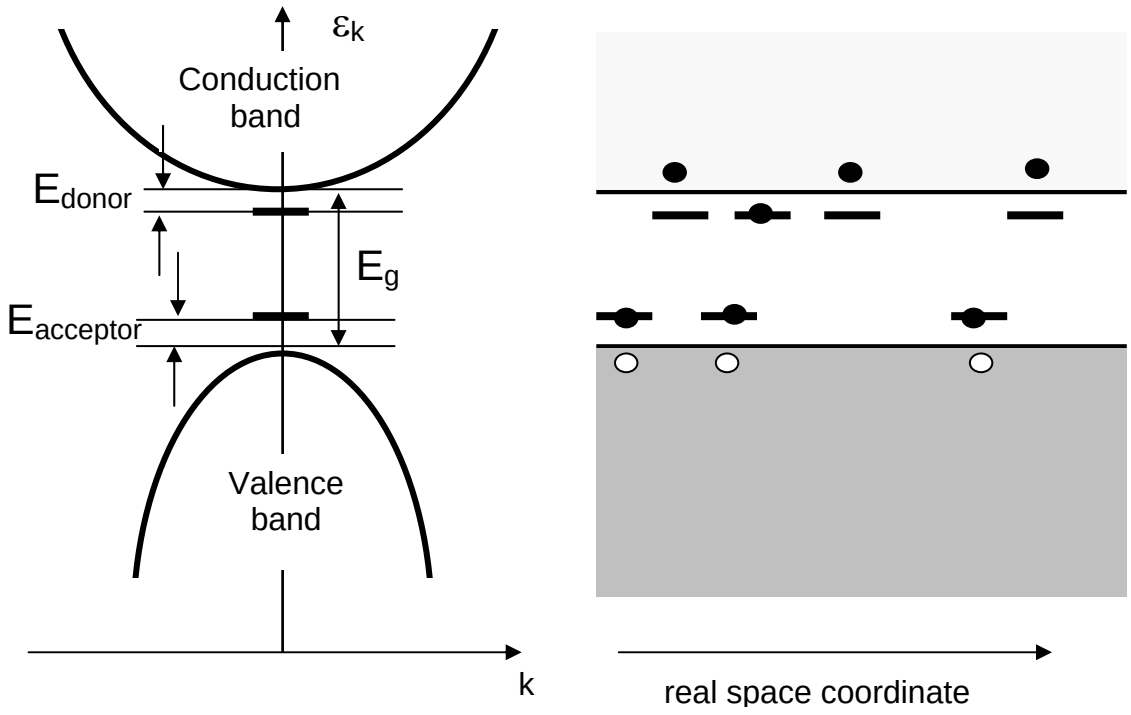
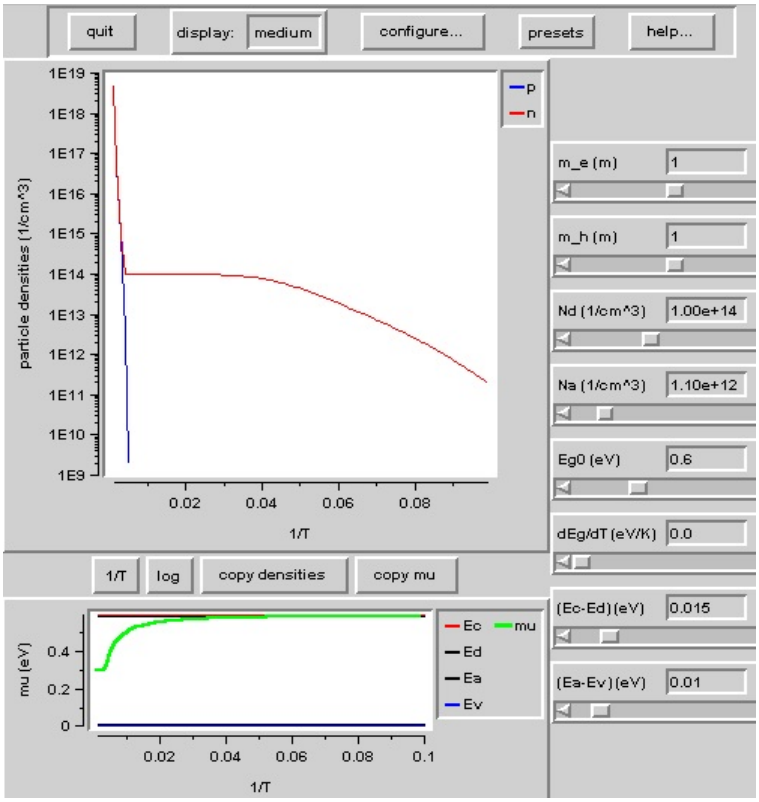


Fig. IX.5: *Left panel*: band structure of a semiconductor with donor levels and acceptor levels. *Right panel*: random distribution of donors and acceptors in a semiconductor. Note that in real space the top of the valence band and the bottom of the conduction band do not depend on position. However the impurity atoms (donors and acceptors) can be ionized or not. In the right panel 3 donor levels are ionized but one is still keeping its electron (black circle). The three acceptors have all captured an electron and thus there are three holes (white circle) in the valence band.



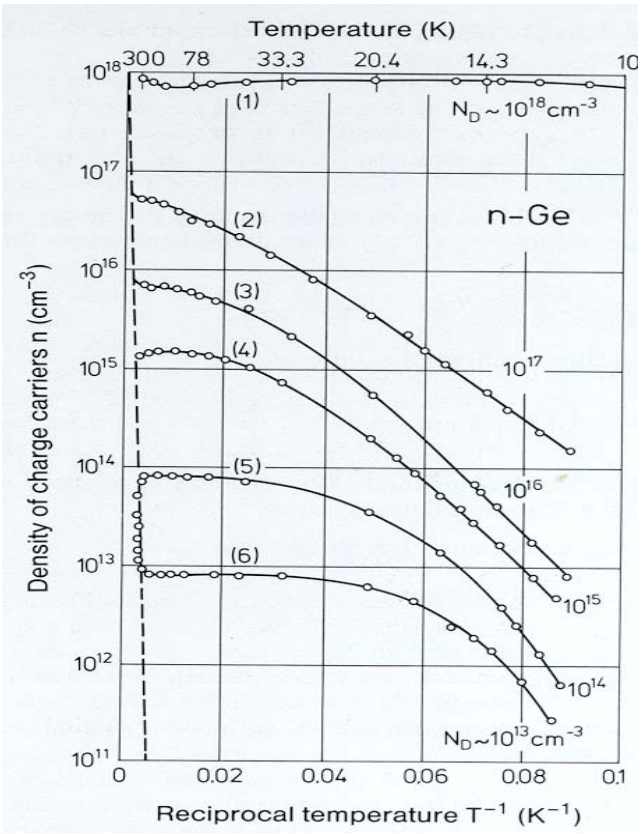


Fig. IX.6: Comparison of a calculated and measured charge carrier density (from Hall effect measurements). The main features are well reproduced. At low temperatures the density of electrons (our n_e is labelled n in the program and n_h is labelled p) varies exponentially with 1/T. The slope is, however much smaller than at high temperatures, since the position of the donors is only 0.015 eV below the conduction band, compared to 0.6 eV for the gap. Note that our E_{donor} corresponds to E_c-E_d in the program. As the density of acceptors is very low, holes in the valence band can only be created by exciting an electron from the valence band to the conduction band. This is not possible at low temperatures and, therefore p is much smaller than n.

IX.4 p-n junctions

It is possible to produce silicon crystals in which there are both p-type and n- type regions separated by a very narrow transition region (called the p-n junction). The width of this junction is of the order of 10^{-6} m and is thus much smaller than the diffusion length of electrons or holes. The n-region is obtained by doping a crystal with donor impurities and the p-region (of the same crystal) is obtained by doping with acceptor impurities. As a model of the junction let us consider the ideal case of a sharp transition as indicated in Fig. IX.7 to Fig. IX.12. In a Gedankenexperiment we visualise the fabrication of the p-n- junction as follows. We first prepare two separate samples: a p-type Si sample and a n-type Si sample. Then, at time t=0, we bring both samples into close contact with each other. We indicate now in steps what happens with the electron and hole distributions as a function of time.

Just after the two separate crystals (one p-type, the other n-type), are brought in contact with each other, the electrons, which are much more concentrated on the n-side than on the p-side start to diffuse into the p-region. Similarly the holes diffuse into the n-region since they are much more concentrated on the p-side. At equilibrium ($t = \infty$) the carrier concentration is as indicated in Fig. IX.8 and Fig. IX.10. It exhibits a very sharp drop at $x = d_n$ and $x = -d_p$. This can be understood as follows: The diffusion of electrons from n to p and the diffusion of holes from p to n cannot last forever because of the resulting space charge of the ionized donors on the n-side and acceptors on the p-side. This dipole-layer induces an electrical field directed in such a way as to inhibit the diffusion of electrons and holes. This electrical field is proportional to $N_d d_n$ and from charge neutrality $N_d d_n = N_a d_p$. This explains why d_n and d_p are finite. The sharp drop at d_n and d_p is a consequence of Eq. IX.14 which states that the product of electron concentration in the conduction band n_c times the hole concentration in the valence band n_v is constant. [Note that we use here n_c and n_v rather than n_e and n_h as in Section IX.1 since the number of conduction electrons is not equal to the number of holes in a doped semiconductor]. Typically $n_c n_v = 10^{26}$ cm^{-6}. Far from the junction $n_c = N_d$ and $n_v = n_v$ $(-\infty)$ on the *n*-side and $n_v = N_a$ and $n_c = n_c$ (∞) on the *p*-side. For a typical semiconductor with $N_d = 10^{17}$ cm^{-3} we have thus n_v $(\infty) = 10^9$ cm^{-3}. Somewhere between $-d_p$ and $+ d_n$ we must therefore have $n_c = n_v$ as can be seen from Fig. IX.8 and Fig. IX.10. This implies $n_c = n_v = 10^{13}$ cm^{-3} at this point. As can be seen by comparing this value with $N_d = 10^{17}$ cm^{-3} the carrier concentration is 10^4 times smaller in the junction region than far away from it. This is the reason why this region is called the **depletion region**.

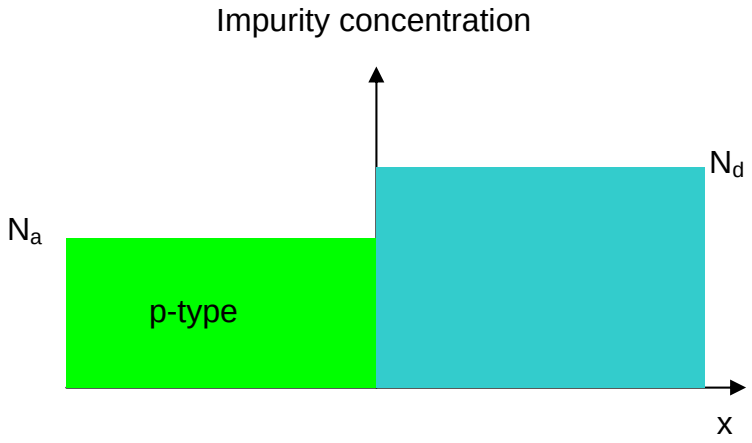


Fig. IX.7: Concentration of donors and acceptors on both sides of our idealised *p-n* junction. On the p-side $N_d = 0$ and on the n- side $N_a = 0$. At sufficiently high temperatures (certainly at 300 K) all the donors are ionised. The electron concentration on the *n*-side is equal to N_d. Similarly, the hole concentration on the p-side is equal to N_a

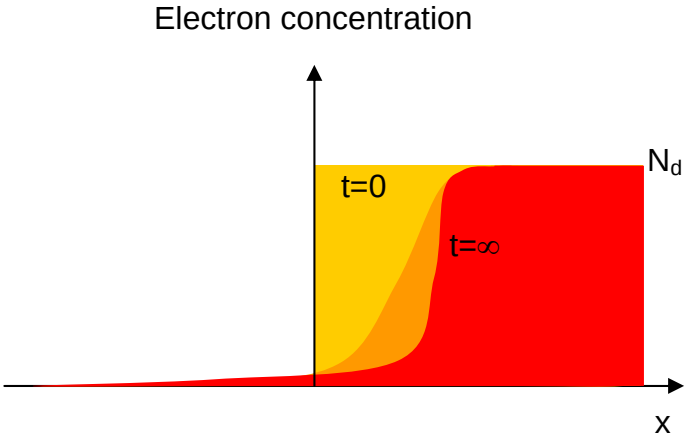


Fig. IX.8: Electron concentration as a function of time. Far from the junction we assume that at the temperature of interest all the donors are ionized. Immediately after "gluing" the *p*-side with the *n*-side the electrons close to the junction spill over to the *p*-side because of the sharp concentration gradient at x = 0. The electric field which is set up leads to an equilibrium electron concentration profile with a sharp edge at a distance d_n, from the junction.

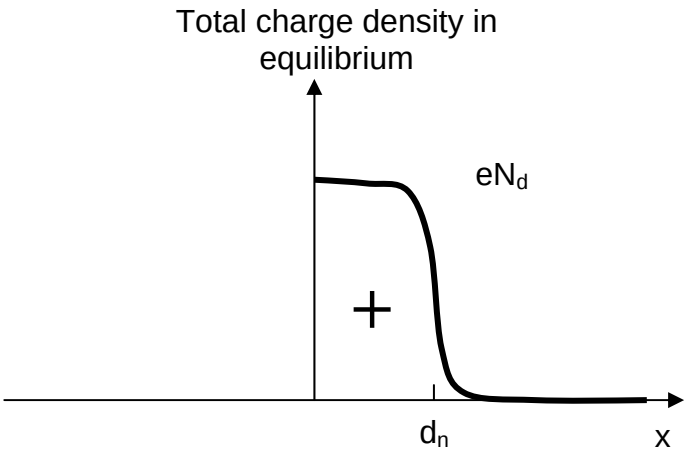


Fig. IX.9: Total charge density on the *n* - side. The electrons that have diffused from the *n*-side to the *p*-side leave an overall positive space charge behind (ionized donors) on the *n*-side

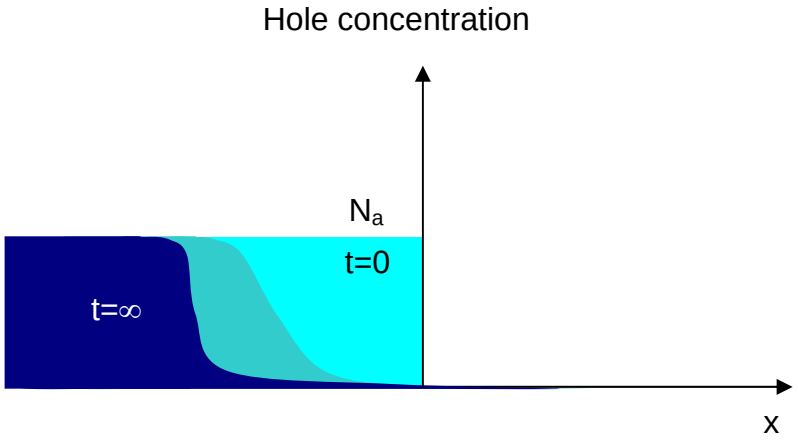


Fig. IX.10: Hole concentration. Far from the junction we assume that at the temperature of interest all the acceptors are ionized. Close to the junction the holes spill over to the *n*-side because of the sharp concentration gradient at x = 0. The electric field which is set up leads to an equilibrium hole concentration profile with a sharp edge at a distance d_p from the junction.

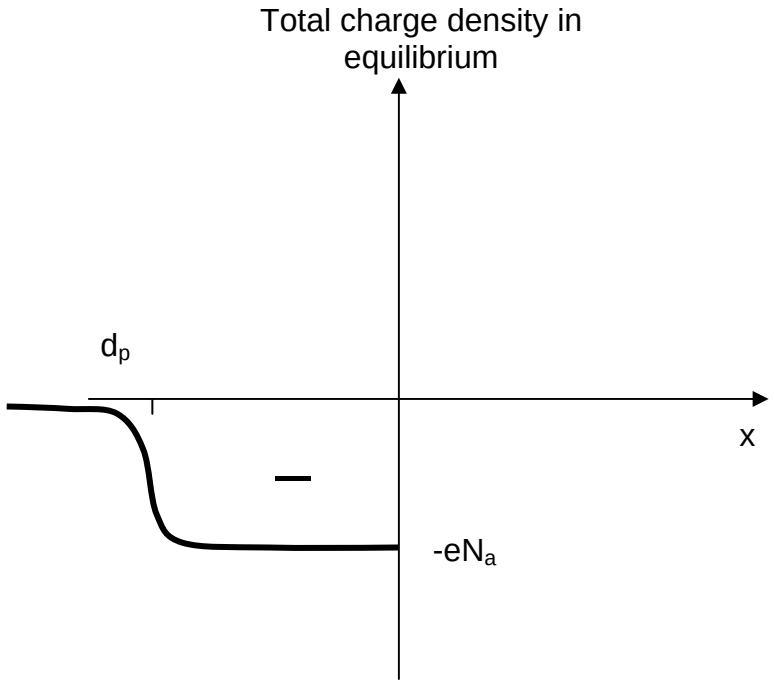


Fig. IX.11: Total charge density on the *p* - side. The holes that have diffused from the p-side to the *n* - side leave an overall negative space charge behind (ionized acceptors) on the *p*-side

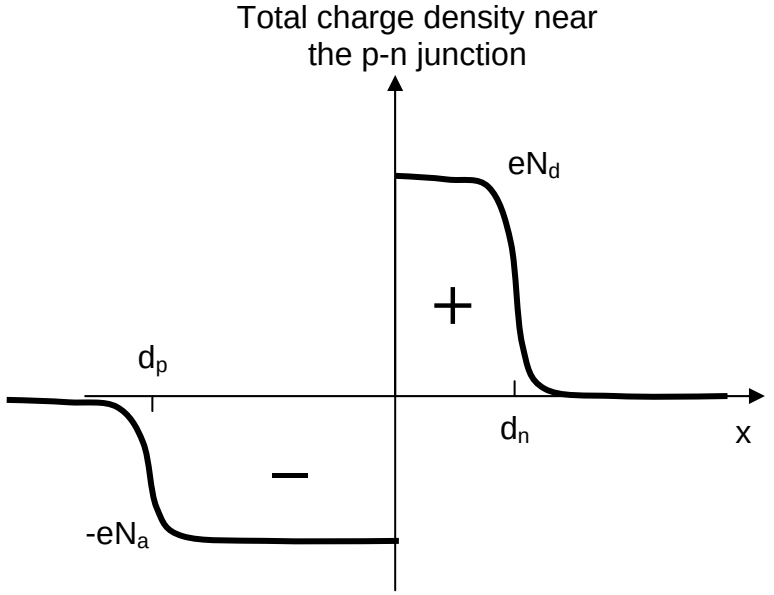


Fig. IX.12: Charge density around the p-n junction obtained by superposition of the charges in **Fig. IX.9** and **Fig. IX.12**. The resulting dipole layer leads to an electric field so that the potential energy of an electron on the *p*-side is **higher** than on the *n*-side

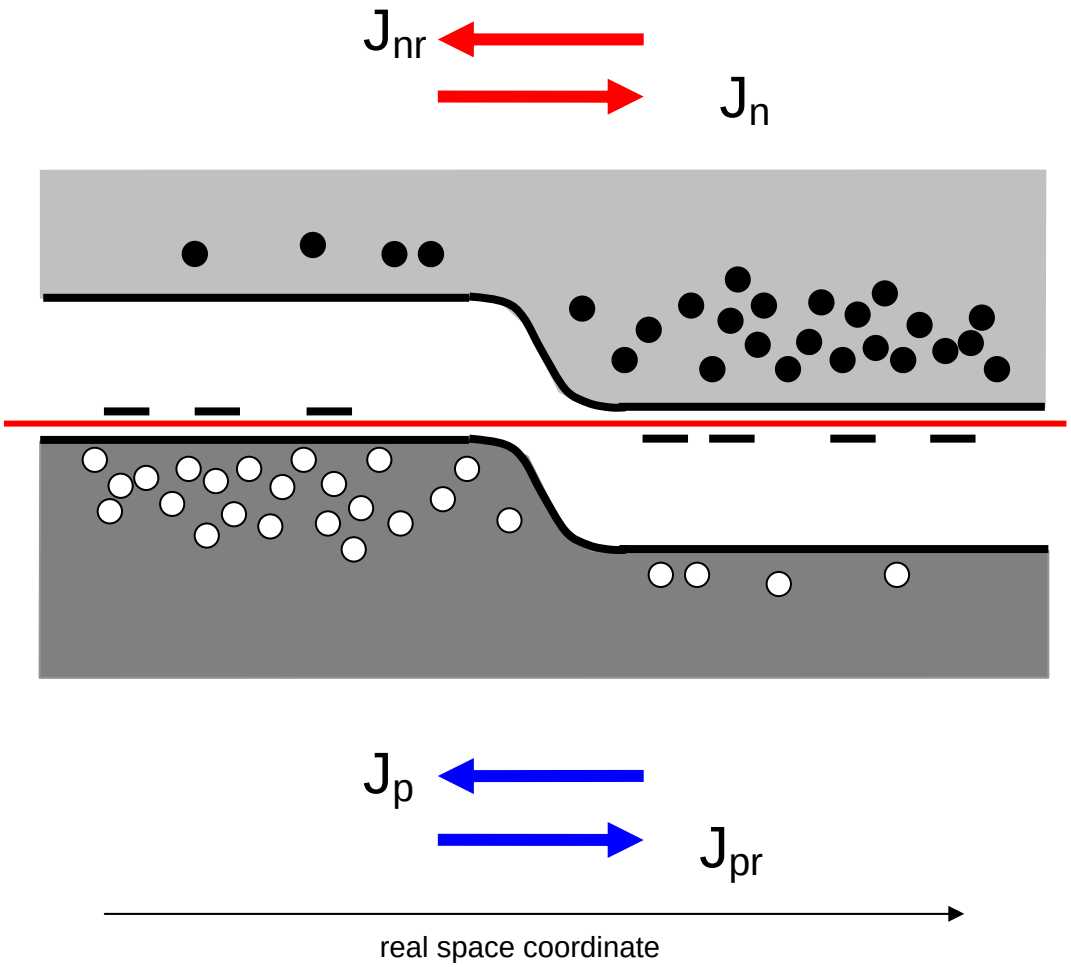


Fig. IX.13: Position of the energy bands near a *p* - *n* junction. The black dots and the white dots indicate symbolically the concentration of electrons and holes, respectively. The chemical potential μ (red line) is constant as required by general thermodynamical considerations.

We have now all ingredients to understand the rectifying properties of a *p*-*n* junction. For this let us represent the position of the top of the valence band and the bottom of the conduction band as a function of *x* by means of the following picture.
The electrical field **E** makes it difficult for electrons to diffuse from *n* to *p* and for holes to diffuse from *p* to *n*. It is, however, not high enough to prevent every electron to travel from *n* to *p* because electrons can recombine with one of the many holes on the *p*-side. There is thus always a certain **recombination current** J_{nr} from *n* to *p* for electrons (similarly J_{pr} from *p* to *n* for holes). At equilibrium, J_{nr} (or J_{pr}) is, however, exactly compensated by J_{ng} (or J_{pg}), the so- called **generation current**: it is obvious from Fig. IX.14 that if an electron excited thermally on the *p*-side reaches the depletion region it will be accelerated by the electrical field towards the *n*-region. The compensation

$$J_{ng} = J_{nr} \qquad \text{(IX.19}$$

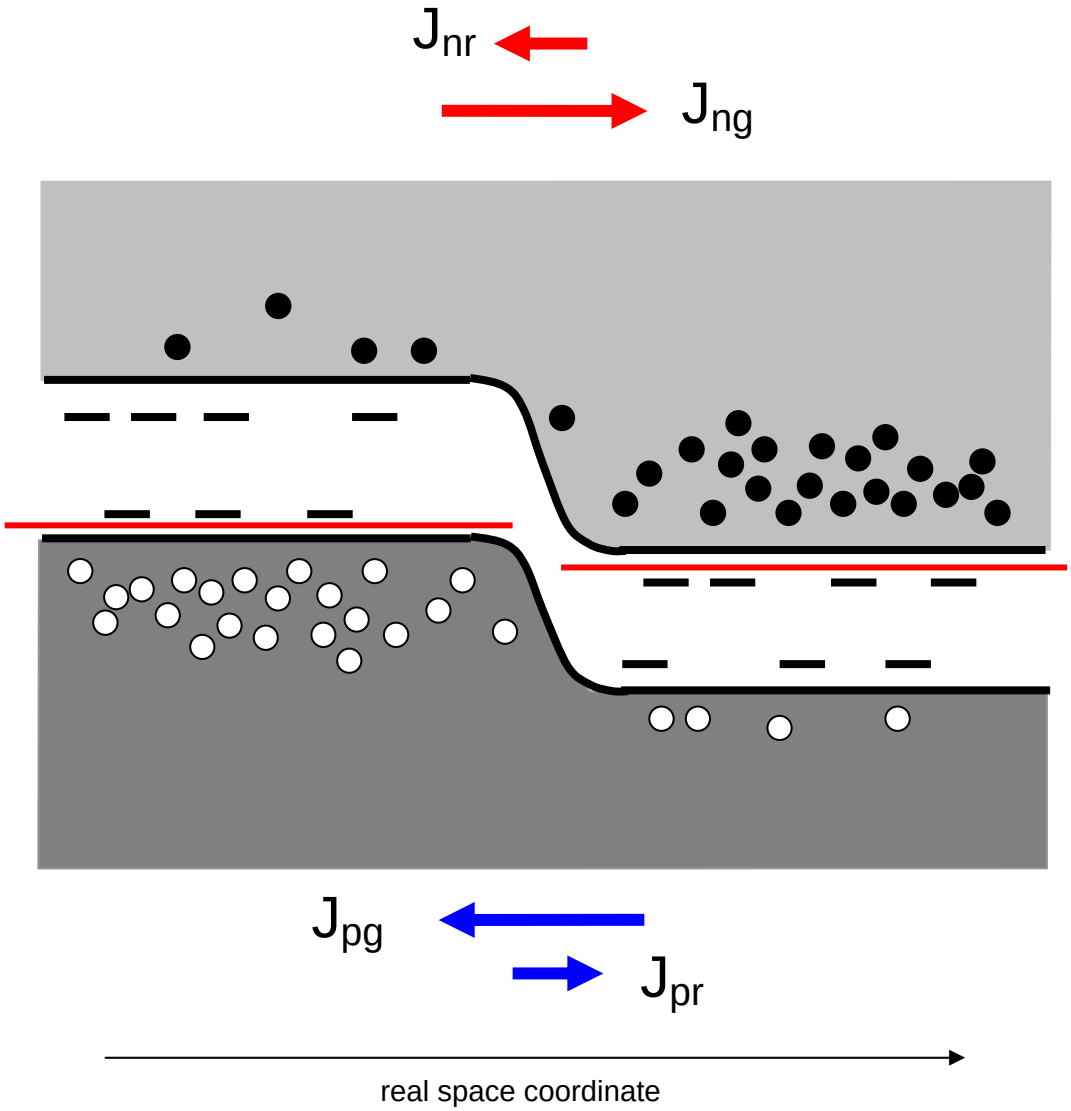


Fig. IX.14: Effect of an external voltage on the energy bands near a *p-n* junction. The voltage is such that the *p*-side becomes less attractive for electrons. In other words the negative electrode of the battery is connected to the *p*-side. The generation currents of electrons and holes is essentially not affected by the voltage. However, the recombination currents decrease strongly since the charge carriers have now to climb up a higher hill. This is the **backward voltage regime.**

is necessary to prevent a piling up of charges on one side of the junction. Let us now apply an external voltage V and see what happens to the bands shown in Fig. IX.14.
The generation current J_{ng} remains approximately constant as it is controlled by the excitation rate of electrons in the bulk of the p-material (far from the junction; do not forget that $d_n + d_p \sim 10^{-4}$ cm while the diffusion length for holes and electrons is 10^{-1}

cm). The recombination current, on the other hand, depends critically on the height of the barrier. We have

$$J_{nr}(V) = J_{nr}(V=0)e^{eV/kT} \qquad \text{(IX.20}$$

if we assume that the Fermi-Dirac distribution can be approximated by a Boltzmann-distribution. Note that the voltage in the backward regime considered here is negative. The total electron current (number of electrons/m^{2}s) is thus

$$\begin{aligned} J_n &= J_{nr}(V) - J_{ng}(V) = \\ &= J_{nr}(V) - J_{ng}(V=0) \\ &= J_{nr}(V=0)e^{eV/kT} - J_{ng}(V=0) = J_{ng}(V=0)\left(e^{eV/kT} - 1\right) \end{aligned} \qquad \text{(IX.21}$$

The electrical current due to the electrons is

$$j_n = -eJ_n = -eJ_{ng}(V=0)\left(e^{eV/kT} - 1\right) \qquad \text{(IX.22}$$

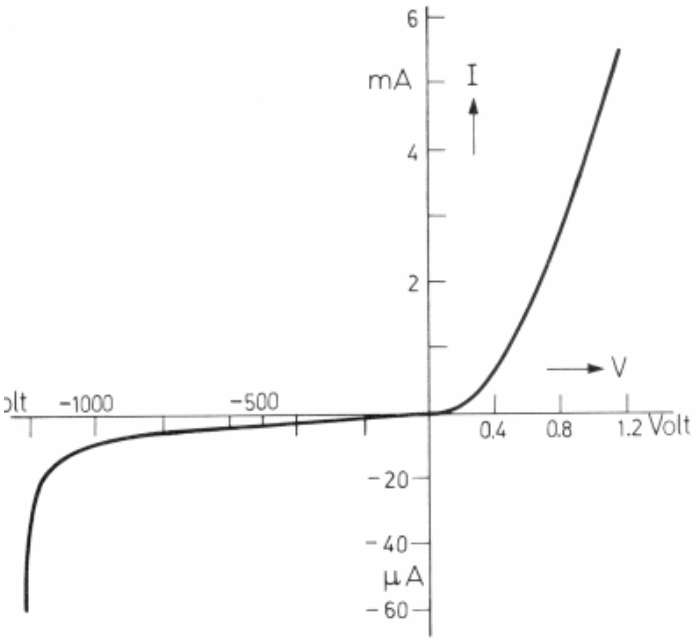


Fig. IX.15: Current(I) versus voltage(V) characteristics for a germanium p-n junction. Note the marked asymmetry between the forward regime (V > 0) and the backward regime (V < 0), which leads to the rectifying property of the p-n junction. Note also the use of completely different scales for the forward and backward voltage regime.

The total electrical current (electrons + holes) is thus (we do not repeat the argument for the holes)

$$j = j_g\left(e^{eV/kT} - 1\right) \qquad \text{(IX.23}$$

where j_g is the sum of the generation electrical currents. This relation is found to be in good agreement with experimental data in germanium.

The *p-n* function is only one of the numerous "solid-state" devices that are found nowadays in almost any apparatus such as radio, television, computers, etc. It is, however, a nice example that demonstrates some of the basic phenomena taking place in the class of semiconducting materials.



To conclude this Chapter let us note once more that the main properties of semiconductors can be understood within the framework of a simple (one-electron) band structure approach. For metals the situation is much more complicated. The conductivity of metals is already large at low temperatures and the concentration of carriers is independent of temperature. It is, however, well known that the resistivity of metals increases with increasing temperature, or equivalently, that the conductivity of metals decreases with increasing temperature. There must therefore be "something" which slows down electrons at higher temperature. These are the phonons (lattice vibrations) treated in Section X.4, which are able to scatter electrons. This scattering increases with increasing temperature. The treatment of electron-phonon scattering falls, however, outside the scope of this introductory lecture notes.

X LATTICE VIBRATIONS AND PHONONS

In previous chapters we were only interested in electronic states and solved Schrödinger's equation for electrons (or one electron) in a (periodic) potential arising from ions. These ions were held fixed. This is certainly not realistic around room temperature (where some metals such as mercury (Hg) and gallium (Ga) are liquids) and at higher temperatures where solids emit radiation due to their vibrating ions (black body radiation).

X.1 Linear chain of atoms

To get some insight in lattice vibrations let us consider a linear chain of N-atoms with a lattice constant equal to a. Between each atom we imagine a spring with a spring-constant K. These springs are simulating the interaction between ions (or atoms) in a solid.

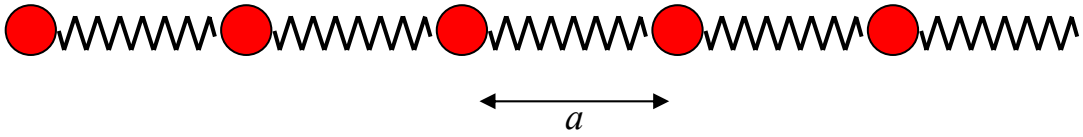


Fig. X.1: A linear chain of N atoms.

Let us assume now that due to thermal agitation all these ions are somehow oscillating around their equilibrium position. At a certain instant we have the situation shown in Fig. X.2. The displacements u(x) are sufficiently small so that on the average the ions remain in the same place.

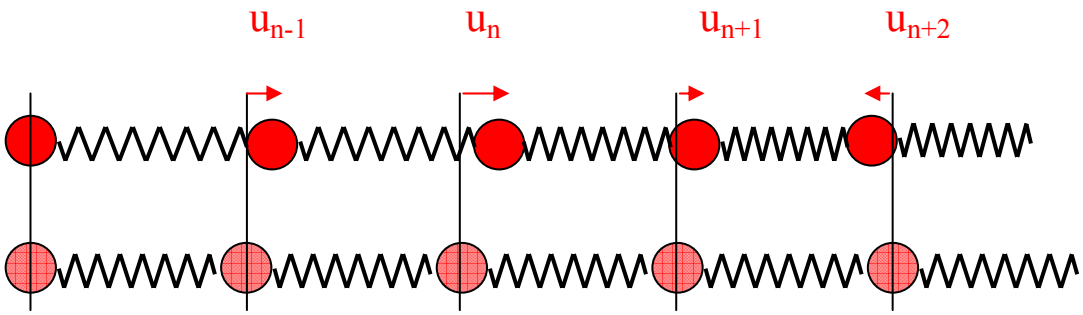


Fig. X.2: A linear chain of N vibrating atoms (upper chain). The displacements u_n are measured with respect to the atomic positions on the non-vibrating chain (lower chain).

The force F acting on the ion at position x = na is given by

$$F = +K\left(u_{n+1} - u_n - \left(u_n - u_{n-1}\right)\right) = +K\left(u_{n+1} - 2u_n + u_{n-1}\right) = M\,\frac{d^2u_n}{dt^2} \qquad \text{(X.1}$$

The last line in Eq.X.1 is nothing but Newton's law. The differential equation to be solved is thus

$$M\,\frac{d^2u_n}{dt^2} = -K\left(2u_n - u_{n+1} - u_{n-1}\right) \qquad \text{(X.2)}$$

By analogy with the problem of a single mass M attached to a fixed point by means of a spring with spring constant K, i.e. a system described by the differential equation

$$M\,\frac{d^2u}{dt^2} = -Ku \qquad \text{(X.3)}$$

which has a solution of the form $e^{i\omega t}$, we try to solve Eq.X.2 with the following Ansatz,

$$u_n(t) = const\, e^{i(qna - \omega t)} \qquad \text{(X.4)}$$

Introducing the Ansatz X.4 into Eq. X.3 we obtain

$$-\omega^2\, e^{i(qna-\omega t)} = -\frac{K}{M}\left[2\, e^{i(qna-\omega t)} - e^{i(q(n+1)a-\omega t)} - e^{i(q(n-1)a-\omega t)}\right]$$

$$\omega^2 = \frac{K}{M}\left[2 - e^{iqa} - e^{-iqa}\right] = \frac{K}{M}2\left[1-\cos(qa)\right] \qquad \text{(X.5)}$$

This shows that the frequency ω of a vibration mode depends on the wave vector $q = 2\pi/\lambda$ of the mode. The dispersion relation $\omega_q = \omega(q)$ is easily obtained by noting that

$$\omega_q = \sqrt{\frac{2K}{M}}\left(1-\cos(qa)\right)^{1/2} = \sqrt{\frac{2K}{M}}\left(2\sin^2\left(\frac{qa}{2}\right)\right)^{1/2} \qquad \text{(X.6)}$$

and finally

$$\omega_q = 2\sqrt{\frac{K}{M}}\left|\sin\left(\frac{qa}{2}\right)\right| \qquad \text{(X.7)}$$

This resembles strongly Eq. III.21 that describes the dispersion relation $\varepsilon_k = \varepsilon(k)$ of a conduction electron in the tight-binding approximation. This resemblance is explicitly shown in Fig. X.5.

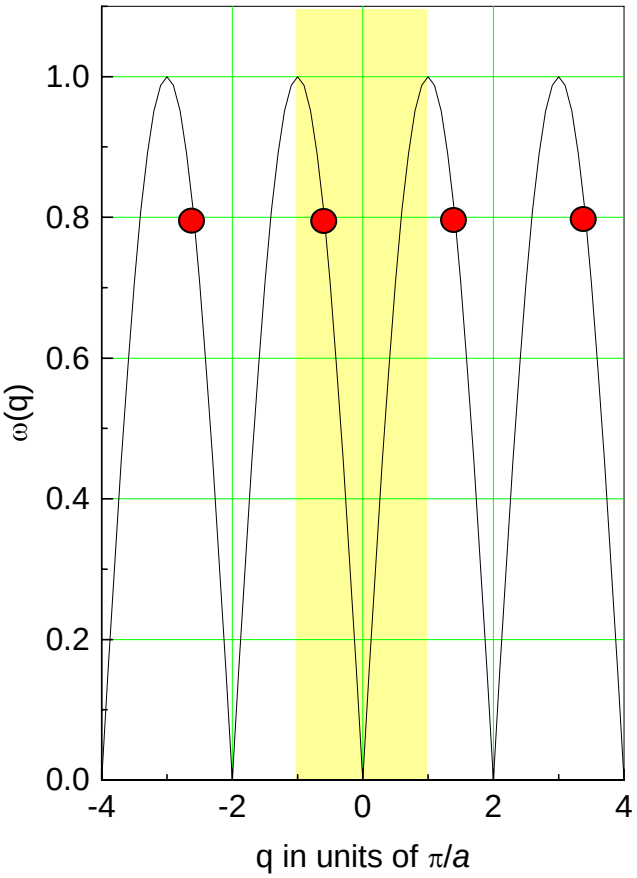


Fig.X.3: Dispersion relation $\omega_q = \omega(q)$ for a linear chain of atoms, as predicted by Eq.X.7. The Brillouin zone is indicated in yellow. All the states in red are equivalent.

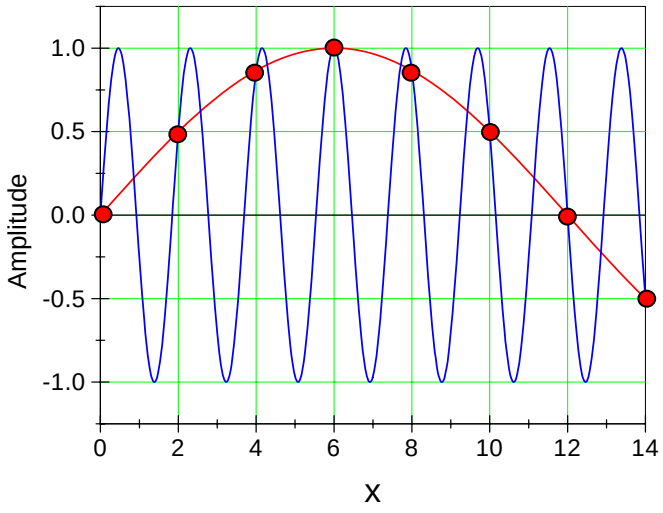


Fig. X.4: It is possible to describe the displacement of ions by means of various waves. The red line has a wavelength $\lambda = 12a$, the blue line $\lambda = (12/13)a$. For clarity, we have chosen a transverse wave.

Another way of seeing the equivalence of states at q and $q+2\pi m/a$ (m: integer) is obtained from Eq.X.4

$$u_{n,q} = const\ e^{i(qna-\omega t)} \qquad \text{(X.8)}$$
$$u_{n,q+2\pi m/a} = const\ e^{i[(q+2\pi m/a)na-\omega t]} = const\ e^{i(qna-\omega t)}\ e^{i2\pi mn}$$

as $m \cdot n = s$ is also an integer, we have $e^{2\pi is} = 1$. As in the case of energy band structures obtained for an electron in a periodic potential we can thus restrict ourselves to the Brillouin zone.

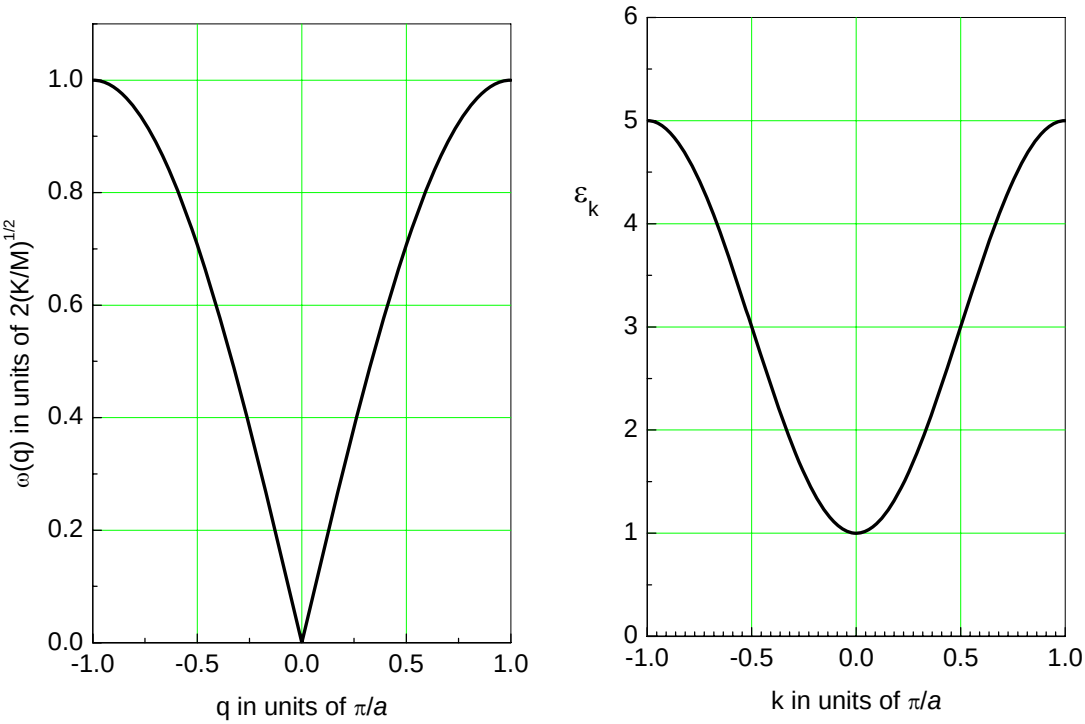


Fig. X.5: Comparison of the phonon dispersion curve *(left)* and the band electronic band structure of a linear chain. The Brillouin zone is the same for both.

X.2 Periodic boundary conditions

Exactly as for an electron in a periodic potential we use here periodic boundary conditions which, according to Born and von Karman can be written as

$$u_{0,q} = u_{N-1,q} \qquad \text{(X.9}$$

This implies that

$$1 = e^{iq\cdot 0\cdot a} = e^{iq\cdot(N-1)\cdot a} = e^{iq\cdot L} \qquad \text{(X.10}$$

Thus

$$q = \frac{2\pi}{L} m \quad \text{with} \quad m = 0, \pm 1, \pm 2, ... \qquad \text{(X.11}$$

which is of the same form as Eq.III.7. As for electrons, we have thus N possible wave vectors in the Brillouin zone.

X.3 Longitudinal and transverse modes

For a given wave vector **q** there are three types of displacements: one with displacement parallel to **q** and two perpendicular to it. There are thus 1 longitudinal and 2 transverse waves. For a linear chain it is evident that the restoring force for a longitudinal displacement is larger than for a transverse displacement. The longitudinal wave has consequently a higher frequency than the transverse one. By symmetry the two transverse waves have the same frequency. In a 3D-solid this is not necessarily true. This is shown for Copper in Fig. X.6. The density of modes is defined in analogy with the density of states for electrons.

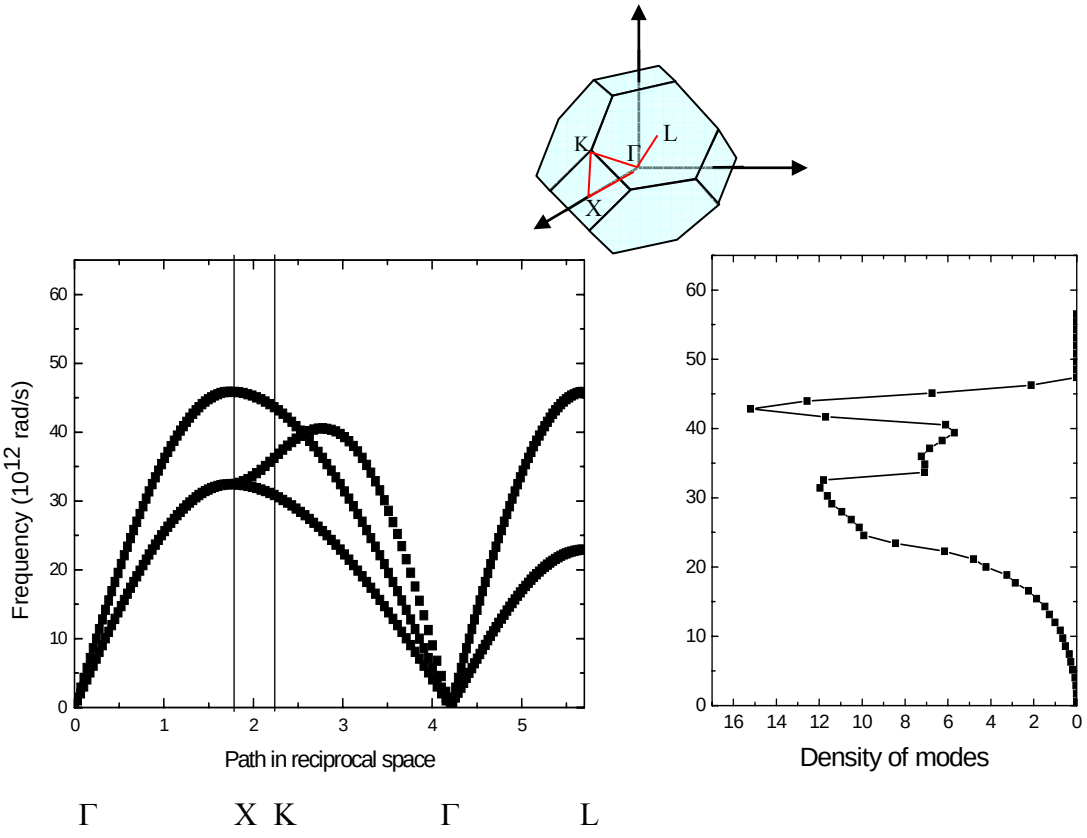


Fig. X.6: Lattice vibration modes *(left panel)* and density of modes *(right panel)* for Copper (Cu). The path chosen for the representation of the vibration modes is shown in the Brillouin zone. For each **q**-vector there are three vibration modes. Note that in contrast to the linear chain, the transverse modes are not always degenerate. The density of modes has sharp peaks whenever the vibration dispersion curves are flat.

X.4 Phonons

Until now the vibrations of ions have been treated within the framework of classical mechanics. Is this a valid approach? One good reason to believe that this is not the case is shown in Fig. X.7. From specific heat measurements it is well known that C decreases with decreasing temperature to vanish at $T = 0$ in agreement with the third law of thermodynamics. If ions were classical objects one would expect that the equipartition principle would hold. (Reminder: the equipartition principle states that the average energy of a particle at temperature T is ½ $k_B T$ per degree of freedom.) For a solid consisting of atoms attached to a rigid lattice by means of a spring (3-dimensional harmonic oscillator) there are 6 degrees of freedom (3 "kinetic"+ 3 "potential"). For a solid consisting of N atoms the total energy would thus be

$$U = N \cdot 6 \cdot \tfrac{1}{2} k_B T = 3 k_B N T \qquad \text{(X.12)}$$

and consequently

$$C_v = \frac{dU}{dT} = 3 k_B N \qquad \text{(X.13)}$$

This result which is known as the law of **Dulong and Petit** is in manifest disagreement with the experimental data in Fig. X.7. These experimental data indicate also clearly that already at room temperature diamond behaves quantum-mechanically!

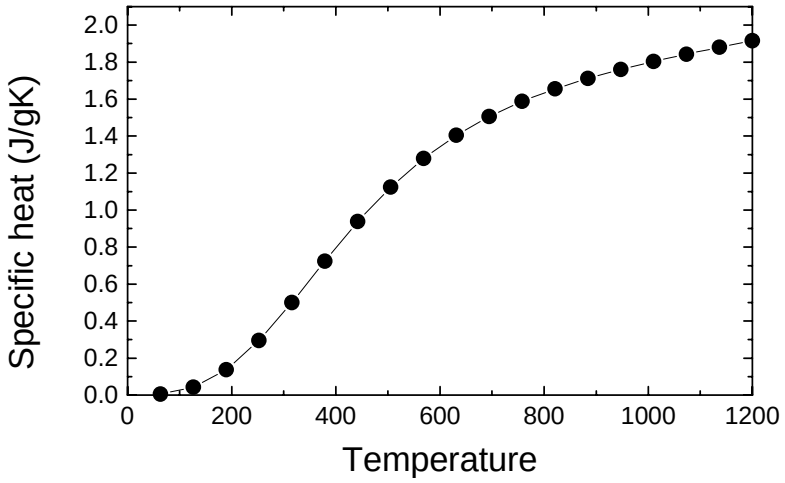


Fig. X.7: Specific heat of diamond. The experimental data (black dots) are in excellent agreement with Debye's model (full line)

Having made this important observation, the problem is now to give a quantum mechanical description of lattice vibrations. This is in fact quite straightforward when one realizes, in a harmonic solid (i.e. a solid in which the displacements of atoms are directly proportional to the forces), that the 3N modes are independent of each other. Each mode can then be viewed as an harmonic oscillator with energy levels

$$\varepsilon_{\mathbf{n,q,s}} = \left(n_{\mathbf{q,s}} + \tfrac{1}{2}\right) \hbar\omega_{\mathbf{q,s}} \qquad \text{(X.14)}$$

The energy $\varepsilon_{\mathbf{n,q,s}}$, the frequency $\omega_{\mathbf{q,s}}$ and the occupation number $n_{\mathbf{q,s}}$ of this vibration mode depend on the wave-vector **q** and the polarisation vector **s**. Except for the indices **q** and **s** Eq. X.14 is just what you learned in first year quantum physics.

Now comes an important point. In solid state physics one does not use too often the name of excitation number $n_{\mathbf{q,s}}$ of a state **q** with polarisation **s**. One follows rather the language of quantum theory of electromagnetic fields and says that there are $n_{\mathbf{q,s}}$ **phonons** (in analogy with **photons** for light) with wave vector **q** and polarisation **s** in the crystal. The phonons are thus viewed as particles. These particles are, however, not usual particles. One phonon corresponds in fact to a vibration mode of all the ions of a solid. Phonons are just one special case of excitations in solids. To distinguish them from usual particles one calls them **quasiparticles**.

Phonons have zero spin: they are therefore **bosons**. Furthermore, the number of phonons (very much like for photons) is not conserved in a crystal in contrast to the number of electrons in a metal. This implies that their chemical potential is zero and that the average occupation number of a given mode is given by the Bose-Einstein distribution function

$$n_{\mathbf{q,s}} = \frac{1}{e^{\hbar\omega_{\mathbf{q,s}}/k_B T} - 1} \qquad \text{(X.15)}$$

At high temperature $\hbar\omega < k_B T$ (we drop the indices **q** and **s** for simplicity)

$$e^{\hbar\omega/k_B T} = 1 + \frac{\hbar\omega}{k_B T} + ... \qquad \text{(X.16)}$$

and thus

$$n = \frac{1}{\frac{\hbar\omega}{k_B T}} = \frac{k_B T}{\hbar\omega} \qquad \text{(X.17)}$$

Consequently each oscillator has an energy (in addition to the zero point energy ½ $\hbar\omega$)

$$n\hbar\omega = k_B T \qquad \text{(X.18)}$$

which is precisely the classical result (equipartition principle $(1/2)k_BT$ per degree of freedom).

At low temperatures, however,

$$n = e^{-\frac{\hbar\omega}{k_BT}} \qquad \text{(X.19)}$$

This means that only the very low frequency oscillators are then excited. In other words, at low temperature only the states with q ≡ 0 are occupied. At high temperatures, all 3N-states are occupied.

X.5 The specific heat of insulators

The specific heat C_v of a system at constant volume is defined as

$$C_v = \left.\frac{dU}{dT}\right|_V \qquad \text{(X.20}$$

where U is the internal energy of the system. The total energy of the vibrating ions is

$$U = \sum_{q,s}(n_{q,s} + \frac{1}{2})\hbar\omega_{q,s} \qquad \text{(X.21}$$

where the summation is over all vibration modes. In analogy with our treatment of electrons it is more practical to define a density of states $g(\omega)$ of vibration modes of frequency ω, such that

$$g(\omega)d\omega = \frac{\text{Number of vibration modes with frequency in the range } \omega \text{ and } \omega + \mathrm{d}\omega}{\text{volume of the sample}} \qquad \text{(X.22}$$

The total energy is thus

$$U = L^3\int_0^\infty \left[n(\omega) + \frac{1}{2}\right] g(\omega)\hbar\omega d\omega \qquad \text{(X.23}$$

where $n(\omega)$ is the Bose-Einstein distribution function and L^3 the volume of the system containing N atoms. For real solids this is a rather complicated calculation. This is the

reason why Debye proposed the linear approximation shown in Fig. X.8. For the purpose of this course we shall however assume that all three modes are degenerate, so that

$$\omega_{\mathrm{L}} = \omega_{\mathrm{T1}} = \omega_{T2} = v_s|\mathbf{q}| \qquad \text{(X.24}$$

where v_s is the sound velocity. We see (similarly to the Fermi surface for electrons) that the constant frequency surfaces (ω = const) are spheres in the three-dimensional **q**-space (the wave vector space). Following the same lines as in Section VII.5 we find

$$g(\omega)d\omega = \frac{1}{L^3}\frac{4\pi q^2 dq}{(2\pi/L)^3}\cdot 3 \qquad \text{(X.25}$$

where

i) $\frac{1}{\mathrm{L}^3}$ = (volume)$^{-1}$

ii) $4\pi\mathrm{q}^2$ = area of sphere of radius q

iii) $4\pi\mathrm{q}^2\mathrm{dq}$ = volume of a shell of thickness dq at the surface of the sphere

iv) 3 = 1 longitudinal + 2 transverse modes

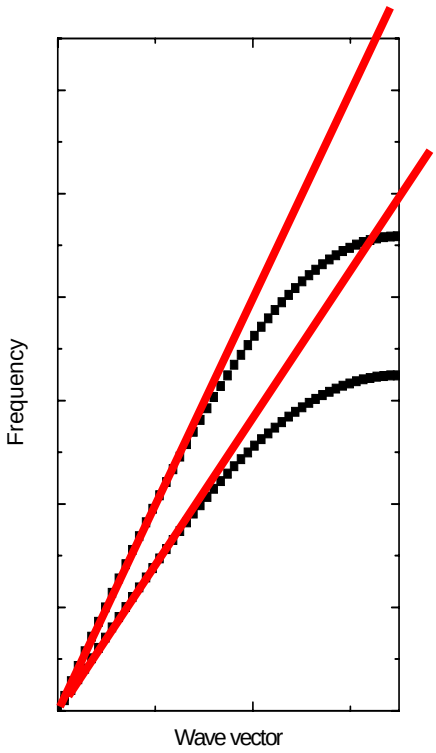


Fig. X.8: Debye approximation of the phonon spectrum. The red straight lines have the same long wave length limit (**q** → 0) as the actual ω(**q**) curves. The model is isotropic in space (i.e. does not depend on the direction of **q**).

As in the Debye approximation

$$d\omega = v_s dq \tag{X.26}$$

we find from eqs X.25 and 26

$$g(\omega) = \frac{3}{2\pi^2 v_s^3}\omega^2 \tag{X.27}$$

and for the total energy

$$U = \frac{3L^3}{2\pi^2 v_s^3}\int_0^{\omega_D}\left[\frac{1}{2} + \frac{1}{e^{\hbar\omega/k_BT} - 1}\right]\omega^2\hbar\omega\, d\omega \tag{X.28}$$

where ω_D, the Debye frequency, is determined by the condition that the Brillouin zone contains exactly 3 N modes, i.e.

$$3N = L^3\int_0^{\omega_D} g(\omega)d\omega = \frac{3L^3}{2\pi^2 v_s^3}\int_0^{\omega_D}\omega^2 d\omega \tag{X.29}$$

from which follows that

$$\omega_D = v_s\left(6\pi^2\frac{N}{L^3}\right)^{1/3} \tag{X.30}$$

where L^3 is the volume of the sample. We set $\hbar\omega/k_BT = x$ in Eq.X.28 and write

$$U = \frac{3L^3 k_B^4 T^4}{2\pi^2 v_s^3 \hbar^3}\int_0^{x_D}\left(\frac{1}{e^x - 1} + \frac{1}{2}\right)x^3 dx \tag{X.31}$$

with

$$x_D = \frac{\hbar\omega_D}{k_BT} \equiv \frac{\theta_D}{T} \tag{X.32}$$

where θ_D is the so-called **Debye temperature**. Combining Eqs.X.30 to 32 we find for the total internal energy,

$$U = 9\,Nk_BT\left(\frac{T}{\theta_D}\right)^3\int_0^{x_D}\left(\frac{1}{e^x - 1} + \frac{1}{2}\right)x^3 dx \tag{X.33}$$

For the specific heat one could now differentiate Eq.X.33 with respect to *T*. It is, however, easier to differentiate Eq.X.28,

$$\frac{dU}{dT} = \frac{3L^3}{2\pi^2 v_s^3}\int_0^{\omega_D} \omega^2 \hbar\omega \frac{\frac{\hbar\omega}{k_B}\frac{1}{T^2} e^{\hbar\omega/k_B T}}{(e^{\hbar\omega/k_B T}-1)^2} d\omega = \tag{X.34}$$

$$= \frac{3\hbar^2 L^3}{2\pi^2 v_s^3 k_B T^2}\int_0^{\omega_D} \frac{\omega^4 e^{\hbar\omega/k_B T}}{(e^{\hbar\omega/k_B T}-1)^2} d\omega$$

$$C_v = 9Nk_B\left(\frac{T}{\theta_D}\right)^3 \int_0^{x_D} dx \frac{x^4 e^x}{(e^x-1)^2} \tag{X.35}$$

for the specific heat. The definite integral is a function of x_D, say $F(x_D)$ so that

$$C_v = 9\,Nk_B\left(\frac{T}{\theta_D}\right)^3 F(x_D) \tag{X.36}$$

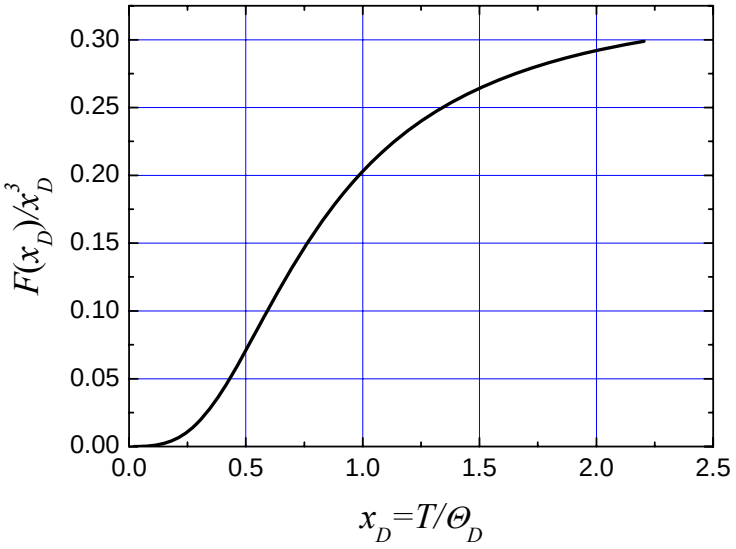


Fig. X.9: The Debye function as a function of the reduced temperature T/θ_D. Values of θ_D for some elements are given in **Table X.1**.

The function *F* is shown in Fig. X.9 as a function of the temperature normalized to the Debye temperature. At low temperature $x_D \to \infty$ and $F(T/\theta_D) = 4\pi^4/15$. We obtain thus

$$C_v = \frac{12\pi^4}{5} Nk_B \left(\frac{T}{\theta_D}\right)^3 \cong 234\, Nk_B \left(\frac{T}{\theta_D}\right)^3 \tag{X.37}$$

At high temperatures $x_D \rightarrow 0$ and $e^x - 1 \cong x$ so that the integral in Eq.X.35 reduces to $x_D^3/3$ and consequently

$$C_v = 3Nk_B \qquad \text{(X.38}$$

in agreement with Dulong-Petit's law (see Eq.X.13).

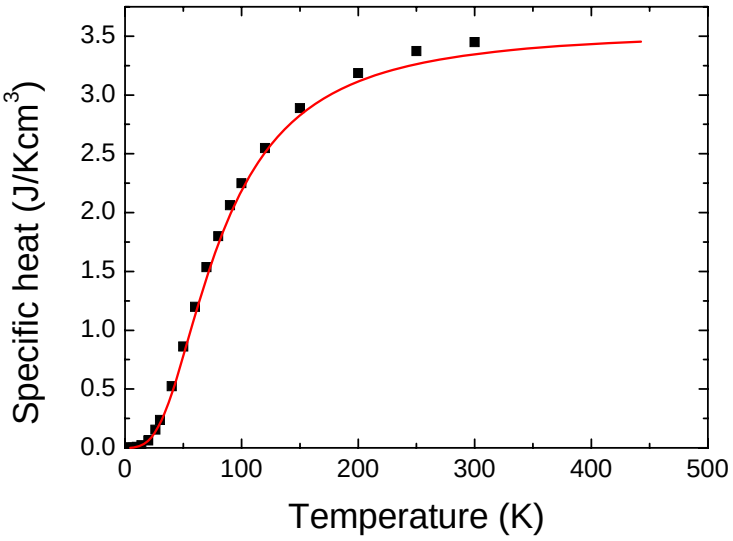


Fig. X.10: Specific heat of Copper compared to the theoretical curve *(red curve)* calculated within the Debye approximation.

Table X.1: Debye temperature for selected elements

Element	**θ_D(K)**	**Element**	**θ_D(K)**
Li	400	Ar	85
Na	150	Ne	63
K	100		
		Cu	315
Be	1000	Ag	215
Mg	318	Au	170
Ca	230		
		Zn	234
B	1250	Cd	120
Al	394	Hg	100
Ga	240		
In	129	Cr	460
Ti	96	Mo	380
		W	310
C(diamond)	1860	Mn	400
Si	625	Fe	420
Ge	360	Co	385
Sn(grey)	260	Ni	375
		Pd	275
Pb	88	Pt	230
As	285	La	132
Sb	200	Gd	152
Bi	120	Pr	74

X.6 Specific heat of electrons compared to that of ions

The overall shape of the theoretical curve in Fig. X.10 is in remarkably good agreement with experimental data. At low temperatures there is however in fact a significant discrepancy that is not visible in the graph. The specific heat does not vanish as T^3 but linearly! This effect must be related to conduction electrons.

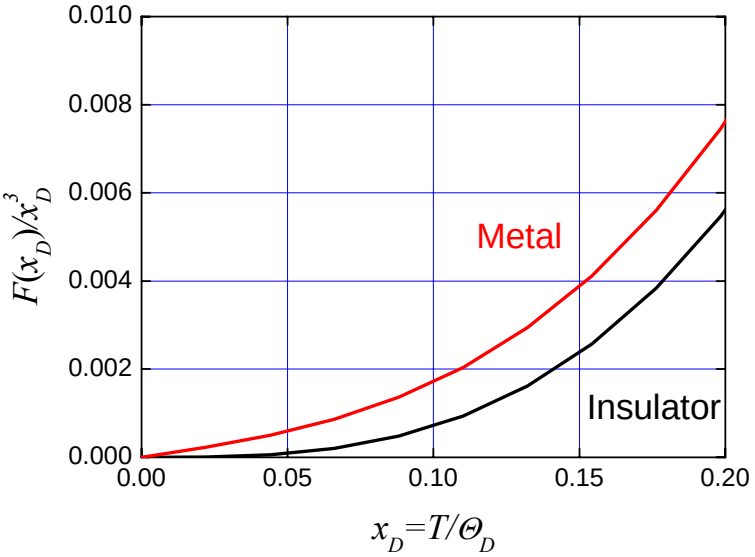


Fig.X.11: At low temperatures the specific heat of a metal has a linear contribution due to the conduction electrons. For a metal there are thus two contributions: one from the conduction electrons and one from the phonons. The contribution of electrons is exaggerated for clarity. For insulators there is only the phononic contribution.

To calculate the specific heat of electrons we proceed exactly as for ions and start from the following expression for the total energy (per unit volume) of a system of independent electrons.

$$U = \int_0^\infty \varepsilon\, f(\varepsilon) g(\varepsilon) d\varepsilon \qquad \text{(X.39}$$

where $g(\varepsilon)$ is the density of states (see Eq. VII.18) and $f(\varepsilon)$ is the Fermi-Dirac distribution function that depends on temperature. At constant volume, the number of electrons being constant, we need to require that

$$n = \int_0^\infty f(\varepsilon) g(\varepsilon) d\varepsilon \qquad \text{(X.40}$$

which implies that the chemical potential μ of the electrons in the Fermi-Dirac distribution function, is a function of temperature. To evaluate Eqs.X.39 and 40 we make use of mathematical expression known as the Sommerfeld expansion.

$$\int_0^{\infty} F(\varepsilon) f(\varepsilon) d\varepsilon \equiv \int_0^{\mu} F(\varepsilon) d\varepsilon + \frac{\pi^2}{6} k_B^2 T^2 \left.\frac{dF}{d\varepsilon}\right|_{\varepsilon=\mu} + O(T^4) \qquad \text{(X.41}$$

where $F(\varepsilon)$ is an arbitrary smooth function of energy and $O(T^4)$ is proportional to $(k_B T/\varepsilon_F)^4 << 1$ for temperatures up to a few thousand degrees. Setting $F(\varepsilon) = \varepsilon g(\varepsilon)$ we obtain

$$U = \int_0^{\mu} \varepsilon\, g(\varepsilon) d\varepsilon + \frac{\pi^2}{6} k_B^2 T^2 \left.\frac{d[\varepsilon g(\varepsilon)]}{d\varepsilon}\right|_{\varepsilon=\mu} \qquad \text{(X.42}$$

similarly

$$n = \int_0^{\mu} g(\varepsilon) d\varepsilon + \frac{\pi^2}{6} k_B^2 T^2 \left.\frac{dg(\varepsilon)}{d\varepsilon}\right|_{\varepsilon=\mu} \qquad \text{(X.43}$$

From the fact that n = const. i.e. $dn/dT = 0$ we obtain that

$$\frac{d\mu}{dT} g(\mu) + \frac{2\pi^2}{6} k_B^2 T \left.\frac{dg}{d\varepsilon}\right|_{\varepsilon=\mu} = 0 \qquad \text{(X.44}$$

For the specific heat we have

$$C_v = \frac{\pi^2 k_B^2 g(\varepsilon_F)}{3} T = \gamma T \qquad \text{(X.45}$$

This result relates a measurable macroscopic quantity, the specific heat C_v to a microscopic quantity of the metal, the electronic density of states $g(\varepsilon_F)$ at the Fermi energy ε_F. This leads to the difference between the specific heat of metals and insulators indicated in Fig.X.11.

In a metal the electronic and phononic contributions can be separated experimentally by plotting $C_v(T)/T$ as a function of T^2. As $C_v(T) = aT + bT^3$

$$\frac{C_v(T)}{T} = a + bT^2 \qquad \text{(X.46}$$

and the intercept a at T = 0 corresponds to the electronic specific heat coefficient γ, which is related to the electronic density at ε_F, i.e. $g(\varepsilon_F)$. For simple metals such as Cu, Ag, Au, Mg, Na, K, Rb, Al, one can evaluate $g(\varepsilon_F)$ by means of the free electron model (see Eq. VII.30).

For transition metals, numerical band structure results are required. The agreement between theory and experiment is relatively good. The theoretical values are, however, always fount to be smaller than the measured values. This is due to the coupling of electrons to phonons that leads to an increase of their effective mass: in a certain sense one can understand this by realizing that each electron is dressed with a “cloud”of phonons. An increase in effective mass corresponds to an effective increase in the density of states. One has to replace $g(\varepsilon_F)$ in Eq.X.45 by $g(\varepsilon_F)(1 + \lambda)$ where λ is the so-called **electron-phonon coupling parameter**. It is interesting to mention that this λ is playing an essential role in the theory of superconductivity of metals.

XI SUPERCONDUCTIVITY

Superconductors, i.e. materials that exert no resistance to the flow of electricity, are one of the most minds bogging scientific discovery. Not only have the limits of superconductivity not yet been reached, but the theories that explain superconductivity seem to be constantly under review. In 1911 superconductivity was first observed in mercury by Heike Kamerlingh Onnes of Leiden University (see Fig. XI.1). When he cooled it to 4 Kelvin, its resistance suddenly disappeared. In his 1913 Nobel lecture, Kamerlingh-Onnes reported that ``mercury at 4.2K has entered a new state, which owing to its particular electrical properties, can be called the state of superconductivity." He noted that the state could be destroyed by applying a sufficiently large magnetic field, while a current induced in a closed loop of superconducting wire persisted for an extraordinarily long time. He demonstrated the latter phenomenon by starting a superconducting current in a coil in his Leiden laboratory, then transporting the coil in a Dewar flask to Cambridge University for a lecture-demonstration on superconductivity.

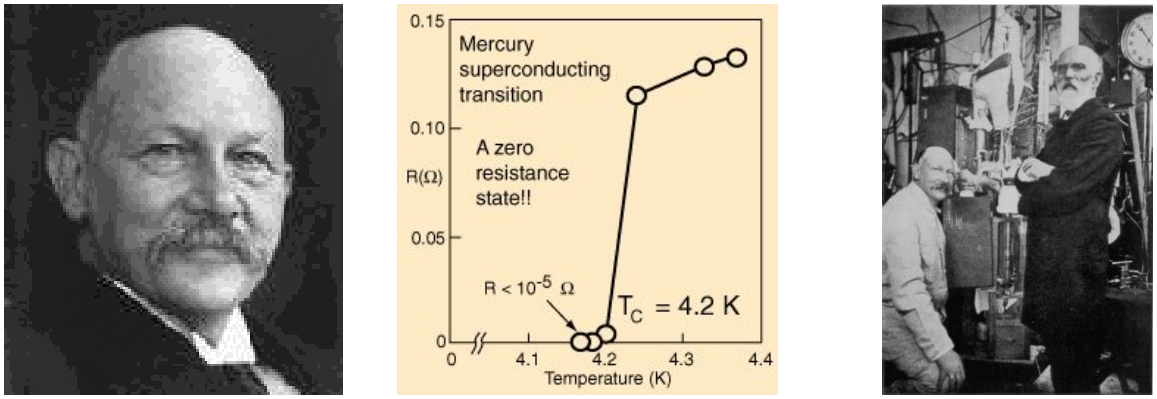


Fig. XI.1: Heike Kamerlingh Onnes, the first measurements of the drop of resistivity in mercury near 4.2 K and Kamerlingh Onnes together with Van der Waals in 1908

Superconductivity represented such a difficult problem in physics that 46 years were necessary to produce a satisfactory explanation. At the beginning, for almost twenty years physicists had to develop the quantum theory of normal metals. Second, it was not until 1934 that a key experiment was performed, the demonstration by Meissner and Ochsenfeld that **the** basic property of a superconductor is in fact **perfect diamagnetism**. Third, once the building blocks were in place, it quickly became clear that the characteristic energy associated with the formation of the superconducting state is amazingly small compared to typical energies in solids (eV for the Fermi energy or 0.1 eV for phonons). Theorists therefore focussed their attention on developing a phenomenological description of superconducting flow. The way was led by Fritz London, who pointed out in 1935 that ``superconductivity is a quantum phenomenon on a macroscopic scale, ...with the lowest energy state separated by a finite interval from the excited states" and that ``diamagnetism is the fundamental property." In the present Chapter we give a very brief introduction to these various phenomena.

XI.1 The Meissner effect

When a superconductor is placed in a magnetic field it expels the field in its interior. As a result a sample placed on top of permanent magnets experiences a repulsive force and is brought in a state of levitation (see Fig. XI.2). At first sight this seems to be a straightforward consequence of the infinite conductivity of a superconductor. According to the induction law

$$\nabla E = -\frac{\partial B}{\partial t} \qquad \text{(XI.1)}$$

and with Ohm's law

$$J_E = \sigma E \qquad \text{(XI.2)}$$

the electric field E is zero since the electrical conductivity is infinite. Thus $\partial B / \partial t = 0$ and the field remains constant. The magnetic field expulsion occurs, however, also when the superconductor is cooled down in a constant magnetic field. This is the most important implication of the Meissner effect. It implies that the superconducting state is uniquely defined and does not depend on the history. In other words, it implies that thermodynamics can be used. This is illustrated in Fig. XI.3. This property cannot be understood within Maxwell's theory but needs an extra assumption about the superconducting state. A phenomenological theory that "explains" the Meissner state was proposed by London.

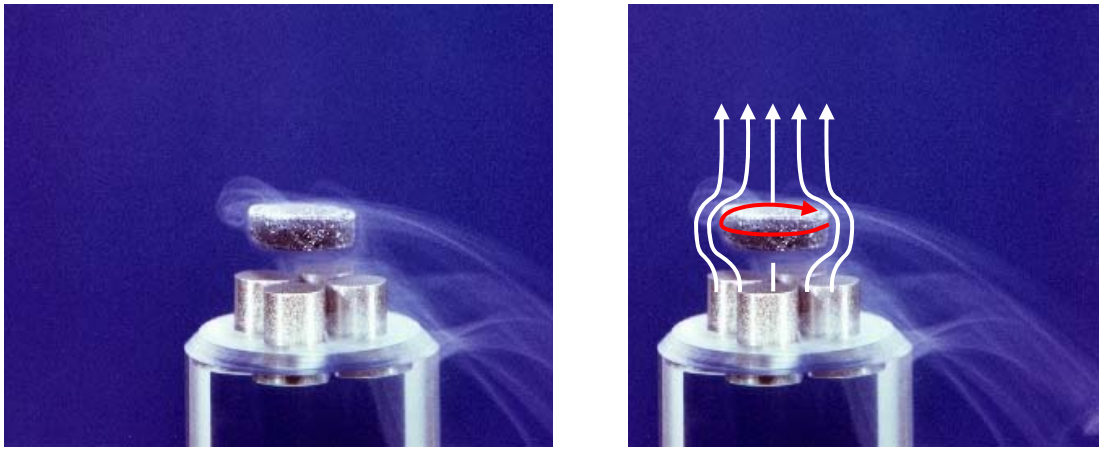


Fig. XI.2: A sample of $YBa_2Cu_3O_7$ levitating above four permanent magnets at 77 K. This material loses all its electrical resistivity as soon as its temperature drops below 91 K.

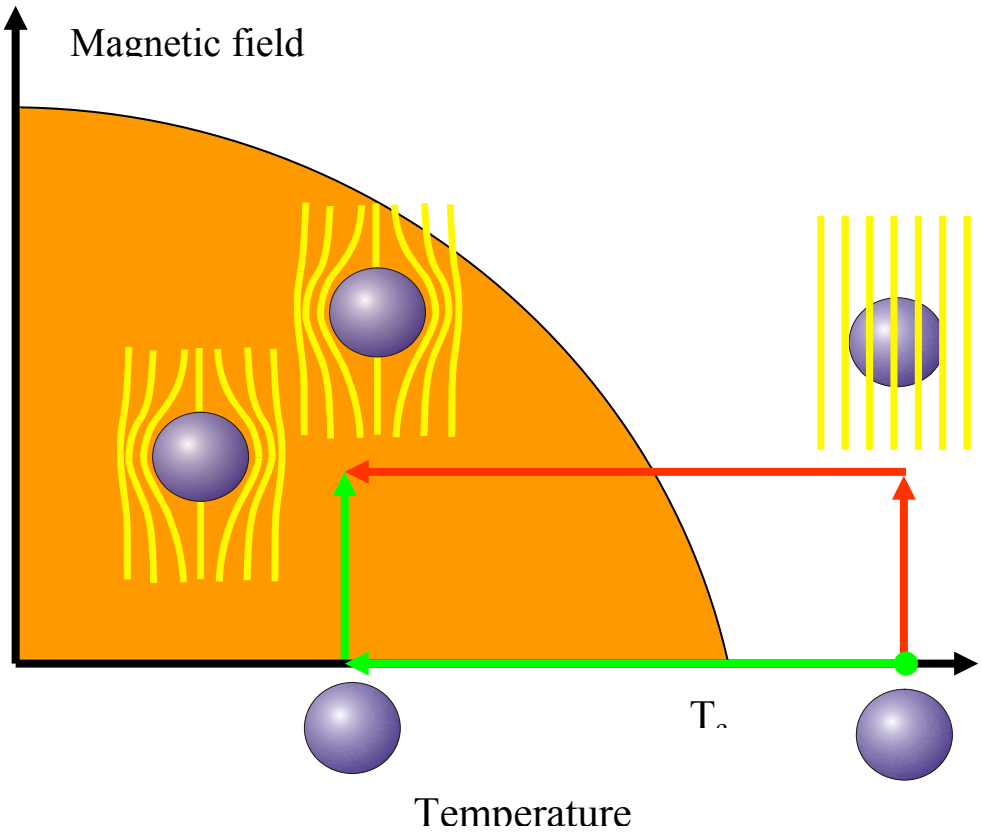


Fig. XI.3**:** The state of a superconductor does not depend on the path followed in the H-T diagram. The field lines of the **B**-field for a sphere are indicated in yellow. For the red path, first one applies a magnetic field at a temperature above T_c when the sphere is a normal metal (not superconducting) and then one cools down the sample to a temperature below T_c. For the green path, one cools the sphere below T_c before applying a magnetic field. The end state is, however, the same for both paths.

XI.2 London theory

London assumes that electrons in a superconductor are completely free to move. In an electric field each electron is accelerated according to Newton's equation

$$-e\mathbf{E} = m\frac{\partial \mathbf{v}}{\partial t} \qquad (\text{XI.3}$$

with m the mass of the electron, e its charge and **E** the electric field. The current density $\boldsymbol{j_s}$ is defined as

$$\mathbf{j}_s = -en_s\mathbf{v} \qquad (\text{XI.4}$$

Its time dependence follows from Eq.XI.3 as

$$\frac{\partial \mathbf{j}_s}{\partial t} = \frac{n_s e^2}{m}\mathbf{E} \qquad (\text{XI.5}$$

This relation and Maxwell's equation

$$\nabla \times \mathbf{E} = -\frac{\partial \mathbf{B}}{\partial t} \qquad (\text{XI.6}$$

lead to

$$\frac{\partial}{\partial t}\left(\frac{m}{n_s e^2}\nabla \times \mathbf{j_s} + \mathbf{B}\right) = 0 \qquad (\text{XI.7}$$

This equation that is derived using classical mechanics and classical electrodynamics describes the behaviour of an ideal conductor, i.e. a conductor with zero resistivity (or equivalently, with infinite conductivity) but it is unable to describe the Meissner effect that occurs during mere cooling of a sample in a constant external magnetic field. However, London noticed that if one would postulate that the expression between brackets vanishes, one could describe the Meissner effect. Indeed if

$$\left(\frac{m}{n_s e^2}\nabla \times \mathbf{j_s} + \mathbf{B}\right) = 0 \qquad (\text{XI.8}$$

we obtain with Maxwell's equation

$$\nabla \times \mathbf{B} = \mu_o \mathbf{j_s} \qquad (\text{XI.9}$$

the so-called London equation

$$\lambda_L \nabla \times \nabla \times \mathbf{B} + \mu_o \mathbf{B} = 0 \qquad (\text{XI.10}$$

where

$$\lambda_L = \frac{m}{n_s e^2} \qquad (\text{XI.11}$$

The solutions of Eq.XI.10 are typically exponentials, which in a 1D case are of the form

$$B \propto e^{-\frac{x}{\Lambda_L}} \qquad (\text{XI.12}$$

with

$$\Lambda_L = \left(\frac{\lambda_L}{\mu_o}\right)^{1/2} = \left(\frac{m}{\mu_o n_s e^2}\right)^{1/2} \qquad (\text{XI.13}$$

the London penetration length. As Λ_L is typically of the order of 100 nm it means that the **B**-field is essentially completely expelled from samples with dimensions of the order of mm or more. It is, however, a phenomenological model.

XI.3 Cooper pairs

The essential physics involved in the microscopic Bardeen-Cooper-Schrieffer theory (the so-called BCS theory) of superconductivity can be understood on the basis of a simple calculation. Consider a system consisting of N electrons and assume that for one reason or the other there is an attractive interaction between them. As it is very difficult to deal with N electrons at once, we assume that the attractive interaction is only operative between two of them and that all the other are doing nothing else than filling the Fermi sphere. This situation is shown in Fig. XI.4.

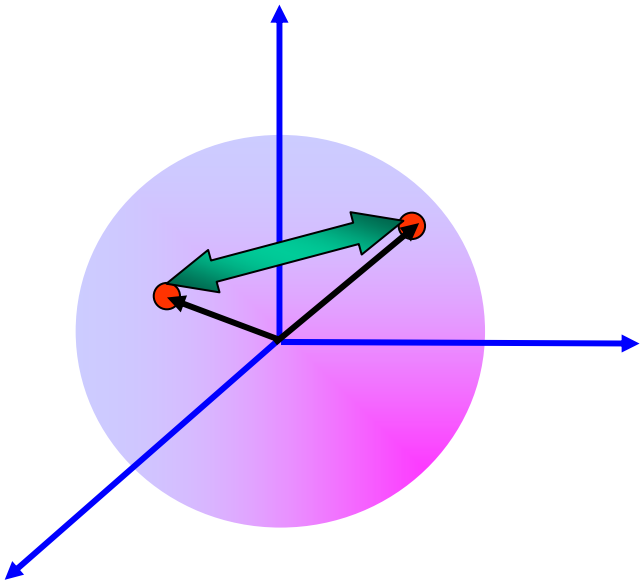


Fig. XI.4: The situation considered by Cooper. Two electrons at the Fermi surface (red) interact attractively (green arrow) with each other. They cannot go inside the Fermi surface as all the states are occupied by the other electrons (Pauli principle). Cooper was able to show that the two electrons form a pair no matter how weak the interaction between the two electron is.

For these two electrons, we can write the following Schrödinger equation

$$-\frac{\hbar^2}{2m}\Delta_1\Psi - \frac{\hbar^2}{2m}\Delta_2\Psi + V(\mathbf{r}_1 - \mathbf{r}_2)\Psi = E\Psi \qquad (\text{XI.14})$$

where $$\Delta_i \equiv \frac{\partial^2}{\partial x_i^2} + \frac{\partial^2}{\partial y_i^2} + \frac{\partial^2}{\partial z_i^2} \qquad (\text{XI.15})$$

and $\mathbf{r_i} = (x_i, y_i, z_i)$ (XI.16)

is the position vector of the electron *i*. The interaction potential is assumed to depend only on the relative position of the two electrons. The wave function Ψ depends both on $\mathbf{r}_1$ and $\mathbf{r}_2$. Introducing the relative position vector

$$\mathbf{r} = (x, y, z) = \mathbf{r}_2 - \mathbf{r}_1 \tag{XI.17}$$

and the position vector **R** of the centre of mass

$$\mathbf{R} = (X, Y, Z) = \frac{\mathbf{r}_2 + \mathbf{r}_1}{2} \tag{XI.18}$$

the Schrödinger equation can be written

$$\begin{aligned} &-\frac{\hbar^2}{2M}\left(\frac{\partial^2}{\partial X^2}+\frac{\partial^2}{\partial Y^2}+\frac{\partial^2}{\partial Z^2}\right)\Psi(\mathbf{R},\mathbf{r}) \\ &-\frac{\hbar^2}{2\mu}\left(\frac{\partial^2}{\partial x^2}+\frac{\partial^2}{\partial y^2}+\frac{\partial^2}{\partial z^2}\right)\Psi(\mathbf{R},\mathbf{r})+V(\mathbf{r})\Psi(\mathbf{R},\mathbf{r}) = E\Psi(\mathbf{R},\mathbf{r}) \end{aligned} \tag{XI.19}$$

with $M=2m$ and $\mu=m/2$. This differential equation can obviously be solved by the method of separation of variables

$$\Psi(\mathbf{R},\mathbf{r}) = \Phi(\mathbf{R}) f(\mathbf{r}) \tag{XI.20}$$

which leads to the following two equations

$$-\frac{\hbar^2}{4m}\left(\frac{\partial^2}{\partial X^2}+\frac{\partial^2}{\partial Y^2}+\frac{\partial^2}{\partial Z^2}\right)\Phi(\mathbf{R}) = E_0\Phi(\mathbf{R}) \tag{XI.21}$$

and

$$-\frac{\hbar^2}{m}\left(\frac{\partial^2}{\partial x^2}+\frac{\partial^2}{\partial y^2}+\frac{\partial^2}{\partial z^2}\right)f(\mathbf{r})+V(\mathbf{r})f(\mathbf{r}) = E_{pair} f(\mathbf{r}) \tag{XI.22}$$

The total energy of the two-electron system is thus

$$E = \frac{P^2}{2M} + E_{pair} \tag{XI.23}$$

where P is the momentum of the centre of mass. The lowest energy is obtained for a pair of electrons with a total momentum equal to zero. Then $E=E_{pair}$. As we are interested in constructing a state with the lowest energy we choose a pair of electrons with $P=0$, i.e. with one electron having a momentum $\hbar\,\mathbf{k}$ and the other $-\hbar\,\mathbf{k}$.
We search for a solution of Eq.XI.22 in the form of a linear combination of plane waves with wave vectors outside the Fermi surface, since all the states with $k<k_F$ are occupied.

$$f(\mathbf{r}) = \frac{1}{\sqrt{\Omega}} \sum_{\mathbf{k'}} g(\mathbf{k'}) e^{i\mathbf{k'r}} \tag{XI.24}$$

where Ω is the volume of the system under consideration, i.e. all the electrons inside the Fermi sphere and the two extra electrons considered here.
The normalisation of the wave function requires that

$$\sum_{\mathbf{k'}} g^*(\mathbf{k}) g(\mathbf{k}) = 1 \tag{XI.25}$$

Introducing Eq.XI.24 in Eq.XI.22 we obtain

$$\sum_{\mathbf{k'}} g(\mathbf{k'}) e^{i\mathbf{k'r}} \frac{\hbar^2 k'^2}{m} + \sum_{\mathbf{k'}} g(\mathbf{k'}) V(\mathbf{r}) e^{i\mathbf{k'r}} = E_{pair} \sum_{\mathbf{k'}} g(\mathbf{k'}) e^{i\mathbf{k'r}} \tag{XI.26}$$

Multiplying by $\frac{1}{\sqrt{\Omega}} e^{-i\mathbf{kr}}$ and integrating over whole space, we obtain

$$g(\mathbf{k}) \left[E_{pair} - 2\frac{\hbar^2 k^2}{2m} \right] = \sum_{\mathbf{k'}} g(\mathbf{k'}) V_{\mathbf{kk'}} \tag{XI.27}$$

where the matrix element $V_{\mathbf{kk'}}$ is defined as

$$V_{\mathbf{kk'}} = \frac{1}{\Omega} \int V(\mathbf{r}) e^{i(\mathbf{k}-\mathbf{k'})\mathbf{r}} d^3 r \tag{XI.28}$$

In order to discuss the properties of Eq.XI.27 let us assume that

$$V_{\mathbf{kk'}} = -F \tag{XI.29}$$

if the energies corresponding to $\mathbf{k}$ and $\mathbf{k}$' are between the Fermi energy E_F and $E_F + \hbar\,\omega_D$ and $V_{\mathbf{kk'}}=0$ for states with energies higher than $E_F + \hbar\,\omega_D$. This choice is justified by the fact that the attractive interaction between two electrons is mediated by the deformation of the metal lattice, i.e. by phonons. Phonons have energies of the order of $\hbar\,\omega_D$. An artist impression about the way phonons can lead to an attractive

interaction between electrons is shown in Fig. XI.5. With Eq.XI.29 equation XI.27 simplifies then to

$$g(\mathbf{k})\left[E_{pair}-2\frac{\hbar^2k^2}{2m}\right]=-F\sum_{\mathbf{k}'}g(\mathbf{k}') \qquad \text{(XI.30)}$$

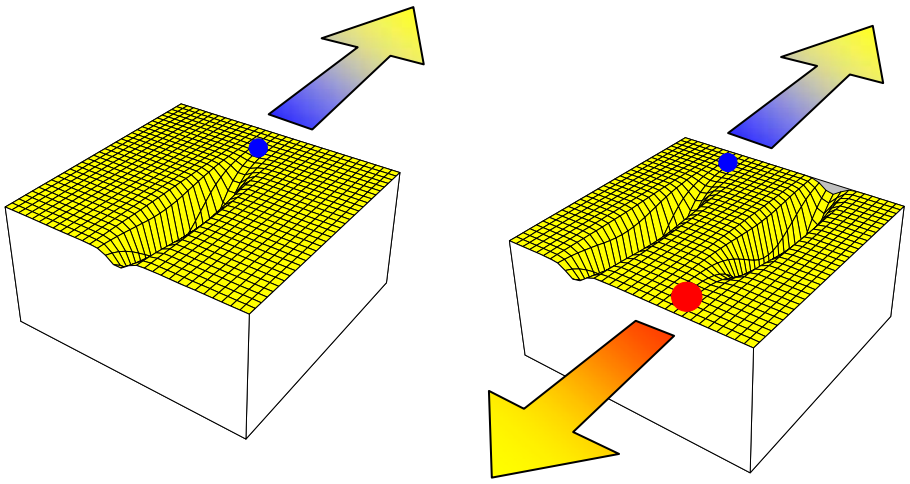


Fig. XI.5: *Left panel*: An electron moving through the ion lattice of a metal creates a compression wave behind him as a result of the attraction between the (negative) electron and the (positive) ions. This compression wave lags behind the electron because ions are slow to respond to the attraction created by the fast moving electron (remember that at the Fermi energy electrons are flying with a velocity of the order of 10^6 m/s !). A compression of ions means that locally a positive cloud is created behind the electron. This cloud is attractive for other electrons: this is the meaning of the dip behind the electron. *Right panel*: When two electrons with opposite velocities pass close to each other electron 1 can lower its energy by moving within the dip of electron 2 and vice versa (for clarity we have slightly shifted the parallel trajectories of the two electrons).

By summing over all **k** we can simplify drastically this relation

$$\sum_{\mathbf{k}}g(\mathbf{k})=-F\sum_{\mathbf{k}}\left(\frac{\sum_{\mathbf{k}'}g(\mathbf{k}')}{\left[E_{pair}-2\frac{\hbar^2k^2}{2m}\right]}\right) \qquad \text{(XI.31)}$$

Since evidently $\sum_{\mathbf{k}}g(\mathbf{k})=\sum_{\mathbf{k}'}g(\mathbf{k}')$ we obtain the so-called self-consistency relation

$$1 = -F\sum_{\mathbf{k}}\left(\frac{1}{E_{pair} - 2\frac{\hbar^2 k^2}{2m}}\right) = -F\sum_{\mathbf{k}}\left(\frac{1}{E_{pair} - 2\varepsilon}\right) \tag{XI.32}$$

The summation is readily evaluated by replacing it by an integral involving the density of particles per unit energy

$$R(\varepsilon)d\varepsilon = \frac{4\pi k^2 dk}{(2\pi)^3} \tag{XI.33}$$

$$\sum_{\mathbf{k}}\left(\frac{1}{E_{pair} - 2\varepsilon_k}\right) = \int_{E_F}^{E_F+\hbar\omega_D} R(\varepsilon)\frac{1}{E_{pair} - 2\varepsilon}d\varepsilon =$$

$$= R(E_F)\int_{E_F}^{E_F+\hbar\omega_D}\frac{1}{E_{pair} - 2\varepsilon}d\varepsilon = \tag{XI.34}$$

$$= -\frac{1}{2}R(E_F)\ln\left[\frac{E_{pair} - 2E_F - 2\hbar\omega_D}{E_{pair} - 2E_F}\right]$$

Combining Eqs.XI.32 ands 34 we obtain

$$E_{pair} = 2E_F - \frac{2\hbar\omega_D}{e^{2/FR} - 1} \tag{XI.35}$$

As F is assumed to be positive (we have assumed an attractive interaction between the two electrons) the pair energy is always lower than $2E_F$, i.e. it is always lower than the energy of the two electrons in absence of attractive interaction. In other words the two electrons do form a pair. This is a remarkable result since in free space two particles form only a pair (bound state) if the attractive interaction is larger than a minimum value. This is the important feature of the Cooper result.

In the limit of a weakly attractive interaction, i.e. when $FR<<1$, then the exponential in Eq.XI.35 is the dominant factor and

$$E_{pair} = 2E_F - 2\hbar\omega_D e^{-2/FR} \tag{XI.36}$$

The binding energy of a pair is consequently

$$E_c = 2\hbar\omega_D e^{-2/FR} \qquad \text{(XI.37)}$$

An estimate of the critical temperature for superconductivity is easily obtained by noting that electron pairs will be broken up when the temperature exceeds T_c defined by

$$T_c \cong \frac{E_c}{k_B} = 2\frac{\hbar}{k_B}\omega_D e^{-2/FR} \qquad \text{(XI.38)}$$

Quite remarkably the simple calculation of Cooper leads to a result that is essentially the same as that of the much more involved Bardeen-Cooper-Schrieffer theory. In the BCS theory all the electrons are treated on the same footing, i.e. they are all allowed to form pairs.

XI.4 High temperature superconductors

A new era in superconductivity opened when, on January 27, 1986, Bednorz and Mueller discovered a sharp drop in the resistance of $La_{2-x}Ba_xCuO_4$ at a temperature of approximately 30 K. They sent off a paper reporting their findings to a European journal, the Zeitschrift für Physik, and continued their study of this novel material in order to be certain that the resistivity change they had observed reflected a transition to the superconducting state. By October they had observed the Meissner effect, and so established that the new material was indeed a superconductor. Word of their results soon spread; a month later, Tanaka and his colleagues in Tokyo confirmed the Bednorz-Mueller results (a confirmation reported in one of Japan's leading newspapers) while their work was further supported by experiments carried out in Beijing by Zhou and his colleagues (whose work was described in the Beijing newspapers that December). In the following month, in a collaborative effort led by Paul Chu of the University of Houston and Mang-Kang Wu of the University of Alabama, a new member of this high temperature superconducting family was discovered, $YBa_2Cu_3O_7$ which possessed a T_c of over 90K. Thus within a year of the original discovery the superconducting transition temperature had increased by a factor of three, and it was clear that a revolution in superconductivity had begun. A celebration of the start of that new era took place at a special evening session of the American Physical Society's 1987 March meeting in New York City, when some 3000 physicists jammed the auditorium in which the session took place, with another 3000 people watching on closed circuit television outside, an event which has become known as the Woodstock of Physics.

Within the next six years a number of additional families of high temperature superconductors were discovered. These included Tl- and Hg- based systems which had maximum T_c of 120K and 160K respectively. All shared the feature which appeared responsible for the occurrence of high temperature superconductivity, the presence of

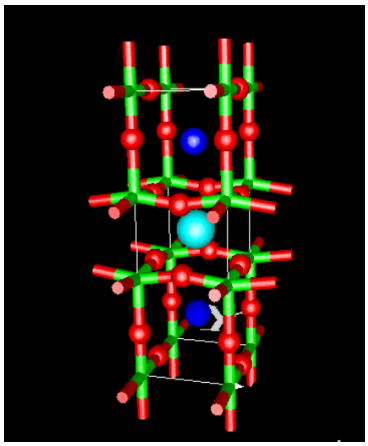


Fig. XI.6: Crystal structure of $YBa_2Cu_3O_7$. The Cu atoms are in red, O in green, Ba in blue and Y in light blue. Superconductivity is believed to occur in the two horizontal CuO planes.

planes containing Cu and O atoms which are separated by bridging materials which act as charge reservoirs for the planes. During this period, some 10,000 papers a year were being published on high temperature superconductors (a pace which continues to the present time) and it became evident that high temperature superconductivity was regarded by many as the major problem in physics in the last decade of this century. There are at least four reasons for the extraordinary interest in high T_c:

- its intrinsic scientific interest;
- its transdisciplinary nature (it reaches across the boundaries which typically divide materials scientists and chemists from experimental and theoretical physicists);
- the potential applications for materials which superconduct at temperatures greater than the temperature at which nitrogen liquefies (77K), applications which might include filters for cellular phone systems, superconducting transmission lines, MRI machines using high T_c magnets, microwave systems which incorporate the new materials, and hybrid semiconductor/superconductor systems;
- and finally, the possibility of finding a room temperature superconductor.

Some common characteristics of the high temperature superconductors are that they are ceramics. They are poor metals at room temperature, are difficult materials with which to work. contain few charge carriers compared to normal metals, and display highly anisotropic electrical and magnetic properties which are remarkably sensitive to oxygen content. While superconducting samples of $YBa_2Cu_3O_7$ can be made by a high school student in a microwave oven, single crystals of the high purity required to determine the intrinsic physical properties of these systems are exceedingly difficult to make. In our group excellent thin films of this material have been done using laser ablation.
Following a decade of work, there is now an experimental and theoretical consensus that the behaviour of the elementary excitations in the Cu-O planes provides the key to understanding the normal state properties of these cuprate superconductors, and that essentially no normal state property (save one) resembles those found in the normal state of a conventional, low T_c superconductor.